Title
On the Mechanics of Hydrogels for Tissue Engineering Applications

Author
López, Gabriel Ricardo

Publication Date
2022

Peer reviewed|Thesis/dissertation

On the Mechanics of Hydrogels for Tissue Engineering Applications

By

Gabriel Ricardo López

A dissertation submitted in partial satisfaction of the

Requirements for the degree of

Doctor in Philosophy

In

Engineering- Mechanical Engineering

In the

Graduate Division

Of the

University of California, Berkeley

Committee in charge:

Professor Grace D. O'Connell, Chair

Professor Tony Keaveny

Professor Kevin Healy

Fall 2022

On the Mechanics of Hydrogels for Tissue Engineering Applications

By

Gabriel Ricardo López

Abstract

On the Mechanics of Hydrogels for Tissue Engineering Applications

By

Gabriel Ricardo López

Doctor of Philosophy in Mechanical Engineering

University of California, Berkeley

Professor Grace D. O'Connell

The dissertation research focused on exploring relationships between composition, structure, and mechanical properties in hydrogels used for tissue engineering application. Specifically, these series of separate but related studies focused on agarose-based gels and co-gels, looking at how different concentrations of agarose, alginate, and collagen affected their ability to serve as a tissue-engineering scaffold with appropriate manufacturability, compressive mechanical properties, and extra-cellular matrix production of embedded cells. These relationships between composition and structure add to the growing literature of tissue-engineering scaffolds, and help researchers move closer towards functional repair of damaged tissues.

The main results of this work identified agarose-alginate co-gels as a suitable candidate for bioprinting tissue engineering scaffolds. Later, it was observed that crosslinking agarose-alginate gels changes the short-term recovery behavior under unconfined compression, and increases elastic mechanical properties. This dissertation work also observed that methods used to quantify collagen content from commercial collagen type I gels vary by species source, and that combining these collagen gels in an agarose-based cell-embedded scaffolds produces a minimal, dose-dependent effect on matrix production and compressive mechanics.

In short, the dissertation has expanded on the known literature of agarose co-gel mechanics under different loading scenarios. It is my hope that researchers will use the relationships between matrix production, initial gel content, and compressive and shear mechanics to continue improving the functionality of tissue engineered constructs.

Table of Contents

List of Figures

Chapter 1

Chapter 2

List of Tables

List of common acronyms

Many acronyms are used throughout this document. While I have made an effort to define new acronyms at the beginning of each chapter, the following list highlights some of the more commonly used acronyms across the dissertation. They are presented here in alphabetical order.

AC – Articular cartilage

ACI – Autologous chondrocyte implantation

AF – Annulus Fibrosus

AFM – atomic force microscopy

Ag-alg – agarose-alginate

AGE – Advanced glycation end-products

ANOVA – Analysis of Variance

CAD – Computer aided design

DW or dw- dry weight

ECM – Extra-cellular matrix

GAG – Glycosaminoglycans

IVD – Intervertebral disc

MSC – mesenchymal stem cells

NP – Nucleus Pulposus

OHP- ortho-hydroxyproline

PG – Proteoglycans

SHG – Second harmonic imaging

TJR – Total joint replacement

TKR – Total knee replacement

w/v – weight over volume

WW or w/w- Wet weight

Acknowledgements

A document 6 years in the making spanned the contributions, directly or indirectly, of a slew of people to whom I am deeply indebted.

Thank you to my research mentor Dr. Grace O'Connell, without whom this dissertation would have been impossible. Grace took a chance on me and has been an incredible mentor during my time at Berkeley. Grace pushed me to be a better scientist, gently guiding me to find my own conclusions and come to my own realizations, never once disparaging my work, and always prioritizing my development as a PhD student. But more importantly, Grace gave me the space to explore my interests outside of the lab, encouraging and being supportive of my involvement in student organizations and teaching me to be a better mentor to those around me. Grace leads through her example, and we are all better off for it.

Thank you to my labmates, past and present, in the Biomechanics lab. Semih Bezci, Shannon Emerzian, Megan Pendleton, Ben Werbner, Minhao Zhou, Thomas Georgiou, Anne Zeng, Saghi Sadoughi, Noah Bonnheim, all of whom taught me as I stumbled my way through the lab in year one. Thanks to Emily Lindberg and Shiyin Lim, who constantly helped me out and give life to the laboratory, as well as Reece Huff, Yishu Yan, Freddie Houghton, Amber Young, Erin Archibeck, and Melissa Abed, who were also a part of the end of my journey in Berkeley.

I am deeply grateful to have had the opportunity to mentor some incredibly ridiculously smart and incredibly kind people. Thank you Kai Littlejohn, Charlie Osuna, Keerthana Elango, Christian Leycam, X Sun, and Cameryn Burnette, who as undergraduates, put in countless hours towards our research goals and help me grow.

I am also thankful for my fellow collaborators, Dr. Jeannette Garcia, Sofia Arevalo, and Gabriel Dorlhiac, who aided me in my moments of scientific need with a willing heart.

I would like to take a moment to also thank my dissertation committee, Dr. Kevin Healy and Dr. Tony Keaveny, for helping me with equipment, with my writing, and finally with my exit seminar. I need to also acknowledge Dr. Lisa Pruitt, who taught me that there's a leader in all of us, and we just have to find them in our own time.

I would be remiss if I didn't thank my Berkeley friends, and especially everyone who formed a part of my time there. Roberto Falcon, who was my biggest support through helping me make sense of graduate school. Michelle and Carli and Michi and Shayan and Liani and Peter, whom I spent so much time with, and Benson and Miguel and Fonseca and everyone else who gave me tips along the way. I would be remiss if I didn't mention LAGSES, and incredible organization in Berkeley who has a lot of Latinx leaders, but more importantly people who are kind, and thoughtful, and deserve the world.

Beyond Berkeley, I need to thank my family and friends. Thank you to Ricardo López and Sandra Marcial, better known as Mami y Papi, for your support not just throughout my academic journey but throughout my whole life. My sister Lisa, abuela Gloyin, Letty, Maro, and everyone else who never doubted I'd be able to get here.

But last and definitely most importantly, I have to thank my wife Milca Nieves. I write this as we are in our Philly apartment, the second time she's packed her bags and journeyed thousands of

miles with me. Milca never doubted I could finish my education, she supported me through all of it, giving me a push when needed and helping me realize when I needed to take a foot of the gas. I'm never kidding when I say that I don't know where I'd be without her, but it would absolutely not be writing an acknowledgement section of a document that lets people call me doctor, and it wouldn't be with the happiness I have right now, because she is always the brightest part of my life.

Chapter 1: Introduction

1.1 Load-bearing tissues

The ability to move is necessary to work, play, eat, or perform most life-sustaining activities. Our musculoskeletal system controls this ability, giving organisms a physical form. This system is composed of bones, muscles, ligaments, cartilage, and other connective tissues that work together to generate or absorb mechanical force. Since these load-bearing tissues actively produce and distribute the forces felt due to our own weight or movement they may be physically damaged due to excessive forces or disease. To understand how to preserve these tissues, we must first understand their composition and their function more closely. Here, we will focus on soft tissues that have explicit load-bearing function but lack blood flow due to low vascularity, and as such are unable to repair quickly. Specifically, we will be looking at tissues such as the knee articular cartilage and the meniscus. These tissues are commonly injured, and may be damaged through a variety of reasons, including age, overuse, and accidental injuries. While these tissues have different functions and structures, they often share similar components such as collagen fibers, water, and glycosaminoglycans (GAG). These components directly affect the mechanical properties of these tissues. The intervertebral disc is briefly described but is not the focus of this work.

Collagen is a structural protein that is subdivided into 28 subtypes, with collagen I and II being the most prevalent in load-bearing tissues. These "major" collagens arrange themselves into a triple-helical structure called a fibril, and a group of fibrils form fibers that provide the tissue with the ability to resist deformation in tension (**Figure 1-1**).

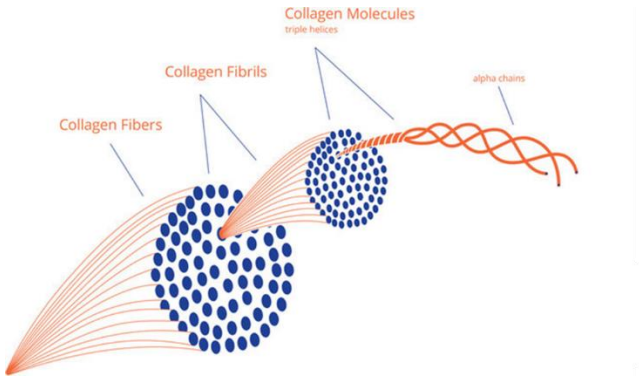

Figure 1-1: *Hierarchical collagen fiber structure. From Nijhuis et al 2019*[1]

Glycosaminoglycans (GAG) are polysaccharides with a repeating unit which attach to a polypeptide core to form proteoglycans (PG's).[7] GAGs are highly polar, negatively charged, and as such attract and store water. This bound water stored within tissues allow them to resist deformation in compression. [8,9]

1.1.1 Articular cartilage

Anatomy and Structure

Articular cartilage is a smooth, white, avascular tissue that can be found in articulating joints (such as the knees, shoulders and hips), where it serves to absorb loads and dissipate energy. Cartilage also exhibits a coefficient of friction lower than any synthetic material (range: 0.002-0.5)[10–12], making it a great sliding surface and enables movement at these synovial joints. [13] It can be described as having three distinct zones (**Figure 1-2B**). The superficial zone near the articular surface is rich in collagen fibers that are tightly packed and oriented parallel to the surface, and comprises 10-20% of the cartilage volume.[14] Below it is the middle zone, which has a high proteoglycan content (40-60% of cartilage volume). Collagen fibers in the middle zone are thicker, but lack a distinct organizational pattern. Finally, the deep zone contains the largest diameter collagen fibers oriented perpendicular to the articular surface, as well as the highest proteoglycan content. [14] This allows it to offer the most resistance to compression. The deep zone comprises 20-30% of the cartilage volume and is connected to the underlying bone.

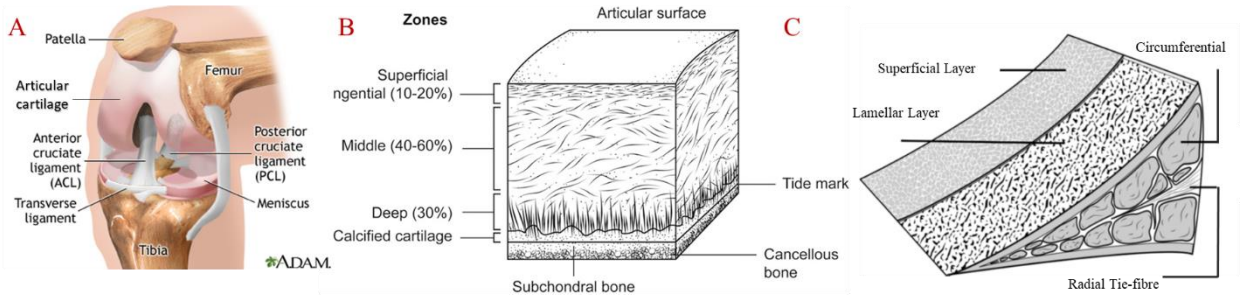

Figure 1-2*: (A) Anatomy of the knee joint. Taken rom https://medlineplus.gov/ency/presentations/100117_1.htm. Collagen fiber structure of (B) articular cartilage (From Brody et al)*[2] *and (C) meniscus (From Choi et al)*[3]

Composition

Articular cartilage is composed of water (80% of wet weight), Collagen type II (~55% of dry weight) and proteoglycans (10-15% of wet weight)[14]. The main proteoglycan found is aggrecan, which is composed primarily of GAG chains.

1.1.2 Meniscus

Anatomy and Structure

The meniscus is a half-moon shaped collagenous tissue that bears loads in the knee between the tibial and femoral articular cartilage. There are two menisci in each knee joint, with the circumferential direction aligning from anterior to posterior direction. The lateral portion of the meniscus is thick but thins into the medial portion, creating a convex shape in its superior surface that conforms to the tibia, while the inferior side is mostly flat.[15] Collagen fibrils are organized across the circumferential direction, with larger tie-fiber bundles across the radial direction. In loading, axial forces in the knee result in hoop stresses in the circumferential direction, borne by

the aligned fibers in that direction. The meniscus serves as a shock absorber, allowing the knee joint to absorb large forces on impact.[16]

Composition

The meniscus is possesses high quantities of water (72% of wet weight) as well as collagen (22% of wet weight)[15]. Collagen type I is predominant, comprising almost 90% of the meniscus dry weight. Other matrix proteins like fibronectin comprise 8-13% of the dry weight, and proteoglycans like GAG contribute 1-2% of the dry weight.[15]

1.1.3 Intervertebral Disc

Anatomy and structure

The intervertebral disc is a structure that rests between the bony vertebrae of the spine, allowing movement and sustaining loads. It is generally described as having two distinct soft tissue regions: a soft nucleus pulposus (NP) in the center, which is surrounded by a stiff annulus fibrosus (AF; **Figure 1-3A**). However, it is more accurately describes as a large structure with a sharp composition gradient at the AF-NP interface (**Figure 1-3B**). When the disc is loaded in compression, the NP expands radially outwards, creating tensile forces along the AF.

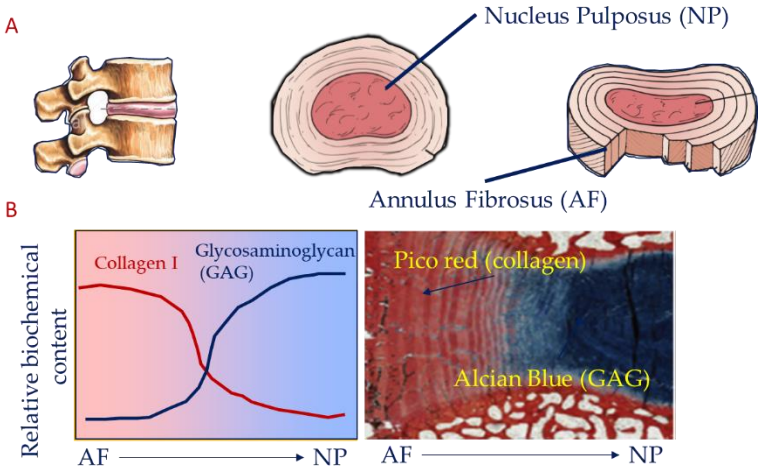

Figure 1-2: *The intervertebral disc (A) general anatomy and (B) simplified composition gradient (From Bonnevie and Mauck, 2018)*[4]

Composition

The NP has high quantities of water (80% of weight), collagen type II, and glycosaminoglycans (GAG; 25% of dry weight). From NP-AF boundary at the inner annulus to the outer AF, water and GAG content gradually decreases while collagen content increases from about 50% of dry weight to 66% of dry weight **(Figure 1-3B)** [4,8,17–19]. The change in GAG composition in the AF contributes to residual strains that are compressive in the inner AF and tensile in the AF.[20].

1.2 Clinical Significance

Chronic knee pain affects approximately 25% of adults in the United States.[21] Many of these cases have been linked to osteoarthritis, a disease characterized by degeneration of articular cartilage due to age or repeated loads.[22,23] In this diseased state, articular cartilage exhibits decreased GAG content, which impacts its ability to absorb water and dissipate energy from loading. This results in a stiff, thinner, brittle tissue, increasing contact stresses to the bone and causing severe knee pain.[13,23,24] A 2019 study that analyzed data from across the United States found increasing prevalence of age-specific arthritis with increasing age and weight, as well as more severe pain with decreasing physical activity.[25] These factors likely compound each other, as people with severe pain will have difficulty staying active and becoming overweight, which increases the load felt by their joints.[26]

Additionally, osteoarthritis may be exacerbated by damage to other knee components. It has been well documented that weakness or injury to the surrounding ligaments in the knee affects stability, increasing the load on the articular cartilage and initiating osteoarthritic symptoms.[27,28] The removal of menisci due to menisectomy (a common treatment for damaged menisci) accelerates the rate of osteoarthritis,[16] but even tears that do not require surgery can increase the likelihood of cartilage degeneration.[29]

Current clinical strategies

The avascular nature of knee tissues, specifically cartilage, makes it difficult for them to regenerate over time. Therefore, there is no current cure for osteoarthritis. In the early stages, medical professionals are most likely to recommend non-surgical treatment such as aerobic exercise and flexibility work to improve mobility and promote weight loss, as well as over the counter pain medication such as non-steroidal anti-inflammatory drugs.[30] If pain persists and the patient is unable to perform daily tasks, a physician may recommend surgical intervention based on a multitude of factors, including the stage of the disease, age, sex, and body composition.[25,31]

Surgical interventions may include arthroscopy, osteotomy, or a total knee arthoplasty (TKA). An arthroscopy would involve removing debris from damaged cartilage and bone around the knee, and maybe even shaving the surface of the articular cartilage to eliminate roughness and restore a sliding surface, while an osteotomy involves rearranging bone around the knee to redistribute loads more evenly in the joint.[31,32] Advanced degeneration may call for a TKA, where the tibio-femoral surfaces are replaced with metal and polymer components. TKA has long been considered the gold standard, with a proven track record of decreasing pain and improving mobility when compared to non-surgical procedures in the short term, as well as being able to delay surgical re-intervention for about 15 years.[31,33]

However, moduli mismatches between the stiff components (190 GPa for CoCr, 0.9 GPa for UHMWPE)[34,35] and the surrounding soft-tissue (0.5-2 MPa)[36–38] may cause a phenomenon known as stress-shielding, leading to bone loss and other long-term damage.[39,40] With increasing numbers of younger patients receiving TKA's, these long-term effects translate into reduced effectiveness of the procedure and more frequent revision surgeries, which are highly invasive and require removal of additional native tissues.[41–43] This has encouraged researchers and clinicians to go beyond traditional surgical procedures and explore biological strategies to replace or regenerate osteoarthritic cartilage.

1.3 Tissue Engineering

Tissue engineering describes the practice of repairing or replacing damaged tissues in the body. It is usually directed at avascular tissues that would not be able to heal themselves due to decreased drug flow, nutrient diffusion, or a normal immune response.

The term tissue engineering encompasses a host of different strategies to achieve this goal. Intra-articular repair therapies include injecting materials such as glucocorticoids or hyaluronic acid into the damaged tissue to promote regeneration, but the efficacy of these treatments has been brought into question.[44] More modern repair approaches are cell-based, including autologous implantation of chondrocytes (ACI) or mesochymal stromal cells (MSCs, more commonly referred to as stem cells).[44,45] ACI in particular has shown limited but very promising clinical results over the past five years, especially when implanted as large spheroids.[46–49] Recent studies documenting 2-year follow-ups of matrix-induced ACI patients have largely seen successful recovery of load-bearing movement given sufficient post-opertaive recovery time.[50,51] However, it is still limited by the need to cultivate large quantities of chondrocytes from the donor.[45] In cases when ACI has failed, some success has been found using cartilage allografts, but even commercially available devices see difficulties in cartilage-bone integration.[52,53]

A more commonly explored way for repair and replacement strategies has been that of scaffolding, which consists of introducing tissue-producing cells into a soft material to match native properties over time. Briefly, cells are isolated from a donor, expanded in 2D cell culture, then implanted into a 3D scaffold, commonly a gel or a fibrous polymer **(Figure 1-4).** The artificial "tissue" can then be implanted back into the donor, replacing damaged tissue and restoring mechanical function over time (Figure 2).[5] This approach aims to repair large osteoarthritic areas, and strives to restore mechanical functionality with biological integration into the surrounding tissues.

Thus, there is a need to develop functional tissue-engineered constructs from materials that will minimize adverse biological reaction while matching mechanical properties of non-degenerated native tissues. While fibrous polymers have been extensively used as 3D scaffolds, especially for tissues such as the intervertebral disc, here we will focus on hydrogel polymers and their applications in the literature.[54–58]

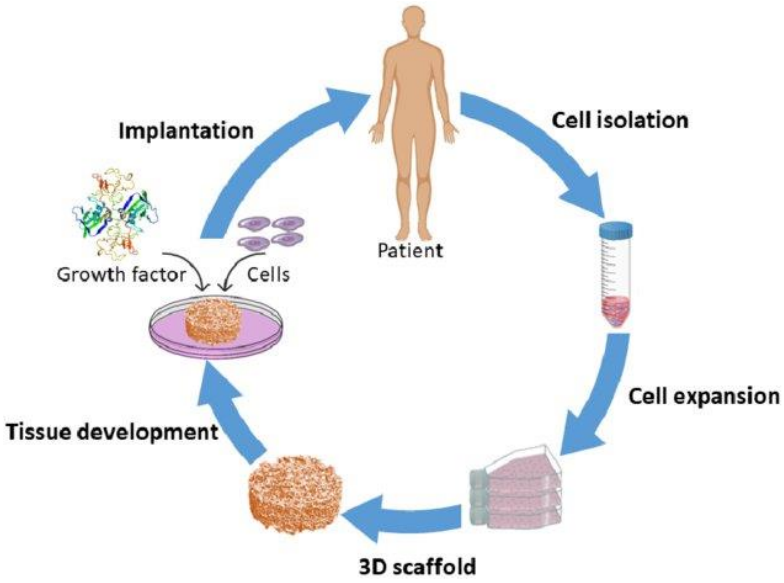

Figure 1-4*: Overview of scaffolding implantation technique. From Asadian et al, 2020*[5]

1.3.1 Hydrogels

Hydrogels are polymers chains that swell in the presence of water. Hydrogels have proven useful as 3D cell culture environments, as they maintain the morphology of certain cell types, including chondrocytes, preventing de-differentiation. Some common hydrogels for scaffolding are agarose, alginate, and reconstituted collagen gels.

1.3.1.1 Agarose

Agarose is a polysaccharide derived from seaweed. It is commercially available as a ground powder. When mixed with water, hydrogen bonds form a network structure that forms a gel. This gel has been extensively used to encapsulate cells due to its mild gelation [59]. It has been especially popular in cartilage tissue engineering as a gel scaffold due to its ability to maintain rounded chondrocyte morphology for long periods of time[60] which in turn leads to near-near native production of GAG within the gel [61–63]. Agarose constructs also regularly exhibit stress relaxation behavior under compression which is similar to that seen in cartilage under similar loading conditions [61,62]. It is usually used in low weight over volume compositions (1-5% w/v) to prevent issues with nutrient diffusion to the embedded cells.[61,64] Since low weight over volume agarose has relatively weak compressive properties (~30kPa linear modulus), this makes the production of native levels of GAG within the scaffold necessary to replicate native cartilage compressive properties.[65–67]

1.3.1.2 Alginate

In addition to being able to form soft hydrogels to promote extra-cellular matrix growth, alginate gels have been particularly useful because of their ability to be crosslinked through ions.[68,69] When exposing a sodium alginate solution to calcium, connections between polymer chains are formed, leading to gelation. Since this can be controlled with calcium concentrations, the simple mechanism gives researchers control over the gelation process and ease of manufacturing gel scaffolds.[68] However, this crosslinking may affect long-term cell-proliferation, limiting the

potential of alginate by itself as a 3D culture medium.[70] This has led researchers to use alginate as a matrix filler in combination with other hydrogels for tissue engineering applications.[63,71,72]

1.3.1.3 Collagen gels

Collagen type I and type II gels may serve as stand-alone scaffold. Since collagen is a structural protein, collagen gels tend to have high bioactivity and thus embedded cells exhibit high attachment and extra-cellular matrix production.[73,74] However, collagen gels by themselves tend to be weaker in shear and compression than other hydrogels.

A common practice is to blend hydrogels to combine their most useful characteristics. For example, agarose-collagen blends have been used to increase cell activity and attachment within stiffer agarose gels[75,76], while agarose-alginate blends alter the shear properties of the gel and allow for manufacturing techniques such as extrusion 3D printing via direct deposition on a surface or a sacrificial slurry.[77,78] These practices have made them popular as structural components in tissue engineering applications, from scaffolding to injectable cell therapies.[79–82]

1.4 Dissertation Objectives and Overview

Given the clinical shift towards more biologically complex tissue repair strategies, this dissertation will focus on the characterization and optimization of hydrogels used for tissue engineering scaffolding strategies. We will describe various mechanical characterizations of agarose-based hydrogels, ranging from flow rheometry to bulk mechanical testing. The studies presented here make an effort to relate mechanical behavior to composition, highlighting the importance of understanding the structure-function relationships present in native tissues and the materials we used to recapitulate native tissue.

Chapter 2 looked at potential of agarose-based hydrogels to be manufactured through 3D printing strategies, aiming towards patient-specific scaffolds and structural complexity. The study presented here focuses on the mechanical properties needed for manufacturing scaffolds while adhering to the constraints presented by the presence of biological material.

Chapter 3 encompasses a series of studies building on the results presented in Chapter 2. Given the success of a 5% agarose-alginate blend as a suitable scaffold material, we investigated ways to improve initial mechanical properties through crosslinking, and moreover investigated the influence of construct dimensions on viscoelastic properties.

Chapter 4 is a short pilot study on biochemical assay methods used to estimate collagen in tissue engineering samples. Briefly, the study evaluated conversion factors used in the literature to convert ortho-hydroxiproline content into collagen content and tried to replicate past studies using pure collagen gels with known collagen content.

Chapter 5 further explores acellular agarose-alginate blends, showing the effect of adding collagen to their printability and evaluating interfaces created between agarose-alginate-collagen gels. We also included the influence of rat-tail collagen on compressive properties of these hydrogels to gain insight into creating gradients of composition in hydrogel scaffolds.

Chapter 6 isolates the influence of bovine collagen type I on the tissue engineering potential of agarose hydrogels. Here we looked at the immediate effects of collagen on gel mechanics, as well as relationships between compressive mechanics and extra-cellular matrix production on agarose-collagen blends.

Chapter 7 investigates the role of structure in the localized mechanical properties of native meniscus tissue. The study presented aimed to validate a localized indentation method for soft materials to broaden the scope of mechanical characterization used in tissues and tissue-engineered constructs with compositional and structural gradients as opposed to the commonly reported bulk properties.

Finally, we look at what's next for hydrogel scaffolds, including scaffolds with inherent interfaces and composition gradients. Chapter 8 exhibits what is being done in the tissue engineering field and how researchers are manufacturing, characterizing, and improving hydrogels towards functional, tissue engineered constructs that might one day be used clinically.

Chapter 2: Agarose-based hydrogels as suitable bioprinting materials for tissue engineering

Gabriel R. López-Marcial, Anne Y. Zeng, Carlos Osuna, Joseph Dennis
Jeannette M. García, Grace D. O'Connell

This work was submitted as a Journal article to the ACS Biomaterials Science & Engineering.

2.1 Abstract

Hydrogels are useful materials as scaffolds for tissue engineering applications. Using hydrogels with additive manufacturing techniques has typically required the addition of techniques such as crosslinking or printing in sacrificial materials that negatively impact tissue growth to remedy inconsistencies in print fidelity. Thus, there is a need for bioinks that can directly print cell-laden constructs. In this study, agarose-based hydrogels commonly used for cartilage tissue engineering were compared to Pluronic, a hydrogel with established printing capabilities. Moreover, new material mixtures were developed for bioprinting by combining alginate and agarose. We compared mechanical and rheological properties, including yield stress, storage modulus, and shear thinning, as well as construct shape fidelity to assess their potential as a bioink for cell-based tissue engineering. The rheological properties and printability of agarose-alginate gels were statistically similar to those of Pluronic for all tests ($p > 0.05$). Alginate-agarose composites prepared with 5% w/v (3:2 agarose to alginate ratio) demonstrated excellent cell viability over a 28-day culture period (>~70% cell survival at day 28), as well matrix production over the same period. Therefore, agarose-alginate mixtures showed the greatest potential as an effective bioink for additive manufacturing of biological materials for cartilage tissue engineering.

2.2 Introduction

Osteoarthritis of articular cartilage leads to chronic pain and reduced joint mobility[22]. The gold-standard treatment strategy for osteoarthritis is total-joint arthroplasty, where the native cartilage and some of the underlying boney tissue are removed and replaced with metal and polymer components. While successful in reducing joint pain, the mismatch in material stiffness between native tissues (0.5-1.0 MPa for cartilage[36,38]) and implanted materials (0.9 GPa for ultra-high molecular weight polyethylene[35]) causes long-term problems, including increased degradation of the surrounding healthy tissue[83]. Alternatively, tissue-engineering strategies aim to recapitulate the function of healthy cartilage in the laboratory to develop implantable biomaterials for cartilage repair and replacement.

Hydrogels have become common scaffolds for cartilage tissue engineering, because of their ability to promote production of extra cellular matrix components in three-dimensional (3D) culture[84,85]. Popular hydrogels for matrix production include sodium alginate and agarose. Agarose has been particularly successful in cultivating engineered cartilage constructs with biochemical and mechanical properties comparable to native values within eight weeks of culture[65,86,87]. Hydrogel selection is largely based on biocompatibility, nanoporosity, support for matrix deposition, and material behavior under specific temperature ranges or loading conditions (*e.g.*, static *vs*. dynamic loading)[88].

Casting is the preferred fabrication method for thermoset hydrogels, with individual constructs being created with diameters that are typically less than 10 mm[66,85,89,90]. Implanting standard casted constructs will require surface shaping to match the patient's native curvature. However, matrix deposition does not occur evenly throughout the construct, with the construct periphery receiving more nutrients, resulting in greater matrix deposition[66]. Therefore, resurfacing an engineered construct during implantation will weakening the implanted material, altering stress distributions between engineered and native tissues, which may affect long-term durability. Recent studies have shown that clinical images (*i.e.*, magnetic resonance images or computed tomography) can be used to develop molds for larger engineered cartilage surfaces with subject-specific topography[36,87,91]. However, cultivating larger constructs is difficult, due to the increase in nutrient path-length between nutrients surrounding the construct and cells at the center of the construct, hindering matrix production and affecting long-term cell viability[64,87,92].

Extrusion-based 3D printing represents an attractive alternative to casting because of the increased versatility in construct design and ability to incorporate macropores throughout the scaffold design[84,93]. However, 3D printing of hydrogels with high shape fidelity has been difficult due to issues during extrusion and material spreading after being dispensed from the nozzle. Useful materials for extrusion-based printing must demonstrate shear thinning behavior (*i.e.*, non-Newtonian behavior), where viscoelastic properties are shear-rate dependent. That is, these materials must stop flowing once deposited onto the print platform to minimize spreading and maintain shape fidelity[89].

Recent work by Mouser *et al.* demonstrated that yield strength was an important material property for determining printability, where materials with higher yield strength had better shape fidelity[94–96]. Thermoset hydrogels are ideal for this purpose, as material properties are tunable based on the concentration of solids in the mixture. Previous studies have also printed hydrogels into a cooling cryogenic liquid (cryoprinting) or into an ion bath to induce crosslinking and improve print fidelity[72,97–99]. However, increasing the solid composition and crosslinking affects nanoporosity, which will alter nutrient diffusion and tissue growth[67,100,101]. Furthermore, cryoprinting may negatively impact long-term cell viability, if temperature gradients are not carefully controlled throughout the construct[97]. Therefore, there is a need to develop bioinks that are able to maintain high shape fidelity with extrusion-based printing, without compromising their ability to support *de novo* matrix growth.

The objective of this study was to identify a suitable non-crosslinked hydrogel for bioprinting. Specifically, we investigated mechanical properties of various concentrations and combinations of biocompatible polymers, including agarose (Type VII) and sodium alginate, which were compared to Pluronic F-127, a gel with known printing capabilities[89] (**Figure 2-1**). Agarose and sodium alginate have been used extensively for cartilage engineering, because of their ability to promote cell proliferation and matrix production[68,72,102–106]. Pluronic was used as a control material for 3D printing; however, it is not considered an ideal bioink for scaffold formation, due to issues with stability in aqueous solutions, and is commonly used for sacrificial support[89,90,107–109]. Gels that printed well were tested for long-term cell viability with chondrocytes for cartilage tissue engineering applications.

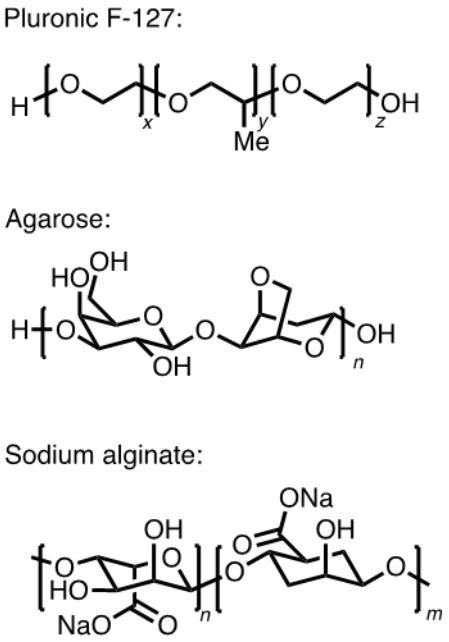

Figure 2-1: *Molecular structure of evaluated materials (Pluronic, agarose, and sodium alginate).*

2.3 Materials and Methods

2.3.1 Hydrogel Preparation

Agarose hydrogels were prepared by mixing agarose in 0.15 M phosphate buffered saline (PBS) for final concentrations of 2%, 3%, or 4% weight by volume (w/v; Type VII powder, Sigma Aldrich, St. Louis, MO). Alginate-agarose hydrogels were prepared by mixing a 3:2 ratio of agarose and sodium alginate in 0.15 M PBS (total solid content = 3.75% or 5% w/v). All agarose-based hydrogels were mixed and sterilized in a bench-top autoclave (120 °C for 25 minutes). Pluronic® F-127 hydrogels were prepared at a final concentration of 30% w/v in 0.15 M PBS and mixed in an ice bath until a homogeneous clear liquid formed. All solutions gelled within 10 minutes at room temperature.

2.3.2 Rheology and Mechanical Testing

Four experiments were performed to evaluate temperature-dependent and strain rate-dependent mechanical properties (Anton Paar MCR302 rheometer, Ashland, VA). Samples (~0.35 g; n = 5 per group) were loaded onto the Peltier plate and a steel plate was lowered to compress the gel sample (conical plate diameter = 25 mm; trimming gap = 64 μm; final gap = 54 μm). Agarose-based gels were re-melted by increasing the temperature of the Peltier plate to 65 °C, then allowed to gel at room temperature before each test.

In the first experiment, the temperature of the Peltier plate was increased at a rate of 5 °C/min from 25-70°C under a constant oscillatory stress (1 Pa at 1 Hz). A smoothing function was used to reduce noise (averaging every 5 points). Storage modulus, loss modulus, and phase angle were recorded. In the second experiment, shear rate was increased from 0.01 to 10.00 s^{-1} and viscosity was measured (temperature = 37 °C). Shear thinning gels were defined as those that followed a power law relationship ($y = \alpha e^{\beta}$); therefore, exhibiting a linear decrease in viscosity with temperature when plotted on logarithmic scale. A power law relationship for non-Newtonian fluids was used to calculate shear rate at the extruder wall (Equation 1)[110]. In Equation 1, *R* and *L*

are the radius and length of the extruder needle, respectively, γ_w is the shear rate at the extruder wall, and ΔP is the pressure difference between the extruder and the atmosphere. Parameters α and β are determined by curve-fitting experimental data to Equation 1.

$$\gamma_w = \left(\frac{R\Delta P}{2\alpha L}\right)^{\frac{1}{\beta+1}} \quad (1)$$

The third experiment consisted of applying the calculated shear rate at the extruder wall (γ_w) for 1000 s at 37°C. The shear yield point was defined as the maximum shear stress measured. The fourth experiment consisted of three steps. First, a constant oscillation was applied at 1 Hz for 100 s. Then, γ_w was applied for 800 s to induce yield, followed by a constant oscillation (1 Hz, 30 minutes, at 37 °C). Storage (G') and loss (G") moduli were measured. The recovery time was defined as the time needed for the storage modulus to be greater than the loss modulus during the second oscillation.

Compressive modulus was determined under unconfined compression. Gels were cast into slabs (thickness = 2.27 mm), and a 6 mm biopsy punch was used to create cylindrical samples. A monotonic ramp test was applied to 90% strain at a rate of 0.3 %/s (n = 10 samples per group; Instron A620-325, Norwood, MA). The compressive yield strength was defined as the stress at the end of the linear portion of the stress-strain curve (**Figure 2-2**).

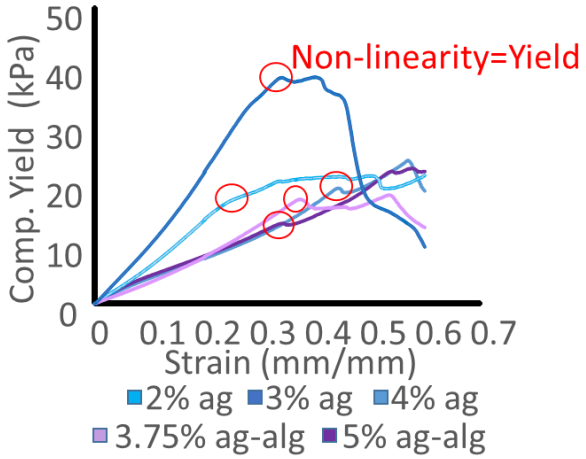

Figure 2-2: *Representative stress-strain curve for unconfined compressive testing. The point of non-linearity (red circles) was defined as the yield point.*

2.3.3 Acellular and Cell-Based Printing

To evaluate print fidelity, a commercially available 3D printer was used to print simple lines or honeycomb structures (BioBots, Philadelphia, PA). Two-dimensional geometries were created using computer-aided design (CAD; AutoCad 2016, Autodesk, San Francisco, CA), which were converted to 3D stereolithography files (STL, 360 Fusion by Autodesk). STL files were then converted into g-code for printing (Repetier software, Willich, Germany). Hydrogels were loaded into a 10 mL syringe and placed into a heated canister to maintain 37 °C during printing. Gels were extruded through a 30-gauge needle by applying 65-75 psi of pressure with an air compressor.

To quantify shape fidelity, a custom written algorithm was developed that overlaid CAD models with pictures of printed constructs. Outputs from the software included the amount of (a) overlap between pixels from the printed gel and the CAD model, (b) gel pixels outside of the model area, and (c) model pixels not covered by the gel (n > 8; MATLAB, Mathworks, Natick, MA). A printing parameter, p, was defined as the percentage of correctly placed pixels (overlapping) minus

the percentage of incorrectly placed pixels (overhanging or uncovered model; $p = \frac{overlapping}{model} - \frac{uncovered}{model} - \frac{overhanging}{gel}$*100; **Figure 2-3**).

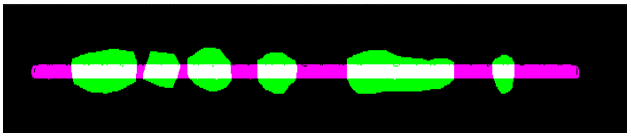

Figure 2-3: Example output of overlaid images from MATLAB code. The code separates gel and model pixels into one of three groups: gel pixels that do not overlap with the model (green), model pixels that are not covered by the printed gel (magenta), and overlapping pixels (white).

Based on results from acellular prints, agarose-alginate mixtures appeared to be the most promising gel formulation for maintaining print integrity; therefore, only agarose-alginate gels were used to evaluate cell viability after printing. Chondrocytes were acquired from juvenile bovine stifle joints within 24 hours of death. Articular cartilage was digested overnight with Type 4 collagenase (Worthington, Lakewood, NJ). 20 M cells/mL were encapsulated within agarose-alginate hydrogels for a final concentration of 3.75% (2.25% agarose + 1.5% alginate) and 5% w/v (3% w/v agarose + 2% w/v alginate) before printing. Constructs were printed as single lines (print width = 0.5 mm, length = 30 mm), cultured for 28 days with chemically-defined media[85,87]. TGFβ-3 10 ng/ml) and vitamin C (1 μg/mL) were added fresh with each media change.

Samples were stained and imaged weekly to assess cell viability (n > 5 per group; Live/Dead kit, Life Technologies, Carlsbad, CA). Images were collected as a z-stack (Swept Field Confocal microscope, Praire Technologies; 10X objective), and a custom written MATLAB algorithm was used to count the number of living (green channel) and dead (red channel) cells. The percentage of living cells was calculated as the number of living cells divided by the total number of cells.

2.3.4 Biochemical assay

On days 7, 21, and 28 samples were collected to measure glycosaminoglycan (GAG) composition (n > 7 per group). Specimens were lyophilized (Labconco, Kansas City, MO) for 48 hours to determine dry weight and digested overnight at 56°C with Protenaise K (MP Biomedical, Burlingame, CA). GAG content was determined using the colorimetric dimethyl methylene blue (DMMB) assay and normalized by wet weight. Data was further normalized to the average GAG content at day 7 to assess tissue growth over time.

2.3.5 Statistics

A one-way analysis of covariance (ANOVA) was performed on the print fidelity parameter, mechanical properties, and cell viability. Significance was assumed at $p < 0.05$. When significance was found, a Bonferroni post-hoc test was performed to compare each agarose or alginate-agarose mixture with the control (Pluronic), where possible.

2.4 Results

Storage modulus changed slightly with temperature (**Figure 2-4A**). At 37°C, the storage modulus of 2% agarose was significantly lower than Pluronic, while there was no significant

difference between Pluronic and the other agarose-based gels (**Figure 2-4B**). The shear yield strength for 3% agarose was significantly greater than Pluronic (**Figure 2-4C**). There were no other significant differences in yield strength in shear, which may be partly due to high variation in agarose-only gels (3 and 4% agarose). Relaxation experiments showed that recovery after yielding in shear was instantaneous for all gels (**Figure 2-5**). Unconfined compression could not be performed on Pluronic because the hydrogel was too soft to test. Agarose gels with 3% w/v and 4% w/v had similar compressive yield strengths, which was greater than 2% w/v agarose and the agarose-alginate mixtures ($p < 0.001$; **Figure 2-4D**).

All gels exhibited shear-thinning behavior, with a logarithmically linear decrease in viscosity at higher shear rates (**Figure 2-6A**). The magnitude of the slope (β) was lowest for Pluronic and increased with solid concentration in agarose-only gels, but not for agarose-alginate mixtures (**Table 2-1**). The gel made of 2% agarose had the lowest shear rate at the extruder wall (**Figure 2-6C**) and the highest viscosity at the extruder wall (**Figure 2-6C**). The shear rate and viscosity for all other gels were statistically similar to Pluronic.

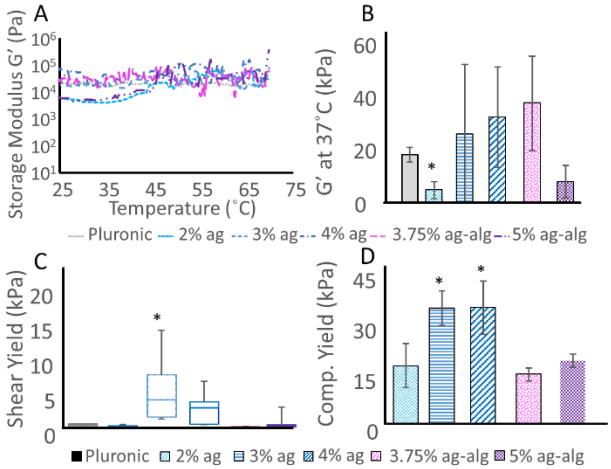

Figure 2-4: *A) Storage Modulus with respect to temperature, B) Storage modulus values at 37°C and C) Shear yield strength for all gels. *represents significant difference ($p < 0.05$) when compared to Pluronic. D) Compressive yield strength for agarose-based gels. *represents significant difference ($p < 0.05$) to other groups.*

Gel	R^2	α	β
Pluronic	0.97	1486 ± 203	-0.80 ± 0.06
2% agarose	0.87*	428 ± 518*	-1.06 ± 0.06
3% agarose	0.90	596 ± 371*	-1.48 ± 0.06*
4% agarose	0.94	367 ± 318*	-1.67* ± 0.30*
3.75% agarose-alginate	0.78*	1641 ± 605	-1.11 ± 0.10
5% agarose-alginate	0.80*	1898 ± 500	-1.11 ± 0.17

Table 2-1: Power fit parameters for viscosity versus shear rate. * represents $p < 0.05$ when compared to Pluronic.

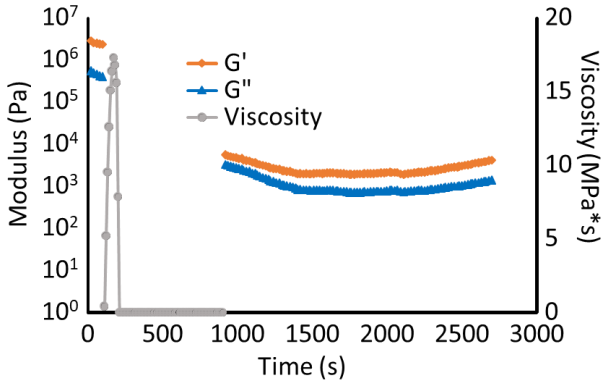

Figure 2-5: *Representative curve for recovery after shear experiments. All samples had a storage modulus that was greater than the loss modulus after shear was removed (orange and blue lines).*

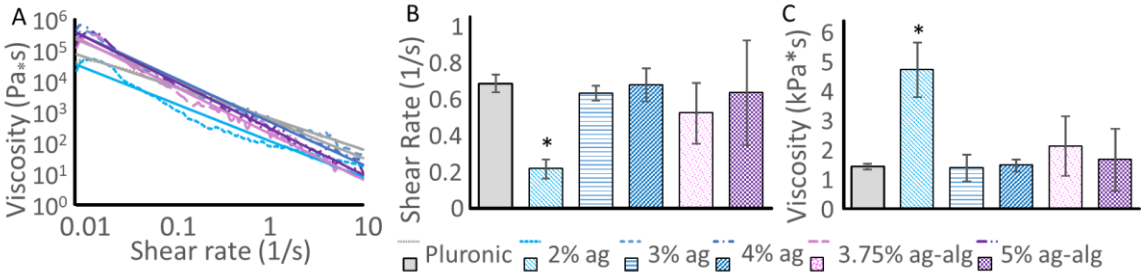

Figure 2-6: *Mechanics: A) Viscosity versus shear rate, B) shear rate at the extruder wall, and C) viscosity at the extruder wall. * represents p < 0.05 when compared to Pluronic.*

Most gels showed limited shape fidelity, meaning that the construct was not similar to the initial model (**Figure 2-7A-F**). Smooth printed lines were achieved with Pluronic, as expected (**Figure 2-7A**). However, printability of agarose-based gels varied significantly depending on the agarose concentration and whether it was mixed with alginate (**Figure 2-7B-F**). 2% w/v agarose and 3.75% w/v agarose-alginate gels tended to spread beyond the specified print area (**Figure 2-7B & 2-7E**), while 3% w/v and 4% w/v agarose were too tough to extrude continuously (**Figure 2-7C & 2-7D**). The calculated print parameter for 3% and 4% agarose was significantly lower than Pluronic ($p < 0.001$; **Figure 2-8**). Based on the results from printed lines, honeycomb printing was only performed with Pluronic and agarose-alginate mixtures (**Figure 2-7G-H**).

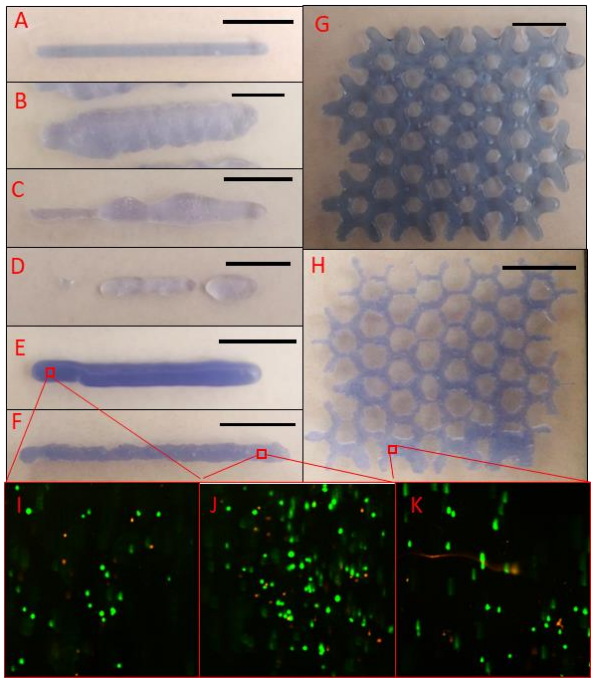

Figure 2-7: *3D printed lines with A) Pluronic, agarose only gels at concentrations of B) 2%, C) 3%, and D) 4% w/v. Agarose-alginate mixtures were printed with final solid concentrations of E) 3.75% and F) 5% w/v. Honeycombs printed with G) Pluronic and H) 5% agarose-alginate. Cell viability at Day 0 of lines printed with I) 3.75% agarose-alginate and J) 5% agarose-alginate. K) Cell viability of a honeycomb printed with 5% agarose-alginate (Day 0). Scale bars = 10 mm.*

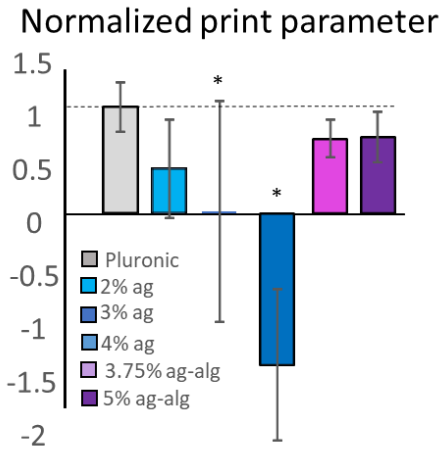

Figure 2-8: *Printing parameter results. Groups with an asterisks (*) were significantly different from Pluronic ($p < 0.001$).*

High cell viability of agarose-alginate gels fabricated through 3D printing or more established casting techniques was maintained over the culture period (**Figure 2-7I-K, Figure 2-9A**). At day 28, there was a ~20% decrease in cell viability in casted constructs (day 0 = 97.4 ± 0.3%, day 28 = 80.3 ± 14.8%) and a 25% decrease in cell viability for printed constructs (day 0 = 93.3 ± 4.3%, day 28 = 69.6 ± 13.1%; **Figure 2-9A**). GAG content for casted and printed constructs

increased with culture time (**Figure 2-9B**). At day 28, the GAG content in printed constructs was 3X greater than casted constructs at Day 7 ($p < 0.001$; **Figure 2-9B**).

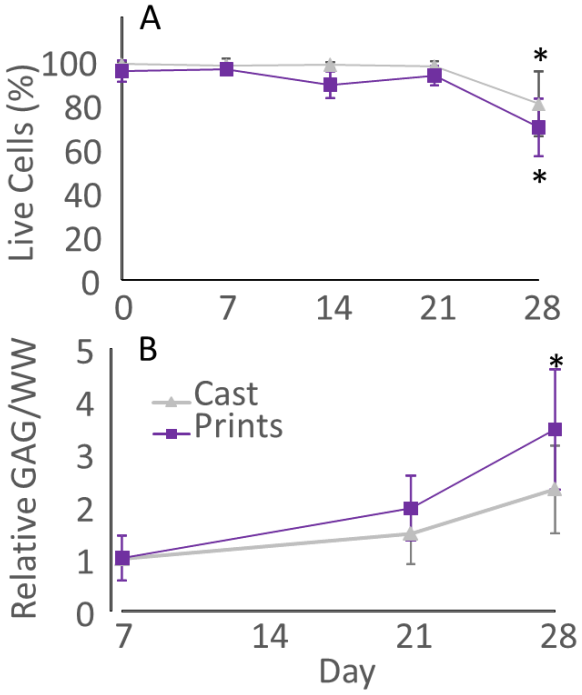

Figure 2-9: *A) Cell viability for 5% agarose-alginate (ag-alg) scaffolds. No differences were observed in cell viability between 3D printed lines and casted constructs ($p > 0.2$), except at Day 28. B) Glycosaminoglycan (GAG) content by wet weight (WW) normalized to the average GAG content at Day 7. Error bars represent standard deviations. * represents $p < 0.05$ between groups.*

2.5 Discussion

We evaluated whether hydrogels, that have been successful in developing *de novo* cartilage, have ideal properties as unmodified bioinks for extrusion-based 3D printing. Rheological properties and printability of five agarose-based gels were analyzed and compared to Pluronic, a gel with known printing capabilities[89]. Agarose mixed with alginate demonstrated similar shear-thinning properties and yield strength to Pluronic. Moreover, agarose-alginate mixtures showed improved print-shape fidelity when compared to agarose-only gels. 3D printed agarose-alginate constructs demonstrated excellent cell viability for up to 21 days in culture, as well as improved GAG production. Based on print integrity and cell viability results, 5% agarose-alginate mixture was determined to be a suitable material for 3D bioprinting for cartilage tissue engineering.

Many variables affect print integrity, including print pressure, gel temperature, and gel mechanics. Previous studies highlighted the importance of extrudable materials exhibiting shear-thinning properties with low yield strength[89,94,96,111,112]. In this study, all agarose-based gels exhibited shear-thinning properties that were similar to Pluronic (**Figure 2-6B; Table 2-1**), but only agarose-alginate mixtures had yield strengths similar to Pluronic (**Figure 2-4B&C**). Previous literature has reported that printability is generally improved with higher shear yield strengths up to a certain limit, which has varied depending on the gel used[94,96]. Our results were consistent with Smith et al, suggesting that gels with a shear yield strength greater than 5kPa had limited success during printing (*e.g.*, 3% & 4% agarose). Based on material properties from rheology experiments,

2% agarose, 3.75% agarose-alginate, and 5% agarose were favorable materials for continuous extrusion and, therefore, are printable materials.

However, it is important to note that extrusion does not necessarily equate to high print fidelity, which is difficult to quantify. Kopf *et al.* printed an agarose-collagen blend around a circle and defined shape fidelity as the percentage of the circle that remained uncovered[77]. Gels that had less spreading around the circle were defined as being a better print. In a similar vein, we developed a printing parameter that accounted for overspreading and the total coverage of the initial model. Parameter results normalized to the control (Pluronic) and showed that 2% agarose, 3.75% agarose-alginate, and 5% agarose-alginate had statistically similar shape fidelity (**Figure 2-6**). However, upon visual inspection it was apparent that 2% agarose and 3.75% agarose-alginate showed significant spreading outside of the model area (**Figure 2-7B & 2-7E**). The difference between visual inspection and the print parameter results suggest that a threshold value may be more appropriate than a direct comparison with Pluronic.

Previous studies have suggested that bioink print fidelity was improved for gels with a storage modulus between 150 and 380 Pa using gelatin and alginate hybrids[112]. While all gels evaluated here had a higher storage modulus than the gels examined by Zhao *et al.*, there may exist a similar range for agarose-based gels[112]. However, it should be noted that 2% agarose had the lowest storage modulus (4796 ± 3250 Pa), while 3.75% agarose-alginate had the highest storage modulus (37820 ± 17927 Pa; **Figure 2-4A**). This finding suggests that storage modulus is not a material property that is predictive of printability or print fidelity.

The 5% agarose-alginate mix demonstrated the best print fidelity, based on visual inspection and the print parameter. Materials are often combined to influence rheological properties of hydrogels for extrusion. However, these combinations commonly require additional manufacturing steps to improve print integrity, such as crosslinking or printing within a sacrificial material[78,86,113–116]. These methods can negatively affect cell viability and, consequently, matrix production, which is vital to cartilage tissue engineering applications[70,117]. In this study, the agarose-alginate combination did not require additional crosslinking or photopolymerization and improved print integrity (print parameter). Moreover, the agarose-alginate mixture maintained excellent cell viability after printing (>95%; **Figure 2-9A**), suggesting that the shear stresses at the nozzle were not high enough to induce cell death, a major concern in bioprinting[72,111]. Lastly, the 5% agarose-alginate gels demonstrated continuous matrix production throughout the culture period. GAG deposition rates of the 5% agarose-alginate mixture was comparable to previous studies that used gels with a lower solid content, suggesting that the increased solid volume in the mixture did not significantly hinder matrix production[65,87]. Thus, the findings from this study suggest that 5% agarose-alginate mixture was a suitable bioink for cartilage engineering applications.

The work presented here is not without limitations. Rheological properties for all gels were evaluated at physiological temperature (37°C) instead of a wider range to match the temperature during cell-based printing. Given that agarose is a thermoset material, it remains plausible that agarose-only gels can produce constructs with high shape fidelity under different temperature conditions. While we believe the shape parameter presented here was useful in identifying suitable printability, it only assessed in-plane print fidelity, and did not account for changes that might occur with multi-layered prints. The incorporation of more advanced imaging techniques will be useful in determining how well gels perform during printing of larger, complex, clinically relevant structures[95,118]. The primary focus of cell-based tests in this study was to evaluate cell viability;

therefore, overall GAG production in future work will be improved by increasing cell density (i.e., greater than $20x10^6$ cells/mL)[65,66,87,119].

2.6 Conclusions

In conclusion, the 5% w/v agarose-alginate mixture was ideal for extrusion-based bioprinting of 3D cartilage constructs. The mixture was able to print high shape fidelity structures comparable to Pluronic, a material known to be ideal for extrusion-based printing, maintained excellent cell viability, and supported matrix production. Moreover, the agarose-alginate mixture did not require additional crosslinking steps or a sacrificial material for the printing process[78,113,120,121], which are techniques that may affect long-term performance[70,117]. Therefore, extrusion-based printing with an agarose-alginate mixture may provide researchers with an easy-to-manufacture technique for developing complex engineered cartilaginous tissues.

2.7 Acknowledgements

This material is based upon work supported by the National Science Foundation Graduate Research Fellowship Program under Grant No. (DGE 1106400) and the National Academy of Engineers (Grainger Foundation). Any opinions, findings, and conclusions or recommendations expressed in this material are those of the authors and do not necessarily reflect the views of the National Science Foundation. We would like to also thank Dr. Kevin Healy (UC Berkeley) for allowing use of his rheometer for this study.

Chapter 3: Stress-relaxation studies on 5% agarose-alginate gel

Gabriel R. López Marcial, Christian Leycam, Grace D. O'Connell

3.1 Introduction

Hydrogels are a commonly used type of scaffold material. These are generally 3D polymer networks made from natural materials such as seaweed or ground protein. Agarose hydrogels have been particularly popular in tissue engineering applications because of their ability to maintain the rounded chondrocyte-like phenotype, which encourages GAG production in 3D culture.[122] Sodium alginate has also been used in tissue engineering applications because of its simple ionic crosslinking mechanism, which allows researchers control over the gels mechanical properties.[68] . Sodium alginate is commonly crosslinked ionically with calcium, which creates a networked structure and gives the gel mechanical stability. When sodium alginate is exposed to a calcium bath, the Ca^{+} ion replaces the Na^{+} ion in the polymer chain, creating a branched and crosslinked structure with stiffer mechanical properties (**Figure 3-1)**.

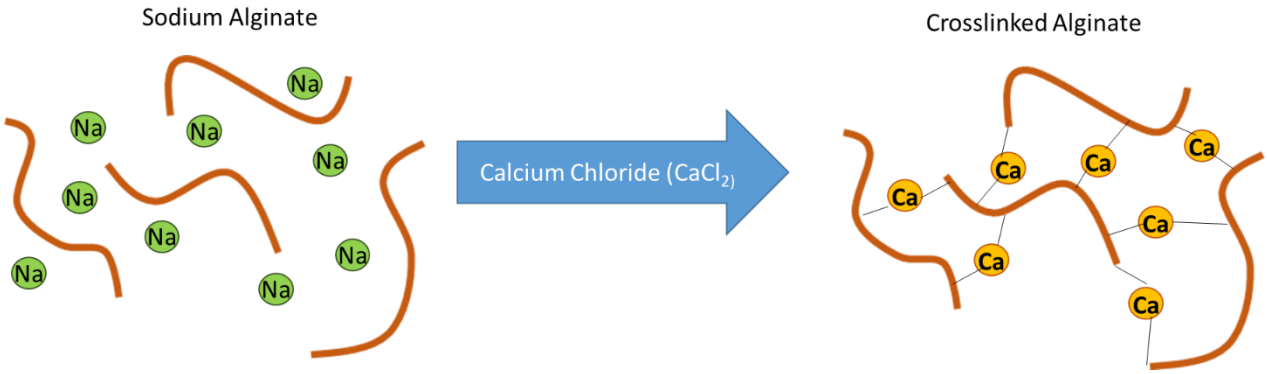

Figure 3-1: *Ionic crosslinking of sodium alginate creates branched structure. Calcium replaces sodium ions and forms two bonds with the negatively charged alginate polysaccharides. Adapted from https://scienceandfooducla.wordpress.com/2013/06/11/deconstructed-apple-pie/*

Chapter 3 demonstrated an agarose-alginate gel with suitable characteristics for cartilage tissue engineering applications.[63] The agarose-alginate combination exhibited comparable mechanical properties to other common agarose hydrogels, as well as the ability to maintain cell viability and encourage matrix production for multiple weeks. However, mechanical characterization of the gel was limited to the context of manufacturability, and is not necessarily representative of the long-term compressive loading scenarios used to evaluate tissue engineered scaffolds.[61,65] While the initially weak mechanical properties of hydrogels may prove beneficial to matrix production, it means that long culture periods are necessary before the material may be functional for implantation Being able to change mechanical properties by selective methods such as cross-linking may also allow for ease of manufacturing biomimetic scaffolds with gradient properties to better match tissue structures.[4,67,123]

Thus, it will be useful to apply common stress-relaxation analysis to the 5% agarose-alginate gels.

While compressive stress-relaxation is popular amongst tissue-engineering researchers, there are no standardized methods for testing native tissue or engineered constructs. Methods can vary in a

many different ways: researchers have reported mechanical properties from confined[124–126] or unconfined compression,[37,61,63] loading rates defined by displacement[127] or strain,[6,37,128] and single[124] or multiple[128,129] strain holds. Additionally, it is common to see wide ranges in peak displacements (from 10-40% strain)[127–129] and length of strain holds (300-7200 s).[37,124,130] Perhaps more concerning is the lack of a standard size for engineering specimens. While ASTM (American Society of Testing Materials) standards for most common engineering materials like metals, ceramics, and ubiquitous polymers include specimen dimensions, even cylindrical tissue-engineering constructs may range from 3-10 mm in diameter and height.[61,127,129,131] While stress and strain aim to represent material properties by normalizing for geometric variables such as length and area, materials with high porosity and water content have previously been reported to demonstrate size-dependence.[132] More recently, geometry measurement techniques in native tissues have been found to contribute to large discrepancies in mechanical properties.[133] Therefore there is a need to investigate if any variation might arise from changes in dimensions under common loading conditions.

Native and engineered tissues typically exhibit time-dependent stresses and strains, known as viscoelastic behavior. A relatively simple way to derive relationships between stress and time has been to represent viscoelastic materials as a combination of springs (purely elastic behavior) and dashpots (viscous behavior) in series or parallel with each other.[134,135] Experimental data can then be curve-fit into equations stemming from spring-dashpot combinations to obtain parameters such as modulus (for the spring component) or viscosity (for the dashpot component). More complicated arrangements of springs and dashpots may improve the data curve-fit, but ultimately create parameters with increasingly limited physical meaning (i.e., the modulus from one spring does not represent the modulus from the material). However, these rheological models can give important information on the behavior of tissues, such as relaxation times and magnitudes, and have been successfully used to describe creep behavior of the intervertebral disc,[136,137] as well as stress-relaxation behavior of cartilage and agarose gels.[130,138]

This chapter will show a series of characterization studies on 5% agarose-alginate. An unconfined compression test with a single stress hold was chosen, as it is one of the most common methods in the literature.[61,65] First, we will determine the effects of inducing ionic crosslinks into the agarose-alginate gel on time-dependent mechanics. Then, we will investigate size as a source of variation in mechanical properties.

3.2 Methods

3.2.1 Sample preparation

Type VII agarose and sodium alginate were mixed into 0.15M Phosphate Buffered Saline (1X PBS) in a 3:2 ratio to produce a 5% weight over volume (w/v – g/mL) agarose-alginate gels, as described previously.[63] The mixture was heated to 121 °C in an autoclave and casted between glass slides, then allowed to cool to room temperature for at least 20 minutes. For the crosslinking study, a 2.3mm spacer was used between glass slides and cylindrical samples were obtained using a 6 mm diameter biopsy punch to obtain samples with dimensions of 2.3 mm in height and 6 mm in diameter. Samples for the crosslink group (**Xlink**) were then submerged in a 30 mM $CaCl_2$ solution for 3 hours, then allowed to re-hydrate in PBS for 20 minutes before testing. The 5% agarose-alginate samples without crosslinks (**Control**) were only submerged in PBS prior to testing.

For the size dependence study two different heights were obtained by using a 2.3 mm (**Short** height) spacer or two 2.3 mm spacers (4.6 mm, **Tall** height) between glass slides during casting. Two different biopsy punches were used to obtain diameters of 4 mm and 6 mm. Full dimensions for each testing group in each of the two studies can be found in **Table 3-1**.

Study	Group	Diameter (mm)	Height (mm)
Crosslinking	Control	6	2.3
	Xlink	6	2.3
Size-dependence	Short	4	2.3
		6	2.3
	Tall	4	4.6
		6	4.6

Table 3-1: *Construct dimensions for stress relaxation studies.*

3.2.2 Mechanical testing

Samples were subjected to stress relaxation under unconfined compression using an Instron mechanical tester (Model A620-325; Norwood, MA), with samples submerged in 1X PBS. A monotonic ramp to 10% strain was applied, followed by a 30-minute hold for the crosslinking study, and a 60-minute hold for the size-dependence study. Young's modulus was calculated as the slope of the linear portion of the loading curve during the ramp to 10% strain, while 30-minute and 60-minute moduli were defined as the average stress of the 50 data-points closest to the 30-minute and 60-minute time-points (**Figure 3-2**). Relaxation was defined as the stress after 30 minutes divided by the peak stress at the end of the ramp subtracted from 1.0 and presented a percentage. Therefore, 0% relaxation represents a fully elastic material, while 100% relaxation represents a material that has undergone complete relaxation.

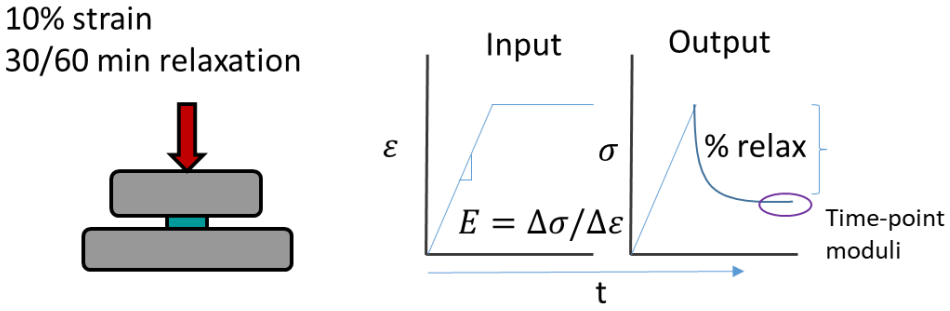

Figure 3-2: *Schematic of how mechanical properties from stress-relaxation testing were defined.*

3.2.3 Model fit: 5-parameter Maxwell model

To evaluate viscoelastic mechanical properties, stress-strain data was fit to a 5-parameter Maxwell model using a custom MATLAB script. This model consists of a spring in parallel with two simple

Maxwell models, which in turn consist of a spring and a dashpot in series (**Figure 3-3**). Each spring is assumed to contribute a linear stress-strain response, while each dashpot contributes to the viscous time-dependent behavior.

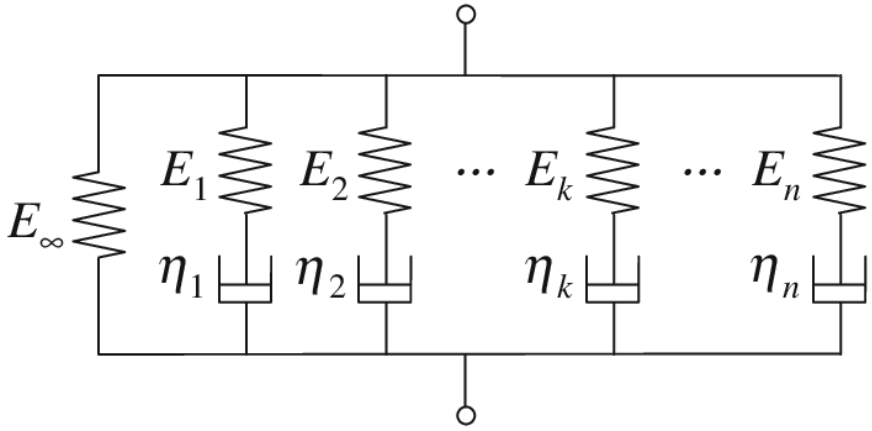

Figure 3-3: *Generalized Maxwell model showing parallel arrangements of a spring-dashpot component in series.*

Setting boundary conditions for stress relaxation (strain is constant; $\frac{d\,\epsilon}{dt} = 0$), we can solve for the stress as a function of time for the generalized form.

$$\sigma(t) = \epsilon[\, E_0 + \sum_{i=1}^{n} E_i e^{\frac{tE_i}{\eta_i}}] \qquad (1)$$

For the 5-parameter case, Equation (1) is simplified to

$$\sigma(t) = \epsilon[\, E_0 + E_1 e^{-\frac{t}{\tau_1}} + E_2 e^{-\frac{t}{2}} \qquad (2)$$

Where $\tau_i = \frac{\eta_i}{E_i}$. This τ is referred to as a "time constant", and represents the time it takes for the element to relax to 36.8% of its original stress value.[134]

Parameters E_0, τ_1, and τ_2 were reported for curves that were determined to have a good fit. Goodness of fit was defined as having a mean of residuals lower than 25, where residuals are defined as the unit distance from the data point given by the model at a certain time point to the actual experimental value at each time point.

3.2.4 Statistics

A non-parametric t-test (Mann-Whitney U-test) was used to compare between crosslinked and non-crosslinked groups. In the size dependence study, a two-way ANOVA to compare between groups of different diameters and different heights because of the absence of a non-parametric alternative in the statistics software used (GraphPad PRISM). A p-value lower than 0.05 was the benchmark used to determine statistical significance.

3.3 Results

3.3.1 Ionic crosslinking

Crosslinking agarose-alginate hydrogel with a calcium bath resulted in a 4.7-fold increase in modulus from 10.4 ± 1.8 kPa to 49.3 ±12.5 kPa ($p < 0.0001$; **Figure 3-4A**). The Xlink group also exhibited a significantly higher stress at the end of the hold, with a 30-minute modulus (0.8 ± 1.2 kPa) that was 8 times greater than that of the control group (0.1 ± 0.3 kPa; $p = 0.03$; **Figure 3-4B**). However, the percent of relaxation was comparable for both groups (92.6 ± 37.3 % and 82.9 ± 20 % for the Control and XLink groups, respectively; $p = 0.7$; **Figure 3-4C**).

Model parameters also showed differences in relaxation behavior between Control and Xlink groups. The average predicted equilibrium modulus for Control group (0.7 ± 12 kPa) was about half that of the Xlink group (1.5 ± 8.6 kPa; $p = 0.002$; **Figure 3-5A**). Time constant τ_1 for the control group (55.2 ± 12.8 s) was significantly lower ($p = 0.001$) than that of the Xlink group (134.1 ± 16.3 s; **Figure 3-5B**). Time constant τ_2, however, was significantly higher for the Control group (2007.6 ± 779.0 s) than for the Xlink group (957.7 ± 252.7 s; $p = 0.02$; **Figure 3-5C**).

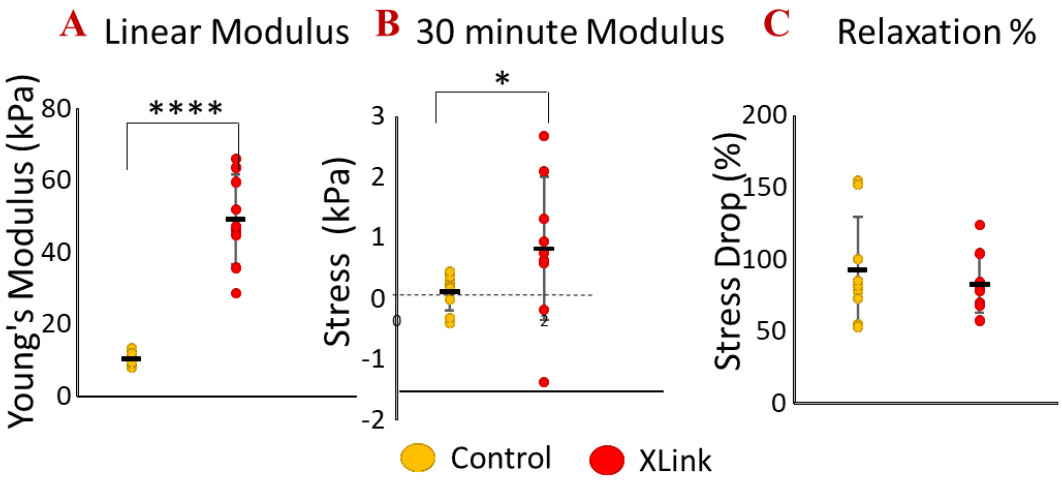

Figure 3-4: *Basic mechanics of 5% agarose-alginate gels (A) Young's modulus, (B) 30-minute modulus, and (C) percent relaxation. * and **** represent $p < 0.05$ and $p < 0.0001$, respectively.*

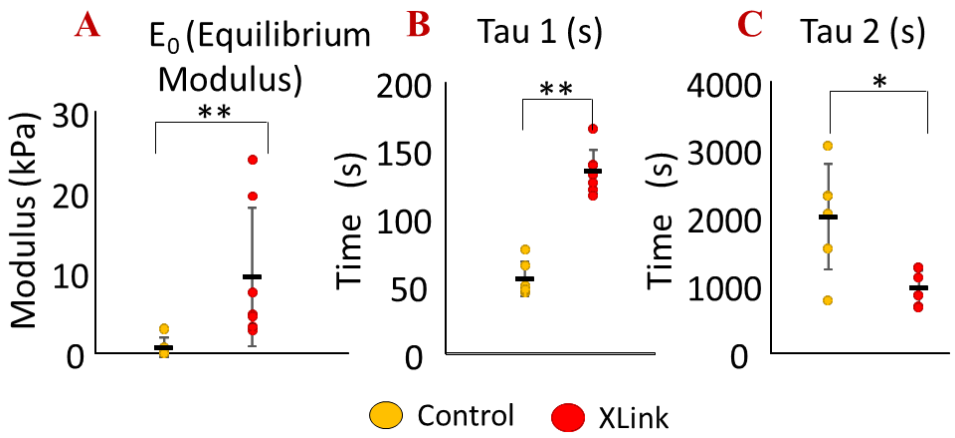

Figure 3-5: *Stress relaxation parameters for 5% agarose alginate gel (from generalized Maxwell model) (A) Predicted equilibrium modulus, (B) short-time constant τ_1, and (C) long-time constant τ_2. * and *** signify $p < 0.05$ and $p < 0.001$, respectively.*

3.3.2 Size dependence

Increasing construct height from 2.3 mm to 4.6 mm significantly increased the linear Young's modulus of 4 mm diameter samples from 17.3 ± 4.1 kPa to 29.7 ± 4.1 kPa ($p = 0.002$; **Figure 3-6A**). Modulus after 30 minutes also increased with increasing height for the 4 mm diameter group, from 1.3 ± 0.4 kPa to 2.4 ± 0.5 kPa ($p = 0.0007$; **Figure 3-6B**). Interestingly, the height effect in the 4mm diameter group disappeared after 60 minutes, with no significant differences between the Short (2.3 mm) and Tall (4.6 mm) height samples with 4mm diameter (0.9 ± 0.4 kPa and 1.6 ± 1.1 kPa; $p = 0.3$; **Figure 3-6C**). Height did not have an effect in the mechanics of the 6mm diameter samples, as Young's modulus for the Short group (16.2 ± 3.5 kPa) was similar to that of the Tall group (14.0 ± 1.1 kPa; **Figure 3-6A**). This trend held up over time, as both the modulus at 30 minutes (0.9 ± 0.1 kPa for Short; 1.1 ± 0.2 kPa for Tall group) and the modulus at 60 minutes (0.7 ± 0.1 kPa for Short, 0.9 ± 0.2 kPa for Tall) were statistically similar ($p > 0.1$; **Figures 3-6B&C**).

There were differences in Young's modulus ($p < 0.0001$) and modulus at 30 minutes ($p = 0.0001$) for Tall samples with differing diameters (**Figures 3-6A&B**). The effect of diameter was not significant for 2mm Short samples.

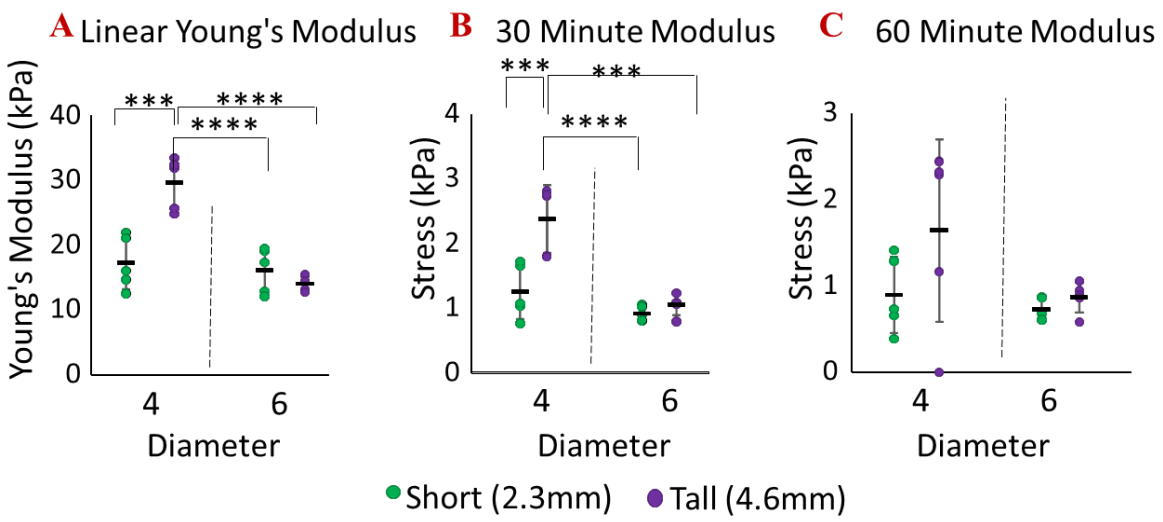

Figure 3-6: *Effects of dimensional changes on basic mechanics (A) Linear Young's modulus, (B) stress after 30 minutes, and (C) stress after 60 minutes. *** and **** represent $p < 0.001$ and $p < 0.0001$, respectively.*

No differences in viscoelastic parameters such as Equilibrium modulus E_0, short time constant τ_1, or long time constant τ_2 were observed with changing dimensions (size or diameter; **Figure 3-7A-C**).

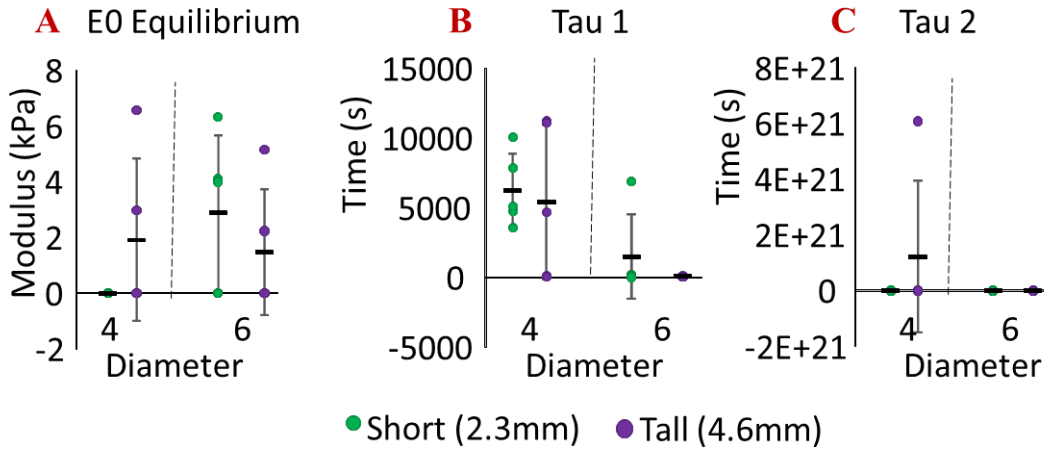

Figure 3-7: *Stress Relaxation model parameters (A) Equilibrium modulus (B) Short time constant τ_1 and (C) Long time constant τ_2 * and **** represent $p < 0.05$ and $p < 0.0001$, respectively.*

3.4 Discussion

This chapter consisted of two separate studies on the mechanical properties of 5% agarose-alginate gel, which our previous work identified as a potential scaffold material for 3D bioprinting cartilage scaffolds.[63] The first study aimed to look at crosslinking of the sodium alginate within the gel through calcium ions with the intention of improving base mechanical properties. The second study aimed to gain insight into variation of measured mechanical properties with size, as well-regulated standards do not exist for biological tissue and different research groups have their own preferences and techniques.[139]

Treatment of the 5% agarose-alginate gel in a calcium bath resulted in stiffer mechanical properties, both instantly and after a 30-minute strain hold. Ionic crosslinks also affected the rate of relaxation, with stiffer Xlink constructs relaxing less initially (higher τ_1) but eventually relaxing to similar percentages of the experienced peak load (**Figures 2 & 3**), suggesting that the calcium crosslink affects more than one relaxation mechanism. Zhao et al suggests that crosslinked regions will relax more quickly, because additional ionic crosslinks will restrict mobility in polymer chains, while un-crosslinked regions relax due to diffusion of displaced sodium ions in the matrix.[140] This would be consistent with what is seen here, and would suggest the long-term relaxation is dominated by the uncrosslinked agarose regions.[130] It should be noted that Control and Xlink samples here were evaluated to only a 30 minute hold, and it has been established that it is difficult to project long-term viscoelastic behaviors from shirt datasets.[141] This was as expected, as it is common for sodium alginate to be crosslinked if a solid structure is desired.[117] It was, however, useful to learn that sodium ions could interpenetrate the porous agarose matrix to reach the sodium alginate. A previous study that made sodium alginate gels with guluronic acid instead of water suggested that a mix could slow gelation time enough so that gel crosslinks are formed more evenly.[68] The increase in stiffness could be useful to study the influence of changing matrix properties on encapsulated cells, as stiffness has been shown to change the differentiation behavior of stem cells and chondrocytes.[142,143]

Comparisons between 5% agarose-alginate samples of different sizes and heights yielded differences in measured mechanical properties, but most of these were confined to the Tall (4.6mm height) 4mm diameter samples when compared to other groups. It should be noted that this group had the only aspect (length/diameter) ratio greater than 1. Low aspect ratios have been associated with higher modulus in tensile testing of fibrous tissues (annulus fibrosus) because of increased fiber engagement, but there are no inherent fibers in our gel materials.[144] The aspect ratio of 1is also well below the aspect ratio of 3 typically associated with buckling in more traditional materials, as well as above lower aspect ratios associated with barreling.[145] The fact that agarose itself has a low friction coefficient, and was tested on smooth plates under submersion conditions also makes barreling unlikely.[138]It is possible these differences are a result of small sample size (n=5 per group), as time-dependent behavior did not change with size and the group presenting differences (Tall 4mm diameter) had the highest standard deviation on mechanical properties between samples (**Figures 3-6 & 3-7**).

Both studies presented used directly measured mechanical properties as well as model parameters from a stress-time curve-fit to show viscoelastic behavior. It should be noted that there was less variance (percentage of standard deviation to average values) in model parameters in samples from the cross-link study than those from the size dependence study. The crosslink study presented high variance in the measured 30-minute modulus, but time constants from the model were fairly

consistent. Conversely, size-dependence samples presented higher variance in time constants and other parameters from the model while showing fairly consistent (< 30%) results in directly measured values like Young's modulus and 30-minute modulus. This speaks to the inherent value of directly measured mechanical properties, whereas models that rely heavily on assumptions may have non-unique solutions and present a wider range of results, making statistical analysis difficult. However, the model parameters here were very useful in highlighting the differences in relaxation behavior between crosslinked and non-crosslinked agarose-alginate gels. In particular, they were able to distinguish two very distinct relaxation time-frames, suggesting different relaxation mechanisms.[140]

The studies presented here had a number of limitations. First, the stress-relaxation hold was only 30 minutes, as at the time of experimentation we focused on comparing to existing literature values versus truly accounting for viscoelastic behavior, which cannot be fully extrapolated from shorter holds.[141] In the size study, a wider range of geometries would have been ideal to establish trends between width, height, and linear modulus. Since size-dependence in the literature has been related to aspect ratio, the study could be improved by having enough aspect ratios below and above 3, which is the generally accepted limit for compressive testing.[144,145] Additionally, the rheological model used was not fully evaluated for uniqueness. While the model performs thousands of iterations based on best fit starting from initial guesses for model parameters, there exist the possibility of having a non-unique solution that will fit the model. Because residuals were used as an evaluation method for fit, sample sizes for model parameter observations are lower than experimental sample sizes.

Here, we further evaluated the mechanical behavior of 5% agarose-alginate gel and explored how changes in composition or dimensions may affect measured mechanical properties. The findings presented in this chapter can be useful in helping tissue-engineering researchers make decisions on mechanical testing conditions and the continued use of hydrogel blends as promising scaffold materials.

Chapter 4: Influence of collagen type I source on gel characterization

Gabriel R. López Marcial, X Sun, Grace D. O'Connell

4.1 Introduction

Collagen is a native structural protein commonly found in soft tissues. Collagen Type II represents more than 90% of the collagen found in compressive load-bearing tissues like articular cartilage and the nucleus pulposus of the intervertebral disc, while collagen Type I represents more than 95% of the collagen found in the meniscus or the annulus fibrosus of the intervertebral disc (**Figure 1-2A**)[8,14,15,17]. Both forms of collagen strongly contribute to the tissue's tensile mechanics[20], making it crucial for researchers to understand how collagen can be quantified in native or engineered constructs.

Tissue engineering researchers often use reconstituted collagen gel as a direct scaffold or as an additive to a hydrogel such as agarose in search of increased cell-interactions.[76,77,82,146] Collagen type I gels are commercially available, and typically consist of ground collagen-rich tissue (such as murine or bovine tails) dissolved in hydrochloric acid. The collagen solution can be gelled by addition of a base, such as sodium hydroxide, and incubation at 37 °C, which accelerates the formation of crosslinks.[147] Previous literature showed that the collagen source is not a factor for the fibril failure properties within the gels, but it does affect the fibril structure and sub-failure properties.[148] More recently, Sorushanova et al observed a species dependence in compressive modulus of sponges made from porcine or bovine collagen.[149] Thus, it is important for researchers to consider characterization of the collagen source before implementation in hydrogel blends.

A common technique to determine the quantity of collagen inside native or engineered tissues has been the ortho-hydroxyproline (OHP) assay. OHP content was strongly correlated with collagen type II by Hollander et al. and as such, became the chemical most widely used to estimate collagen content in collagen type II-rich tissues like articular cartilage and the nucleus pulposus.[128,150] However, conversion factors between OHP content and actual collagen are inconsistent between groups[128,151] and have been used for tissues with other predominant collagen types such as Type I, including tendons, ligaments, meniscus, and the annulus fibrosus.[152–154] Additionally, it is unclear from the original data if the relationship between OHP and collagen was obtained from a curve with more than a single sample at each concentration, which would fail to account for variability within groups. Thus, it would be helpful to highlight how correlations may be affected by using averages as opposed to fitting individual data points.

This short study aimed to identify variation induced by collagen gels sources on tissue engineering techniques. More specifically, our objectives were (1) to verify the commonly used OHP to collagen ratios used in the literature were applicable to type I collagen, (2) to determine if the collagen source in gels produced variation in compressive mechanics when used in a collagen-agarose blend, and (3) to determine if the dilution of commercially available gels affect the measured OHP.

4.2 Methodology

4.2.1 Sample Preparation for OHP assay: Rat-tail (Corning Life Sciences, 354249) and bovine (FIBRICOL, 5133) collagen type I gels were used either directly (9.33mg/mL, 3.52mg/mL for rat

tail, 10.4mg/ml for bovine) or diluted. Samples (n > 5 per group) were diluted with either 0.15M PBS or a 5% weight over volume hydrogel (3:2 agarose to alginate ratio; g/100mL) into a range of final concentrations (10.40, 9.33, 7.30, 6.22, 5.20, 4.67, 3.52, 2.51, 1.76 mg/ml; **Table 4-1**). 5% agarose-alginate (Ag-Alg) was also used as a negative control (0 mg/mL). OHP/Collagen ratio was compared between groups with different collagen sources (Bovine vs Rat-tail) regardless of concentration or dilution method. OHP/Collagen ratio was also compared between dilution methods (PBS vs Ag-Alg) from Rat-tail samples and similar concentrations (4.67 & 1.76 mg/mL).

4.2.2 Assay: Hydroxyproline (OHP) content was obtained by a colorimetric assay. Briefly, hydrochloric acid was used to break off OHP from polypeptide chains in the sample. The acid was then evaporated from the sample and the sample was re-suspended in assay buffer. Chloramine-T and p-dimethylaminobenzaldehyde are used to oxidize free hydroxyproline in the sample and create a chromophore[155], which is then measured using a plate reader at a primary wavelength of 540nm, providing an OHP concentration reading (μg/mL) when compared to standards of known OHP content.

4.2.3 Sample preparation, mechanics: A stock solution of 4% agarose was made by dissolving agarose in 0.15M PBS and autoclaving at 121°C. The stock solution was diluted down with either PBS, Rat-tail collagen Type I, or Bovine Collagen Type I to create final solutions with an agarose concentration of 2% and a collagen concentration of 0 mg/mL (NOCOLL), 2 mg/mL (LO-RAT, LO-BOV) or 5 mg/mL (HI-RAT, HI-BOV). These were casted between two glass slides and allowed to cool before being punched into cylindrical samples for mechanical testing (d = 4mm, h = 2.3 mm).

4.2.4 Compressive testing: Cylindrical samples were subjected to unconfined compression while submerged in PBS. Briefly, a 10% strain ramp (2%/min) was applied and then strain was held for 60 minutes. Linear Young's modulus was obtained by applying a linear fit to the ramp, while 30-minute modulus was defined as the stress value average of 50 data points before and after the 30 minute time point.

Table 4-1: Overview of sample groups for OHP assay

Final Concentration (mg/mL)	Dilution Method	Collagen Source	Number of samples
9.33	none	Rat-Tail	15
6.22	PBS	Rat-Tail	10
4.67	PBS	Rat-Tail	5
4.67	Ag-Alg	Rat-Tail	6
3.52	PBS	Rat-Tail	5
1.76	PBS	Rat-Tail	5
1.76	Ag-Alg	Rat-Tail	6
10.40	none	Bovine	5
7.3	PBS	Bovine	6
5.20	PBS	Bovine	5
2.51	PBS	Bovine	5
0	Ag-Alg	None (control)	5

4.2.5 Statistics: A non-parametric t-test (Mann Whitney) assuming unequal variances was used to highlight differences between two groups when appropriate (Bovine vs Rat-tail groups, PBS vs hydrogel dilution). To obtain the relationships between OHP and collagen content, a simple linear regression was performed and degree of correlation was used by obtaining Spearman's correlation coefficient r_s (GraphPad PRISM software). Values of r_s greater than 0.3 were considered a strong correlation, according to suggested guidelines.[156] Significance was assumed for p values lesser than 0.05.

4.3 Results:

4.3.1 Species difference: OHP was measured for known concentrations of both rat-tail and bovine collagen type I, as well as a negative control. The Collagen to OHP ratio was significantly different ($p < 0.02$) between species (**Figure 4-1**). When OHP vs Collagen data is plotted separately, we see different linear relationships between rat-tail (**Figure 4-2A**) and bovine (**Figure 4-2B**) groups. Both groups show strong correlations between OHP concentration and the known collagen content ($r_s = 0.85$, $p < 0.0001$; $r_s = 0.78$, $p < 0.0001$for rat-tail and bovine collagen, respectively). When linear correlation and regression are performed for these same datasets as averaged values at each concentration as opposed to individual samples, both correlation coefficients (from 0.78 to 0.9 and 0.85 to 0.9 for bovine and rat-tail, respectively) and goodness of fit coefficients improve (from R^2 values of 0.66 to 0.76 and 0.56 to 0.86 for bovine and rat-tail, respectively). However, we obtain a much steeper slope for the relationship between OHP and collagen in rat-tail samples (4.14 to 6.27; **Figure 4-3A**), and a slightly steeper slope for bovine (3.89 to 4.00; **Figure 4-3B**).

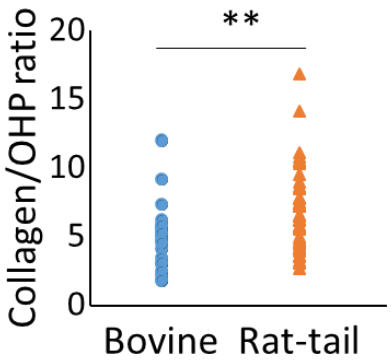

Figure 4-1: *Collagen/OHP ratio by species source. (** signifies $p < 0.01$, $n > 22$)*

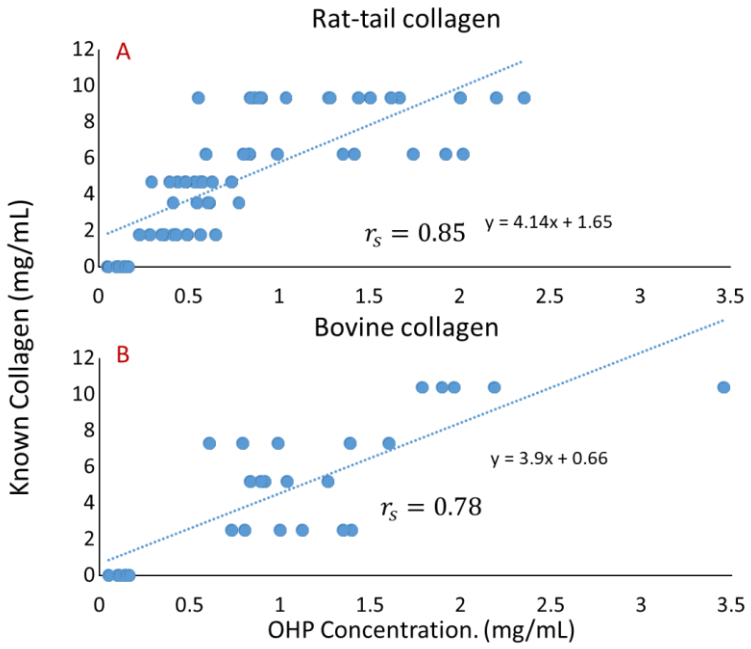

Figure 4-2: *Collagen presents different linear relationships with respect to OHP by species* ***A)*** *Rat-tail and* ***B****) Bovine.*

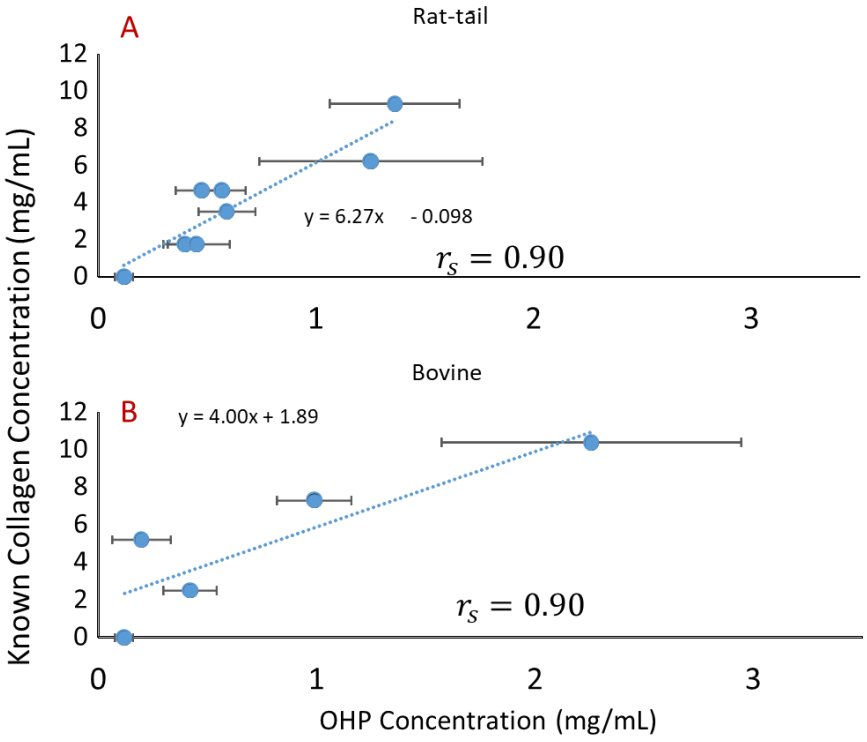

Figure 4-3: *Linear relationships change when plotting averages vs raw data points for species A) Rat-tail B) Bovine*

4.3.2 Dilution methods: We observed no significant difference in measured OHP content due to dilution methods (p = 0.87, **Figure 4-4**).

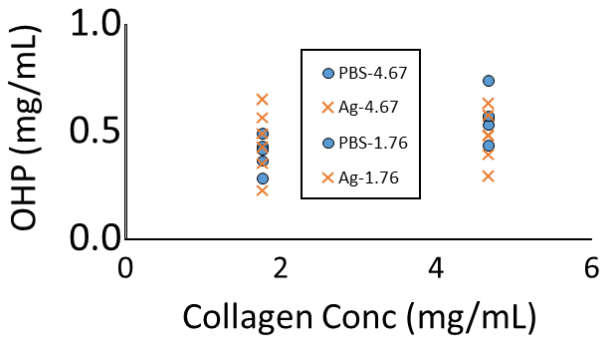

Figure 4-4: No differences between dilution methods.

4.3.3 Compressive mechanics: Young's modulus for the LO-RAT group (32.0 ± 5.1 kPa) was significantly higher than that of LO-BOV (17.0 ± 3.0 kPa; p = 0.000001; **Figure. 4-5A**). This increased stiffness was also observed in stress values after 30 minutes, where modulus for the LO-RAT group (1.9 ± 0.4 kPa) was significantly higher than that of LO-BOV (1.2 ± 0.4 kPa; p = 0.001). This trend did not extend to higher collagen concentration, as there were no differences in Young's modulus (35.9 ± 8.9 kPa for HI-RAT; 31.9 ± 15.8 kPa for HI-BOV) or 30 minute modulus (2.2 ± 0.9 kPa for HI-RAT; 1.9 ± 0.9 kPa for HI-BOV).

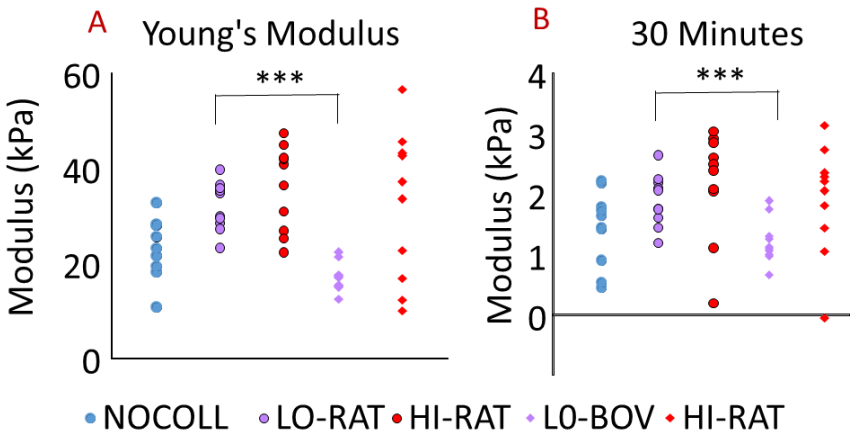

Figure 4-5: *Mechanics of agarose-collagen cylinders (A) Young's Modulus (B) 30 Minute Modulus. *** indicates p < 0.0001.*

4.4 Discussion

This short study aimed to establish a relationship between measured OHP content from a traditional OHP assay and collagen type I content in samples containing collagen hydrogels typically used for tissue engineering. We measured OHP content in rat-tail and bovine collagen type I gels and looked at differences in collagen to OHP ratio by species and sample preparation, as well as the actual collagen to OHP ratios to establish a "multiplier" that will allow us to report collagen content from the OHP assay.

Strong linear correlations ($r_s > 0.75$) were observed between measured OHP content and known collagen content is observed for collagen type I (**Figures 4-2, 4-3**). The slopes of these curves could be interpreted as "conversion" factors for collagen type I, where the actual collagen may be estimated from the measured OHP content. Previous studies have applied a conversion factor of a 1:7.4 OHP to collagen type II ratio[8] based on work by Hollander et al., where the authors showed a strong linear relationship between average OHP and collagen content.[150] However, we observe that there exists high variation within groups, with the average standard deviation for each group being approximately 30% of the average OHP value measured. We can also observe that the actual value of the slope changes when fitting to averages as opposed to a pool of individual values, amplifying differences between measured collagen to OHP ratios between collagen sources **(Figure 4-1).** This implies we could be observing what is called an "ecological fallacy", which maintains that the behavior of a group is not necessarily an accurate representation of an individual behavior.[157]

This does not mean that the relationships described here are useless, as relationships are still useful as estimates in many studies.[158] Since OHP to Collagen Type I ratio was observed to vary significantly across species (**Figure 4-1**), a quick reference table outlining these relationships is presented in **Table 4-2**. The conversion was obtained by plotting the OHP averages for all groups against known collagen content and extracting the slope with a forced 0 intercept.

Table 4-2: OHP-to-Collagen ratios as conversion factors.

Group	Collagen/ OHP	Correlation Coefficient (r_s)	Reference
Collagen Type II	7.40	-	Hollander et al 1994[150]
Collagen Type I	5.4	0.71	Internal
Bovine Collagen I	5.2	0.90	Internal
Rat-Tail Collagen I	6.1	0.89	Internal

There are some limitations that must be mentioned. A species difference was determined by pooling all rat-tail and bovine specimens, but a more apt comparison might have been comparing rat-tail and bovine samples with the same known collagen content.

Agarose-collagen blends with low collagen content (2 mg/mL) exhibited a species difference, with LO-BOV samples being less stiff than LO-RAT samples when subjected to compression.

However, no such difference was observed when collagen content was increased to 5 mg/mL, as both HI-RAT and HI-BOV samples exhibited similar mechanics. It has previously been reported that collagen source may influence the size of reconstituted collagen fibers between gels, and that at such low concentrations thinner fibers may simply not have been engaged enough to contribute to bulk mechanics, as the LO-BOV group was less stiff than the NOCOLL group as well.[148,149,159] It should also be noted that high variance was observed in higher concentration collagen groups as opposed to lower concentrations (**Figure 4-5**). Researchers are advised, however, to keep collagen source in mind when designing studies based on mechanical findings from different groups, and are encouraged to replicate results when possible.

In conclusion, a high variation in OHP to collagen ratios was observed for various type I collagen groups using a traditional OHP assay. As such, caution is advised when reporting collagen content extrapolated from OHP content in tissue-engineering samples. Additionally, it is apparent that OHP reading are influenced by different factors (collagen type, species), and it might be useful to simply report the measured OHP content from native or engineered tissues instead of extrapolating collagen content, as native and engineered tissues typically contain a range of different collagen types.

Chapter 5: Towards engineering a collagen gradient

Gabriel R. López, Keerthana Elango, Grace D. O'Connell

A version of this work was submitted as an abstract and presented as a poster talk at the 2020 Annual Meeting of the Orthopaedic Research Society (ORS) by Keerthana Elango.

5.1 Introduction

Lower back pain due to damaged or degenerated intervertebral discs is a highly prevalent issue in the United States.[160] There is growing interest in developing biological replacement strategies for the disc.[151,161] Engineered discs are commonly created with separate materials for the annulus fibrosus (AF) and nucleus pulposus (NP), resulting in a distinct interface between materials,[56,162] which does not recapitulate the natural gradient in tissue-composition and mechanics.[56] The intervertebral disc has been shown to experience bulging or damage initiating at tissue interfaces such as the NP-AF boundary and the boundary between the disc and the vertebral endplate.[163] Work in tissues such as tendon-to-bone insertion has suggested that changes in both composition (collagen, mineralization content) and structure (collagen fiber orientation) work together to alleviate mechanical mismatches and transfer loads.[164,165] However, native tissues are complex and highly variable across individual organisms, making it difficult to evaluate the individual contribution of each one of these changes on the bulk mechanics. Thus, there is a need for a tissue-analog that replicates the NP-AF gradients to better understand mechanisms of intradiscal stress distribution and, possibly, to ensure long-term success of replacement strategies.

While the manufacturing of such scaffolds has proved to be difficult, advances such as targeted photocrosslinking and layered casting have been successful in creating linear gradients.[4,166,167] 3D printing has emerged as a promising alternative, with commercial and custom printers having the ability to print multiple materials separately or at controlled volume fractions.[168] Chapter 2 identified 5% agarose-alginate gels as suitable materials for 3D printing, as they were able to create simple structures with similar shape fidelity to commonly used extrusion inks and maintain viability of encapsulated chondrocytes.

To avoid having bulk mechanical and characterization be dominated by the stiffest part of a gradient interface, the individual regions or components must first be evaluated separately. Thus, the objective of this work was to evaluate mechanical behavior between two hydrogels for developing engineered tissues. For this study, we focused collagen I to investigate one of the gradient effects present at the NP-AF interface, using alginate-agarose hydrogel as the base, due to its biocompatibility and 3D printing capabilities.[63] We assessed the effect of collagen to hydrogel mechanics. We hypothesized that adding collagen to an agarose-alginate base would alter bulk compressive modulus, as well as bulk relaxation behaviors by adding a fibrous component. Then, we analyzed interface strength between hydrogels to ensure the creation of a soft gel interface would not weaken the bulk tensile mechanics of the gel constucts. Finally, we assessed printability of the hydrogel with collagen.

5.2 Methods

5.2.1 Sample preparation

Agarose-alginate gels were made in 0.15 M PBS as described previously (Chapter 2) [6] and served as the control (5 w/v%; 3:2 agarose-alginate ratio). Collagen Type I (from Rat-tail, as seen in Chapter 4) was added to the hydrogel (LoColl = 1 mg/mL and HiColl = 3 mg/mL). Gels were casted between glass slides using a rubber divider. Compressive samples were made using a cylindrical biopsy punch (d = 6 mm, h = 2.3 mm). Interfaces were created by initially including a rubber divider in the center of the glass slide and removing it immediately after both gels were poured, allowing gels to contact each other during gelation (**Figure 5-1)**.

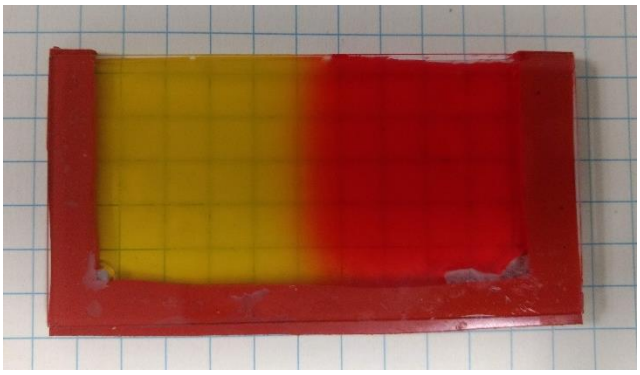

Figure 5-1: *Gel interface after casting. A barrier was removed between two casted gels, allowing them to join. Distinct gels colored yellow and red for visibility.*

5.2.2 Compression

Stress-relaxation tests were performed to 10% strain to evaluate compressive Young's modulus and time-dependent behavior (10% strain, rate = 2%/min, 60 min hold; diameter = 6 mm, thickness = 2.3 mm). Data from hold period was curve-fit to a 5-parameter Maxell-Weichert model to describe the time-dependent response, as described in Chapter 3 (n > 5 per group).

5.2.3 Tension

Gels were cut to create dogbone specimens for tensile testing (n ≥ 7 per group; ASTM D638 dimensions were scaled up by a factor of 1.57 to improve specimen stability during testing; **Figure 5-2A**). A monotonic ramp was applied to failure (rate = 20 mm/min) and the yield stress was defined as the point of maximum stress (**Figure 5-2B**). Tensile testing groups (CTL-no interface, CTL-CTL, CTL-LoColl, LoColl-LoColl, CTL-HiColl, LoColl-HiColl, HiColl-HiColl) are defined by the gels at each side of the casting barrier. For example, CTL-LoColl means that a CTL and a LoColl cast were casted in either side of the rubber divider and allowed to form an interface (**Figure 5-2B**).

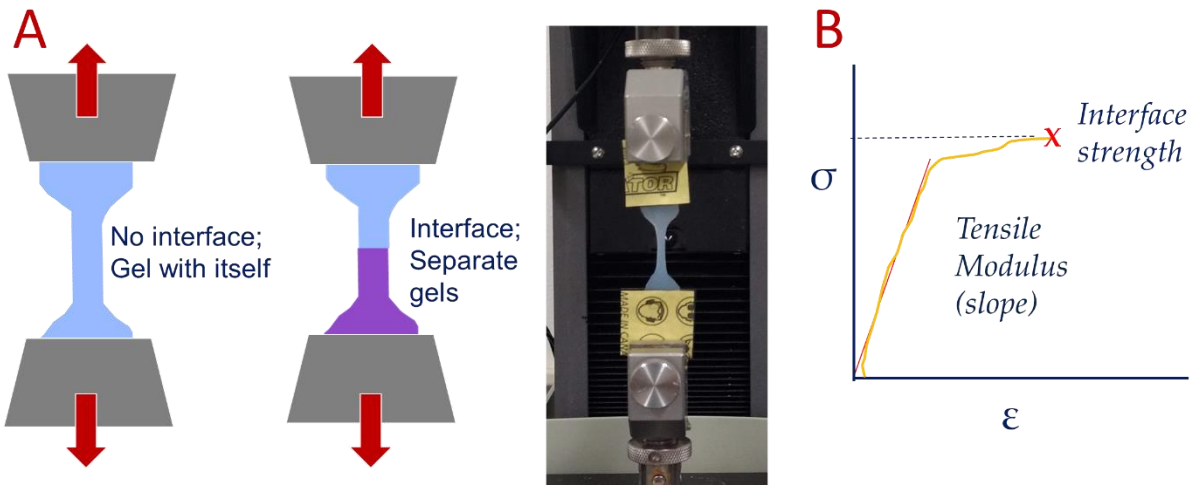

Figure 5-2: *Tensile testing (A) Schematic of gels without and with an interface. Representative image of tensile test setup. (B) Representative stress-strain response.*

5.2.4 3D Printing

Lines were printed with a commercially available bioprinter (37°C; n ≥ 5; Allevi, Philadelphia, PA). Photos of completed prints were compared to the CAD model to assess print quality, as seen in Chapter 2.[6] Print accuracy was calculated as $p = \frac{overlapping}{model} - \frac{uncovered}{model} - \frac{overhanging}{gel}$, and material spreading during the print (s) was calculated as the average distance between the gel boundary and CAD model boundary.

5.2.5 Statistics

A one-way non- parametric ANOVA (Kruskal-Wallis) with a Dunn post-hoc analysis was performed to compare mechanical properties across hydrogel types for compressive mechanical properties, stress relaxation model parameters, and tensile mechanical properties. Significance was assumed at $p < 0.05$. Spearman's correlation coefficient r_s was calculated between tensile Yield and Young's modulus values, as described in Chapter 4.

5.3 Results

Adding collagen type I into the agarose-alginate hydrogel increased both compressive Young's modulus, where the compressive Young's modulus of the HiColl group (18.9 ± 5.8 kPa) was 40% greater than the CTL group (11.8 ± 2.9 kPa; $p = 0.03$). (**Figure 5-3**). No differences were observed between modulus the LoColl group (13.7 ± 3.2 kPa) and the other two groups.

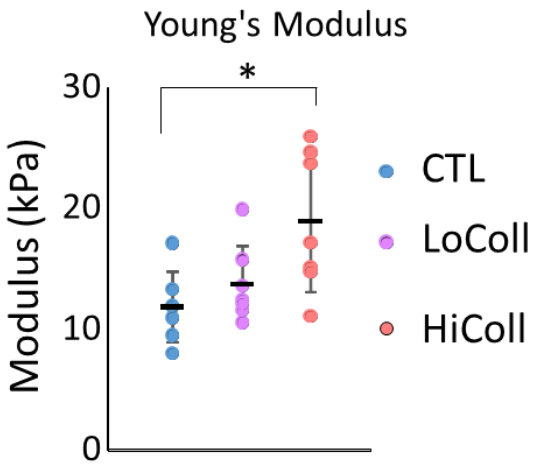

Figure 5-3: Compressive Young's modulus for agarose-alginate-collagen gels. * signifies $p < 0.05$.

Qualitatively, HiColl gels generally exhibited less relaxation than CTL or LoColl gels (**Figure 5-4A**). The initial relaxation rate significantly decreased with the higher concentration of collagen, as τ_1 was more than 3 times higher for the HiColl group (168.4 ± 44.6 s) than for the CTL group (54.4 ± 12.6 s; $p < 0.002$), but no such distinction was present between these groups and the LoColl group (99.5 ± 48.3 s; **Figure 5-4B**). This effect subsided over time, as there were no differences in long-term relaxation rates between groups (**Figure 5-4C**)

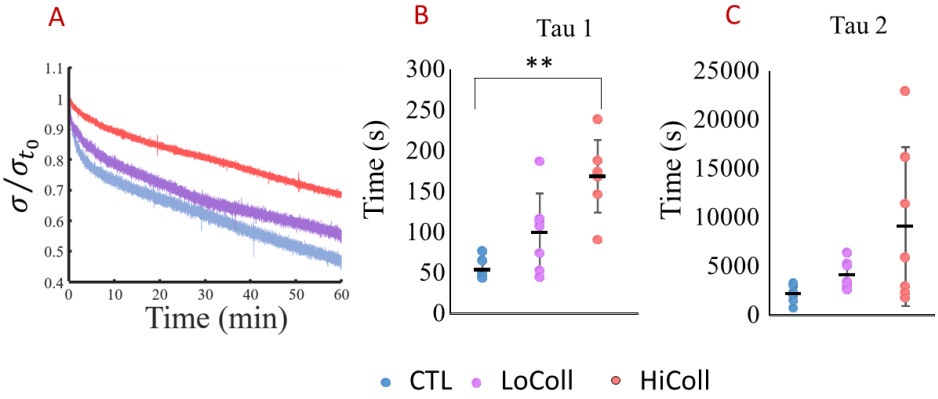

Figure 5-4: *Time dependent response of Agarose-alginate-collagen gels. (A) Representative curves of relaxation response (B) Time constant τ_1 (B) Time constant τ_2. ** signifies $p < 0.01$.*

The tensile Young's modulus of the HiColl-HiColl group (141.9 ± 14.2 kPa; $p < 0.05$) and the the CTL-HiColl group (102.7 ± 8.6; $p = 0.007$) were significantly higher than the CTL group with no interface (36.0 ± 12.6 kPa) , while the LoColl-LoColl group had a significantly lower modulus

than the control (77.9 ± 5.7 kPa). The CTL-LoColl group had a tensile modulus (36.1 ± 1.4 kPa), significantly lower than both the CTL-HiColl group (102.7 ± 8.6 kPa; p = 0.02) and the HiColl-HiColl group (p = 0.003). Uniaxial tensile failure occurred at the mid-substance for all specimens, and ~50% of specimens with an interface failed at the interface. The yield strength of the interface followed the same trends, with the groups with higher Young's modulus withstanding a higher stress to failure as well (**Figure 5-5A**). Yield strength and Young;s modulus exhibited a strong linear correlation, with a correlation coefficient of r_s = 0.83 (**Figure 5-5B**, p < 0.0001).

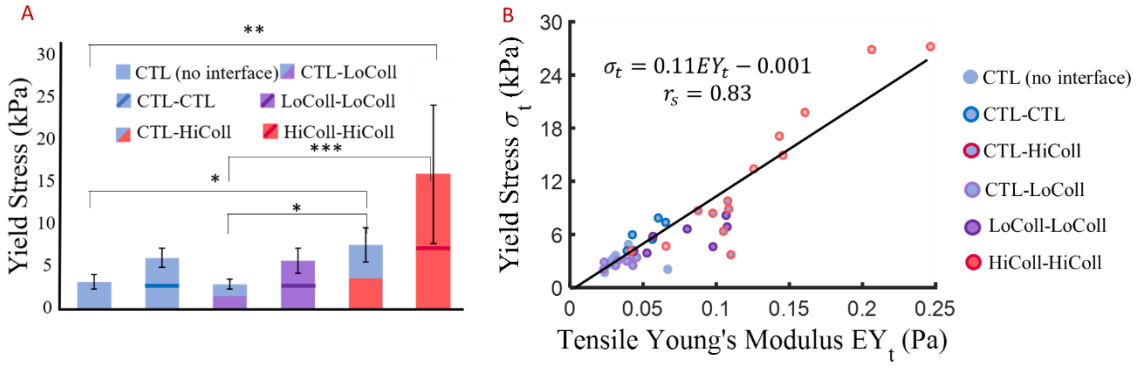

Figure 5-5: *Tensile testing of hydrogel interfaces (A) Yield strength of all tensile groups (B) Linear correlation between Yield strength and Young's modulus. *, **, and *** signify p < 0.05, 0.01, and 0.001, respectively.*

The three hydrogels had no significant differences in print quality (*p*), but the LoColl group experienced more spreading during printing (Figure 5-6; Table 5-1)).

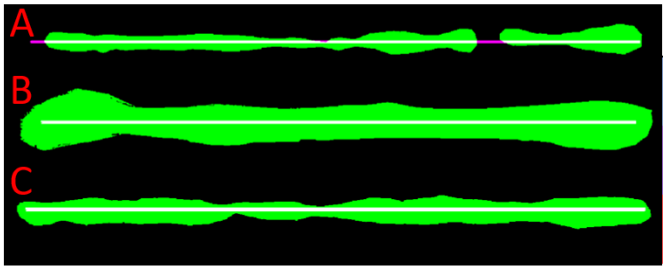

Figure 5-6: Representative overlay of printed lines for (A) CTL, (B) LoColl, and (C) HiColl over model CAD. As outlined in Chapter 2[6], green shows gel pixels while white and magenta show covered and uncovered model pixels, respectively.

Table 5-1*: Print and spread parameters for printed lines of agarose-alginate-collagen gels. * signifies $p < 0.05$ with respect to control.*

Group	Print parameter *p*	Spread *s* (mm)
CTL	-0.01± 0.15	0.48 ± 0.12
LoColl	0.08 ± 0.04	1.03* ± 0.1
HiColl	-0.01 ± 0.19	0.62* ± 0.04

5.4 Discussion

In this study, the acellular mechanical properties of adding collagen type I into a printable agarose-alginate gel were evaluated with the intention of later using this mixture to fabricate gradient agarose-alginate-collagen interfaces that might mimic the collagen gradient present on native tissue. With that end, the strength of interfaces between dissimilar gels were evaluated through tensile testing as well as the effect on 3D printability caused by the addition of the collagen to the agarose-alginate matrix.

We observed a dose-dependent increase in agarose-alginate hydrogel stiffness with the addition of collagen fibers, which may be used to aid in the formation of fibrous materials. Some previous studies that evaluated the effect of collagen supplementation in an agarose-based hydrogel observed a decrease in shear stiffness.[76,77] Differences are likely due to a variety of different factors. First, differences in gel preparation such as varying of both agarose and collagen concentrations had made it difficult to evaluate collagen content as a single variable[77], whereas here the initial agarose-matrix weight over volume was calculated such that all groups had the same final weight over volume concentration. A dose-dependent effect was also observed in relaxation behavior, with HiColl groups initially relaxing more slowly than CTL or LoColl groups. It is possible the fibrous concentration of the LoColl group (1mg/mL of collagen) was too low for fibers to be mechanically engaged, or for the fibers to affect bulk properties in a significant way. Previous studies have suggested that agarose dominates the relaxation behavior by attracting water, thus making the agarose matrix relax more slowly than collagen due to increased flow into the porous agarose matrix, which contradicts the behavior seen here.[130] However, given the increased stiffness seen in the ramp, it is reasonable to assume that engaged collagen fibers simply offered more resistance to compressive deformation initially.

Visually, we observed good integration between materials at the interface. Implementation of the gel interface did not inherently lower failure strength, even when the interface was between materials with different mechanical properties (**Figure 5-5A**). While there is little information regarding failure properties between the NP and AF, due to a lack of a defined boundary, failure stress for hydrogels in this study was an order of magnitude lower than AF failure stress in the radial direction (0.2 ± 0.2 MPa).[169] The strong correlation between yield stress and Young's modulus suggests that the interface contributed less to overall mechanical integrity than material elasticity (**Figure 5-5B**). Collagen fibers contribute to tensile strength in native tissues like the AF, where this correlation between failure and sub-failure stress has also been observed.[152] The integration of similar and dissimilar gels is important for bioprinting applications, as the process inherently creates many interfaces. In conclusion, we found that the addition of collagen to agarose-alginate gels did not significantly alter bioprinting and can be used to create scaffolds with initial collagen for developing fiber based engineered tissues. Future work will evaluate matrix

deposition in multi-material scaffolds to produce engineered tissues that better replicate the biochemical gradients observed in native tissues, as well as an expanded range of collagen concentrations.

Chapter 6: The addition of collagen type I in agarose created a dose-dependent effect on matrix production in engineered cartilage

Gabriel R. López-Marcial, Keerthana Elango, Grace D. O'Connell

A version of this work was published in Regenerative Materials in 2022.

6.1 Introduction

As explored in Chapter 5, gradients in tissue composition are found throughout the body, connecting materials with different stiffnesses, in turn, creating gradients in mechanical properties.[170] Mechanical gradients are of particular importance at interfaces of soft and hard tissues, like tendon or cartilage to bone, where sudden mismatches in stiffness create stress concentrations that contribute to tissue failure.[4] Gradients in fiber architecture and tissue composition can alleviate stress concentrations between materials with mismatched mechanical properties.[170,171] Replicating tissue and mechanical gradients is important for successful integration of engineered tissue with surrounding native tissues.

Gradients in tissue stiffness, fiber orientation, and tissue composition exist through the thickness of articular cartilage (Chapter 1).[14] This organization results in increasing compressive and shear moduli from the superficial to deep zone, while tensile modulus decreases, allowing energy to be dissipated through the depth of the tissue.[4,172]

Hydrogels have been used as tissue-engineering scaffolds because of their ability to maintain a rounded chondrogenic phenotype, as seen in Chapter 1. Agarose has been specifically useful in cartilage tissue engineering, as it has been able to stimulate enough GAG production to approach native values, resulting in compressive mechanical properties that are comparable to native values.[61] Collagen Type I hydrogels mixed with other gels, including agarose, alginate, and collagen type II, have resulted in increased cell-matrix interactions and GAG production. [76,82,146]

Studies that used an agarose-collagen mixture have shown an increase in cell bioactivity. These studies have evaluated gene-expression over multiple weeks. [76,77,173] However, we have little insight into whether collagen-agarose blends develop functional engineered cartilage, as gene expression is an imperfect indicator of protein production.[174,175] Hydrogels by themselves exhibit relatively weak mechanical properties and are dependent on extracellular matrix deposition to approach native mechanical properties. While the addition of collagen may result in weaker initial mechanical properties, due to a disruption in the agarose network [76], potential increases in protein production due to greater bioactivity may result in a greater long-term benefit.

Thus, the objective of this work was to characterize the effect of collagen type I on matrix production of bovine chondrocytes embedded in an agarose scaffold. We hypothesized that the addition of collagen type I will increase extra-cellular matrix production and mechanical properties. Furthermore, a low and high dose of collagen was assessed to determine whether there is a dose-dependent effect on matrix production and mechanical behavior.

6.2 Materials and Methods

6.2.1 Sample preparation

An agarose gel stock was created by dissolving Type VII agarose powder (Sigma-Aldrich, St Louis, MO) in 0.15M phosphate-buffered saline at a concentration of 6% weight over volume by heating to 121°C in an autoclave for approximately 20 minutes. The stock gel was then diluted with saline and Type I collagen (Bovine, Advanced Biomatrix, CA) to obtain a final concentration of 2% agarose gels. Collagen was added at concentrations of 0 mg/mL for the control (CTL), 2 mg/mL for the low concentration group (LoColl), or 5 mg/mL for the high collagen group (HiColl).

For cell-based experiments, the stock gel was cooled to ~40 ° C before being mixed with chondrocytes (final concentration of $30x10^6$ cells/mL) and cast between glass slides before being allowed to cool to room temperature to obtain cylindrical samples using a biopsy punch. Junior bovine knee joints were obtained from an abattoir (Green Village Packing, NJ) and chondrocytes were obtained by digesting cartilage with type 4 collagenase (activity 375 units/mg dry weight; Worthington Biochemical, Lakewoond, NJ) dissolved in media (DMEM with 5% FBS, 1% non-essential amino acids, 1% TES, 1% BES, 1% HEPES, 1% sodium bicarbonate, 1% penicillin streptomycin antimycotic (PS/AM), 2% minimum essential aminoacids) and shaken overnight inside an incubator (37 ° C, 5% CO2). Cells ($1x10^6$ per vial) were frozen in liquid nitrogen with DMSO until use. Frozen vials were thawed rapidly (< 2 minutes) in a 37 ° C water bath then plated in a culture flask. Cells were cultured in growth media (DMEM with 10% FBS, 1% PS/AM, 5ng/mL FGF, 10 ng/mL PDGF, 1 ng/mL TGFβ-1) until passage 6 until they were seeded into gels.

6.2.2 Rheology

Oscillatory rheology (Anton Paar) was performed on cylindrical, acellular gel samples (height = 2.3 mm; n = 8) using a sandblasted parallel plate with a diameter of 8 mm and a gap size of 2mm. Samples were created with a diameter of 8 mm to match the diameter of the testing plate. A temperature ramp (2°C/ min) was performed from 25-37°C, followed by a 5-minute isothermal step at 37° C with an oscillatory shear of 1% at 1 Hz. Storage (G') and Loss (G") moduli were defined as the average of all values recorded at the isothermal step (50 data points).

6.2.3 Engineered Cartilage

Cylindrical samples (diameter = 4mm, thickness = 2.3 mm; n=5 per group for each timepoint for mechanics and biochemical assays) were cultured in serum-free chondrogenic media (DMEM with 4.5g/L glucose and L-glutamine, 1% ITS+Premix, 1% Penicillin-streptomycin, 100μg/mL Sodium Pyruvate) for four weeks. Media was changed 3 times a week and supplemented to final concentrations of 50 μg/mL ascorbic acid and 100nM dexamethasone on the day of feeding. Media was additionally supplemented with 10 ng/mL of TGFβ-3 for the first 2 weeks of culture.

Stress-relaxation tests were performed to 10% strain to evaluate compressive Young's modulus and time-dependent behavior (10% strain, rate = 2%/min) on cell-laden cylindrical samples (diameter = 4 mm, thickness = 2.3 mm) at Weeks 0 and 4 under unconfined compression in a saline bath. Young's modulus was calculated as the slope of the linear portion of the loading curve during the ramp to 10% strain. Relaxation was defined as the stress after 30 minutes divided by the peak stress at the end of the ramp subtracted from 1.0 and presented a percentage. Therefore, 0% relaxation represents a fully elastic material, while 100% relaxation represents a material that has undergone complete relaxation.

Samples were stained and imaged at Weeks 1 and 3 to assess cell viability and observe changes in morphology (n = 3 from each group; Live/Dead kit, Life Technologies, Carlsbad CA). Z-stack images were collected at 533nm for live cells (green) and 640 nm for dead cells (red) using a confocal microscope (Praire Technologies; 10X objective). A custom MATLAB program was used to estimate the number of objects in each channel using a grayscale threshold (grayscale level > 35,000). Cell viability was measured as the number of live cells divided by the total cell count in the image stack and reported as a percent.

After mechanical testing, samples were re-hydrated (>20 min), weighed, and collected to measure DNA, GAG, and collagen contents. Specimens were lyophilized (Labconco, Kansas City, MO) for 48 hours to determine dry weight and digested overnight at 56°C with Protenaise K (MP Biomedical, Burlingame, CA). DNA content was determined using the fluorescent PicoGreen assay, GAG content was determined using the colorimetric dimethyl methylene blue (DMMB) assay, and collagen content was determined using the hydroxiproline (OHP) assay. Both GAG and OHP content were normalized by DNA content and the sample wet weight.

6.2.4 Statistics

Due to the relatively small sample size, normality was not assumed. A one-way non-parametric ANOVA (Kruskal-Wallis) was performed to assess differences among groups. Comparisons were evaluated for initial and final properties (*i.e.*, at Weeks 0 and 4). A Dunn's multiple comparison post-hoc was used to determine specific p-values between groups. Significance was assumed for $p \leq 0.05$. Statistical analyses were performed using GraphPad PRISM version 9.3 (GraphPad, San Diego, CA).

6.3 Results

Changes in Mechanical Properties:

Acellular mechanical properties were evaluated using a rheometer. The storage modulus for the control group was G' = 3.6 ± 1.8 kPa and the loss modulus was G" = 0.2 ± 0.1 kPa. There were no significant differences observed in storage or loss modulus with the addition of collagen to the hydrogel ($p = 0.2$ for G'; $p = 0.06$ for G"; **Figure 6-1A & B**). Variability in measured mechanical properties increased with the addition of collagen, which impacted the power of the analysis ($\beta = 0.14$). There were significant differences in initial mechanical properties of seeded scaffolds tested under unconfined compression ($p < 0.01$; **Figure 6-1C** – Week 0). Specifically, the Young's modulus of the HiColl group was 47.8 ± 33.0 kPa, which was more than 3X greater than the CTL group (14.4 ± 2.6 kPa) at Week 0 (**Figure 6-1C**; $p = 0.009$). All scaffolds experienced 50-60% relaxation during the 30-minute hold, with no significant differences with respect to collagen supplementation ($p = 0.11$; **Figure 6-1D**). Final bulk mechanical properties measured at Week 4 showed that the Young's modulus for CTL and LoColl groups were 2.6X stiffer than the HiColl group ($p < 0.01$; **Figure 6-1C**). There were no significant differences in compressive Young's modulus between CTL and LoColl groups. At Week 4, the percent of relaxation for the LoColl group was 21% lower than HiColl (38.9 ± 9.8% and 59.7 ± 16.5%, respectively; $p = 0.02$; **Figure 6-1D**. However, there were no significant differences in percent relaxation with respect to the CTL group ($p = 0.35$).

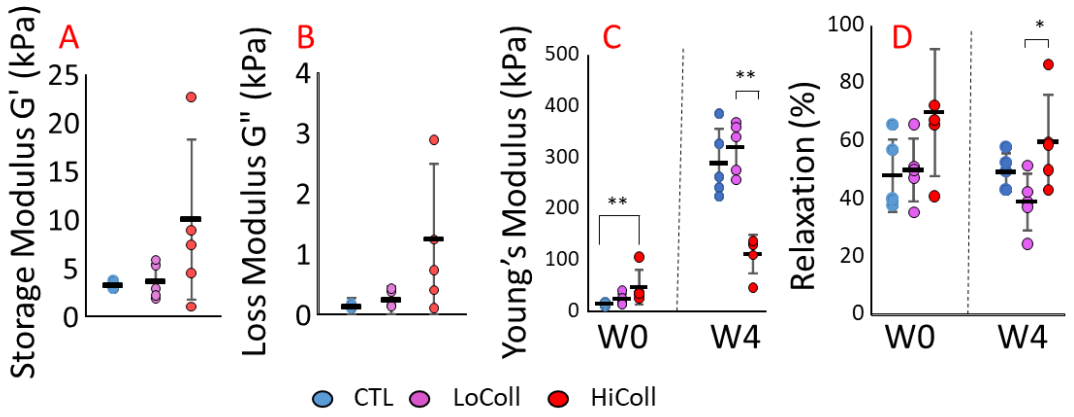

Figure 6-1: *(A-B) Rheological properties of acellular hydrogels. (A) Storage modulus and (B) loss modulus at 37° C. No significant differences were observed between groups (p > 0.2). (C-D) Initial (W0) and final (W4) compressive mechanics of engineered cartilage constructs. (C) Linear region Young's modulus and (D) percent relaxation measured during the hold period of a stress-relaxation test. * represents p < 0.05. ** represents p < 0.001*

Changes in Matrix Production

The HiColl group presented a larger diameter than the CTL group when normalized by Week 0 diameter (p = 0.006; **Figure 6-2A**). This difference was due to a 6% decrease in diameter for the CTL group and a ~10% increase in diameter for the HiColl group from initial values (i.e., Week 0). However, these differences did not translate to significant differences in construct height or volume at Week 4 (p > 0.05; **Figure 6-2B & C**).

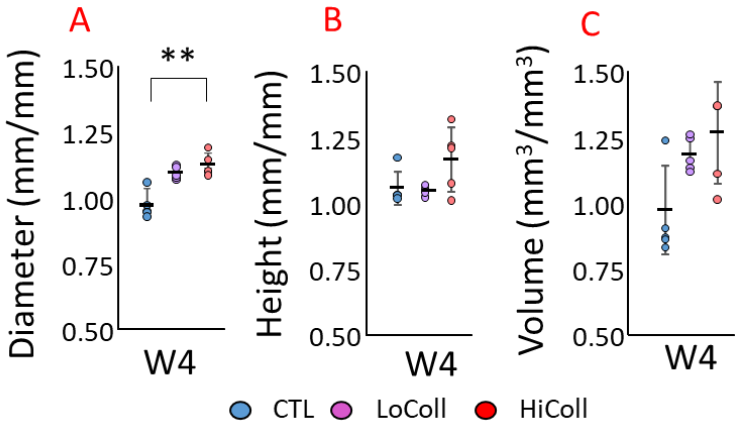

Figure 2: *Dimensions of engineered cartilage constructs at Week 4 (W4), normalized by dimensions at Week 0: (A) diameter (d), (B) height (h), and (C) volume ($V = \pi(\frac{d}{2})^2 h$). ** represents p < 0.01.*

No differences in DNA content were observed between groups at Week 0 or Week 4, suggesting that cells were seeded evenly, and the added initial collagen did not alter cell proliferation (**Figure 6-3A**). At Week 1, all groups had high cell viability (> 90%; p = 0.23; **Figure 6-3B**), and there were no noticeable differences in cell morphology (**Figure 6-3C** – top row). After 3 weeks of culture, cell viability was lower for the CTL (75.8 ± 13.2%) and LoColl groups (78.6

± 2.1%; **Figure 6-3B**) and cells from all groups showed an elongated phenotype (**Figure 6-3C** – bottom row).

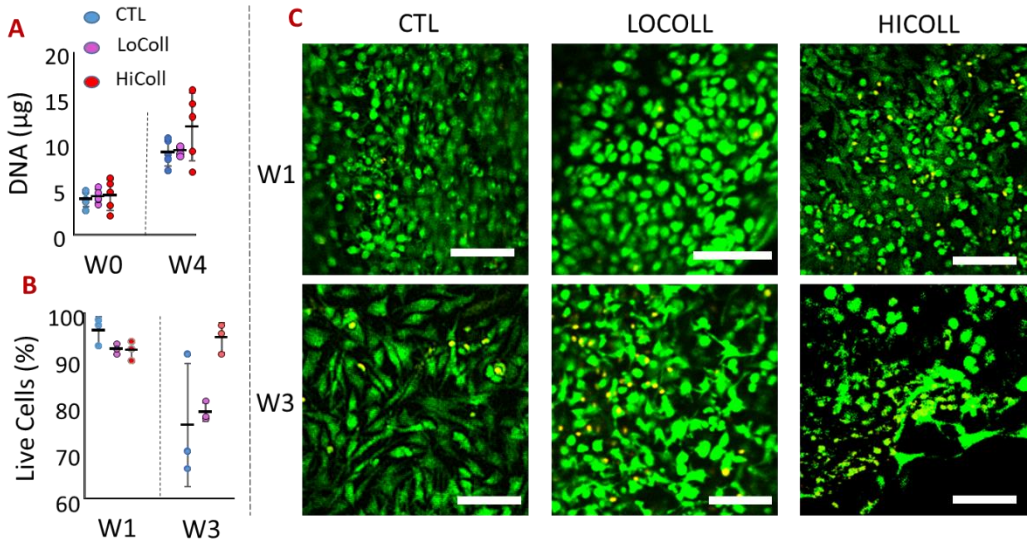

Figure 6-3: *(A) DNA content, (B) percentage of living cells, and (C) live/dead imaging, where green represents live cells and yellow represents dead cells. Scale bars = 100 µm. No statistical differences were observed for DNA content or percentage of living cells counted at either time point (p > 0.4).*

The addition of collagen resulted in statistically significant differences in the initial collagen content, as expected (**Figure 6-4A & C** - Week 0). At Week 4, the LoColl group was more metabolically active than CTL, based on OHP/DNA (LoColl = 6.7 g/g CTL = 4.2 g/g; p = 0.02), but not significantly more active than the HiColl group (5.1 g/g; p = 0.23**, Figure 6-4A**). There was also a trend for greater metabolic activity in the LoColl group with respect to GAG production (**Figure 6-4B**; p = 0.059). However, these differences in metabolic activity were not reflected in overall differences in tissue composition when normalized by wet weight, as commonly performed in the literature (**Figure 6-4C & D**).

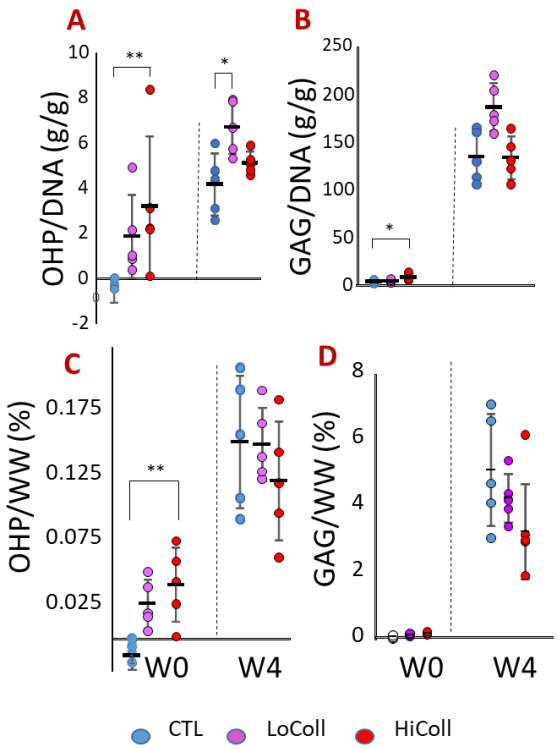

Figure 6-4: *Biochemical content was normalized by (A & B) DNA content to assess metabolic activity and (C & D) wet weight (WW) to compare to data in the literature. (A & C) * represents $p < 0.05$. ** represents $p < 0.01$.*

6.4 Discussion

The objective of this study was to evaluate the effect of incorporating collagen within agarose to increase matrix synthesis during a month-long 3D culture. GAG growth in CTL and LoColl groups were similar to previously reported values for agarose-only gels[61], resulting in compressive properties within the range of native values (240-850 kPa).[176] A previous study found that the addition of collagen type I in the range of 2-4.5 mg/mL increased GAG production from nucleus pulposus cells embedded in agarose.[76] The addition of collagen to the agarose hydrogel in this study demonstrated a dose-dependent effect on cell bioactivity, where 2 mg/mL of collagen improved bioactivity but the higher concentration had a negative impact on cell bioactivity.

The addition of collagen to the agarose scaffold only altered elastic mechanical properties at higher strains. The increase in Young's modulus of agarose-collagen gels agreed with an experimental study by Kopf *et al.*[77] The increase in stiffness may be due to greater fiber engagement as the non-fibrillar agarose matrix experiences deformation.[177] Similarly, insensitivity of collagen on rheological mechanics agreed with data from Cambria *et al.*, when correcting the reported p-value for the number of observations (*i.e.*, running a one-way ANOVA rather than multiple t-tests).[76] The discrepancy in findings between testing modalities may be explained by a decrease in fiber engagement during rheology. That is, unconfined compression testing was performed at 10% strain, while oscillatory rheology reached maximum strains of 1%, which is not high enough to detect strain-stiffening behavior in collagen gels.[159] The non-linear behavior of engineered cartilage suggests that greater differences may have been observed at higher strains;[178] however, 10% strain was used in this study to represent moderate physiological loading and compare to exiting data in the literature.[103,128,179] Initial time-dependent relaxation behavior was

not altered by collagen, agreeing with previous work that evaluated time-dependent behavior of agarose-collagen gels with indentation testing.[130] Relaxation behavior of the scaffold is thought to be dominated by the non-fibrillar agarose;[130,166] thus, it was unaffected by the relatively low quantities of collagen (0.1-0.5% w/v).

A dose-dependent effect was also observed in matrix deposition, with the greatest GAG/DNA and OHP/DNA content at Week 4 in the LoColl group (**Figure 6-4A & B**). GAG content is directly linked to compressive mechanics, which was also observed in this study, where the HiColl group was initially stiffer than the CTL and LoColl groups (Week 0) but was less stiff at Week 4 when the GAG content was also lower. The lower GAG content also resulted in a greater relaxation response when compared to other groups (**Figure 6-1D**), agreeing with trends of energy dissipation seen in native articular cartilage.[180] Extra-cellular matrix deposition did not affect overall construct size between groups, as all groups showed similar values for volume at Week 4 relative to their initial volume (**Figure 6-2C**). Previous research has shown that collagen gels may experience a decrease in size over time due to contractile cell forces on fibers,[76,181] but this was not observed in this study. The lack of scaffold contraction was likely due the much higher agarose concentration and the use of chondrocytes, both of which have been shown to counter the effects of cell-mediated contraction in collagen gels.[173,182]

While collagen type II is the predominate type in native cartilage, collagen type I was used here based on previous *in vitro* studies.[79,173] However, a recent study showed that that blending both type I and II collagen had a greater impact on GAG production and gene expression (Sox9, aggrecan, Coll I,II,X) when compared to pure collagen I scaffolds, suggesting the mechanical function of our gels could have been further improved by including both collagen type I and II.[82] Improving collagen production in engineered cartilage has been a significant challenge. Degrading early production of GAGs with chondroitinaseABC has resulted in greater improvements in collagen production (75% increase over wet weight when compared to the control) than what was observed in this study.[60]

This study is not without limitations. First, collagen is expected to have a greater impact on tensile properties, which was not assessed here due to challenges of culturing longer specimens for tensile testing. Second, this study had a low sample size per group. Regardless, our findings support the notion that collagen supplementation at a lower concentration can increase chondrocyte bioactivity within an agarose hydrogel, as suggested in the literature. However, the increase in bioactivity did not greatly increase collagen production outside the range of previously reported values for engineered cartilage (~1.5%/WW versus native ~10%/ WW). Thus, the overall impact of using a collagen-agarose blend to increase collagen production in engineered cartilage is low under static culture conditions.

6.5 Acknowledgements

We would like to thank Dr. Kevin Healy and Dr. Anouk Killars for their help with rheological measurements.

6.6 Funding

This work was supported by the National Science Foundation (NSF) [DGE 1752814].

Chapter 7: Effect of collagen fiber structure on the localized mechanical properties of meniscus

Gabriel R. López-Marcial, X Sun, Gabriel Dorlhiac, Sofia Arevalo, Grace O'Connell

7.1 Introduction

Previous chapters (Chapters 5 & 6) highlighted the need to create analog tissue structures to study the role of gradients on tissue mechanics at the interface between two or more different types of tissues. In addition to the relationships between bulk mechanics and composition, it is important for the local or spatial changes in mechanics to be studied as well. Nanoindentation is an important tool for characterization of local material mechanical behavior that has been widely used for characterizing hydrogels, despite challenges relating to adhesion and low stiffnesses.[183,184] Here, we aim to validate a nanoindentation setup as a method to detect localized stiffness changes due to composition and structure in analog tissues by characterizing stiffness in different regions of native meniscus tissue. We selected meniscus because of its availability, well documented regional variations in tissue composition, and limited swelling ex vivo.

Meniscus is load-bearing collagenous tissue in the knee joint and contributes to stability, energy absorption, and decreased contact stresses to surrounding tissues like articular cartilage (**Figure 1-2A**).[15] Each knee has 2 menisci (medial and lateral), and they can be thought of as having a middle, anterior horn, and a posterior horn (**Figure 7-1**). Damage to the meniscus often results in increased risk of osteoarthritis, highlighting its ability to distribute stresses.[185] Damage in need of clinical intervention often appears as tears, which have been found to occur most often in the posterior horn of the medial meniscus.[185]

The observed change in prevalence would suggest site-dependent differences in loading or mechanical properties, which are strongly correlated to composition and structure. The bulk composition and structure of the meniscus was described in Chapter 1. Briefly, the meniscus is 65-70% water and contains glycoproteins, such as glycosaminoglycans (1-2% of dry weight) and fibronectin (8% of dry weight), yet the extracellular matrix is dominated by collagen type I fibers (90% of dry weight). These fibers are organized mainly as large bundles in the circumferential direction with a network of radial tie-fibers in between.[3,186] However, the prevalence of radial tie-fibers has been seen to increase from the anterior to the posterior horn with maturation in bovine and equine animal models.[186,187] There also exists a small superficial layer where fibers are aligned randomly, creating a "shell" layer structure around the more directionally aligned fiber structures (**Figure 1-2C**), with this layer showing a size-dependent effect on stiffness.[3,15,186,188] Bulk and localized mechanical testing has confirmed that the meniscus is, like most soft tissue, highly anisotropic, with collagen fiber orientation affecting measured tensile and compressive modulus.[189,190] In the radial direction, studies by Sanchez *et al.* found higher GAG content in the inner regions that contributes to ECM stiffness.[191,192] Danso *et al.* observed greater GAG content in the center regions of the circumferential plane,[193] reaffirming changes in local mechanical properties with structure and composition.[189]

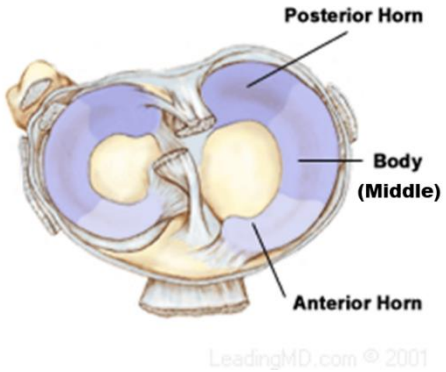

Figure 7-1: *Superior view of the knee joint menisci. From (https://www.thesteadmanclinic.com/patient-education/knee/meniscus-injuries)*

However, the influence of these regional structural and compositional effects on mechanics have been more widely observed using mechanical characterization techniques at very small (atomic force microscopy, < 5μm) or relatively large (uniaxial tension and compression, > 10mm) length scales, likely capturing individual components like single collagen fibers (10-50 μm in diameter) or bulk portions of tissue.[3,190,194–197] Studies that used a more intermediate but still localized length scale failed to observe differences between anterior, middle, and posterior meniscus regions, but it should be noted that all of their indentation was on the lamellar surface layer, where fibers are randomly aligned.[198–200] There is also limited literature on the differences between the lamellar layer and the center region as indented from the same plane, as other studies that have looked at both regions have generally rotated the sample in between.[189,201] Thus, there is an opportunity to expand the literature on localized structure-function relationships of the meniscus while validating a localized approach that could be used to characterize composition-function changes in gradient tissues and tissue-analogs discussed in previous chapters (Chapters 5 & 6).

The main objective of this study is to characterize the relationships between structure, function, and indentation mechanics between the surface layer and the larger center meniscus region in the circumferential plane. We expect to see a difference in GAG content, collagen organization, and stiffness between these regions. This will serve to (1) confirm previously observed structure differences in these regions and (2) validate a characterization method to studying gradient related mechanics in soft materials.

7.2 Methods

7.2.1 Sample Preparation: Menisci were obtained from juvenile bovine knee joints (3-6 weeks old, n = 9), wrapped in 0.15M PBS-soaked gauze and stored at -20°C until preparation. Since the knee joints were initially acquired for an unrelated study that harvested the articular cartilage, neither were the medial and lateral menisci nor the anterior and posterior regions of said menisci labeled during dissection. Therefore, the anterior and posterior regions horn regions were identified simply as “horn” regions. A scalpel was used to prepare ~5 mm thick slices from each 1/3 region (two horn regions and the center region; **Figure 7-2**). A freezing stage microtome was then used to create a flat surface for indentation testing.

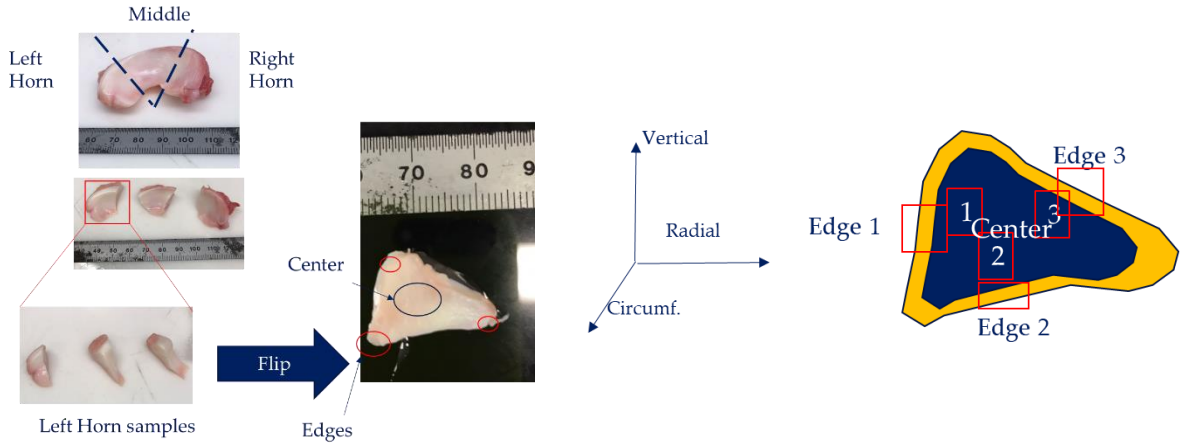

Figure 7-2: *(Left) Diagram of specimen preparation (Right) Center and edge regions for SHG imaging and nanoindentation.*

7.2.2 Imaging: Second Harmonic (SHG) imaging[186] was used to image menisci samples in the circumferential plane. SHG is a label-free technique that has proved particularly useful because of its ability to obtain high-resolution images (~200nm) and its non-destructive nature[202]. This has allowed researchers to monitor the growth and directionality of collagen fiber structures over time[203]. Briefly, the edge and center regions of each specimen was excited using an 850 nm or 1450 nm wavelength to obtain a 600 x 600 μm image. At the edge, 9 images were stitched together to create a 3x3 image composite. A larger composite image was created at the center using a 12 x 12 grid (144 images).

To highlight the directionality of the collagen fibers, a custom Python code was used to create a similar analysis to that used by Li et al.[189] The code further segments each image into 12 x 12 μm window. In each window, the angle of each element (i.e., fibers) was recorded. Features in windows with a wide distribution of angles (many elements with different angles) were re-colored with low intensity, while features in windows with a narrow distribution (i.e., most fibers in a single or similar directions) had higher intensity (**Figure 7-3**). These windows are then re-stitched together to make a larger image with high color intensity in regions of high organization, and is darker in regions of random organization

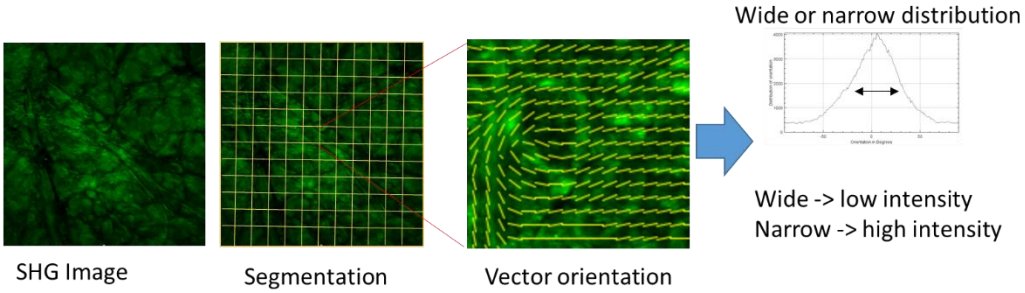

Figure 7-3: *Overview schematic of image orientation processing.*

7.2.3 Nanoindentation: Mechanical testing was performed using a Hysitron Triboscan indenter with an ESP 301 motor controller (Bruker, Bullerica CA). Samples were laid flat (circumferential side up) on a petri dish and were surrounded with 10% w/v saline polyethylene glycol (SPEG) during mechanical testing. SPEG was used because of its ability to hydrate native tissues with

minimal swelling, as swelling or dehydration would impact tissue mechanics and disrupt the flat surface needed for indentation.[204] Care was taken for the fluid line to match the top of the sample, as preliminary experiments that completely submerged demonstrated difficulties with sample detection and adhesion that led to noisy or unusable data (**Figure 7-4**).

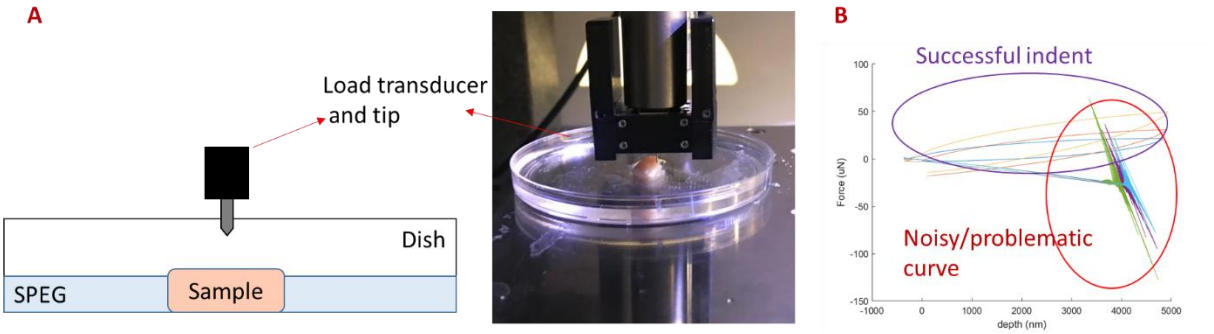

Figure 7-4: *Indentation overview (A) Schematic and picture of hydrated indentation setup (B) Representative force-displacement datasets from indentation.*

Samples were indented with a conical fluid-cell tip (d=100 μm) in six regions (3 edge regions and 3 center regions, **Figure 7-2**) using a 3x3 pattern of indents spaced 400um. A pre-load of 50 μN was applied to detect the surface, followed by a 5000nm displacement at a rate of 1μm/s, a 5-second hold at the maximum depth. The sample was then unloaded at a rate of 1um/s. Young's Modulus, E, was calculated using the method proposed by Oliver & Pharr.[205] Briefly, the force-displacement data from the unloading portion was curve-fit to an exponential function of the form

$$P = \propto \left(h - h_f\right)^m \quad (1)$$

Where P is load, h and h_f represent current and final displacement, respectively, and α and m are the curve-fit parameters.[205] To clarify, the unloading part of the curve is used while loading is an elastic-plastic deformation, unloading is purely elastic. The exponential curve-fit parameters are used to define stiffness, S, defined as the change in force over the change in height, which can be used to determine the Young's modulus:

$$S = \frac{dP}{dh} = \frac{2}{\sqrt{\pi}} E_r \sqrt{A} \quad (2)^{205}$$

$$E = \frac{E_i E_r (1-\nu^2)}{E_r (1-\nu_i^2) - E_i} \quad (3)$$

Where E_r is the reduced modulus, E_i is the modulus from the indenter, ν_i is the Poisson's ratio of the indenter, and ν is the Poisson's ratio of the material. The reduced modulus is essentially the measured modulus, which includes the modulus of the indenter as well as that of the sample (think two springs in series). Since the indenter is much stiffer than the sample, equation (3) may be simplified to

$$E = E_r (1 - \nu^2) \quad (4).$$

In this study, Poisson's ratio was assumed to be 0.4, based on previous experimental data on bovine meniscus.[126] While nine indents were performed for each region, curves that were unable to be

evaluated due to clear issues with surface detection or curve-fitting were eliminated (**Figure 7-4B**). Regardless, a minimum of three indents per region were averaged to determine the modulus value for each region, and replicate measurements of each region were averaged to obtain the value of each sample. In summary, there were two samples (horn and center) from nine different menisci (n = 9), with each of these samples indented in six different regions (three edge, three center for each) between 3-9 times).

7.2.4 Biochemical content: Tissue punches (diameter = 1 mm) was collected from 3 center and 3 edge regions for one slice from each meniscus (i.e., either horn or middle region). Samples were weighed to obtain the sample wet weight (ww), lyophilized for 48 hours, and re-weighed to determine the dry weights (dw). Samples were digested overnight in 2 mg/mL Papain (Spectrum Chemical; Gardena, CA). Glycosaminoglycan (GAG) content was determined using a dimethyl-methylene blue (DMMB) colorimetric assay, and the ortho-hydroxiproline (OHP) assay was used a proxy for collagen content.[155] OHP was directly reported, however, collagen content is typically reported in the literature. Therefore, a 5.2:1 collagen to OHP ratio was used to place these results in context of collagen content, in accordance with our findings and suggestions from Chapter 4. Water content was calculated as $\frac{ww-dw}{ww}x100$ and reported as a percentage. To quantify collagen crosslinking through advanced-glycation end-product (AGE) content, quinine sulfate content was measured using a fluorescence assay.[152]

7.2.5 Statistics: Statistical analyses were performed using GraphPad PRISM version 9.4 for Windows (San Diego, CA). A non-parametric paired t-test (Wilcoxon test) was used to compare biochemical (GAG, Collagen, AGE) content and mechanical properties (indentation modulus) between edge (the superficial layer of the meniscus) and center (the main organizational region). Overall modulus of horn and middle regions were compared using the Wilcoxon test. Statistical significance was assumed for $p \leq 0.05$.

7.3 Results

7.3.1 Nanoindentation

No statistical differences in Young's modulus were observed between the center (5.4 ± 2.2 MPa) and edge (4.24 ± 1.6 MPa) regions of the menisci when averaging values obtained from middle and horn region samples ($p = 0.12$; **Figure 7-5A**). In the middle meniscus, there were no significant differences observed between center region (5.3 ± 2.8 MPa; $p = 0.38$) and edge (5.0 ± 2.4 MPa; **Figure 7-5B**). However, the horn region did have greater variations in mechanical properties between the center (5.5 ± 3.24 MPa) and edge (3.5 ± 2.0 MPa; $p = 0.023$; **Figure 7-5C**). No significant differences ($p = 0.65$) were observed between averaged center and edge regions of horn (4.5 ± 2.5 MPa) and middle samples (5.1 ± 2.1 MPa; **Figure 7-5D**). A power analysis assuming normality of the data suggests that we would have seen a difference between these groups ($\beta = 0.2$) with a sample size of 12.

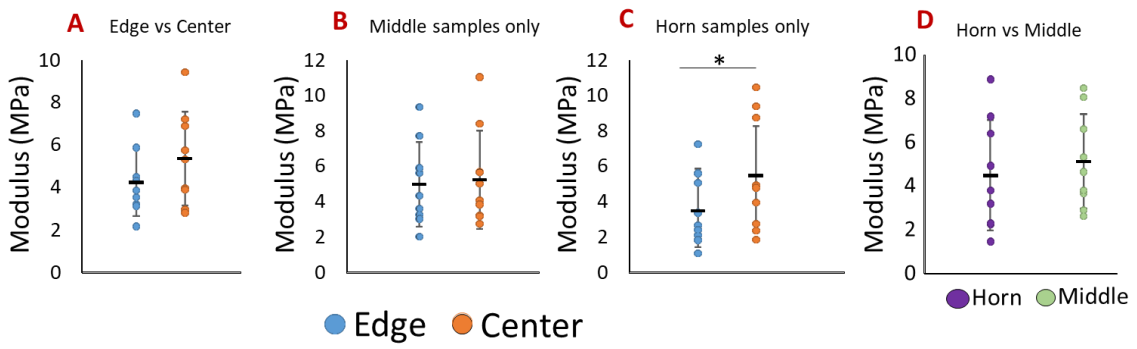

Figure 7-5*: Indentation modulus of (A) Averaged horn and middle meniscus samples (B) Middle samples and (C) Horn samples. (D) Averaged center and edge samples * signifies p < 0.05 between groups.*

7.3.2 Biochemical Composition

No differences were observed between center and edge regions in biochemical content. Water content at the edge (55.1 ± 9.5 %) was not statistically different from the center (66.0 ± 8.6 %; **Figure 7-6A;** p = 0.054). GAG content was nearly identical for edge (1.5 ± 0.7 %/ww or 3.4 ± 1.3 %/dw) and center regions (1.4 ± 0.8 %/ww or 5.1 ± 4.6 %/dw; p = 0.5 for GAG/ww, p = 0.25 for GAG/dw; **Figure 7-6B & 7-6C**). OHP content normalized by wet weight (**Figure 7-7A**) was identical between regions (7.2 ± 5.5 %/ww; p = 0.57) and presented high standard deviations when normalized by dry weight (**Figure 7-7B**; 19.5 ± 18.0 %/dw and 27.9 ± 26.5 %/dw for edge and center regions, respectively; p = 0.43). These comparisons hold for collagen content, where OHP values are multiplied by a conversion factor (**Figure 7-7C & 7-7D**).

AGE content was similar between all regions. The amount of quinine in the edge regions (0.7 ± 0.4 %) and center regions (0.76 ± 0.4 %) was nearly identical when normalized by wet weight (**Figure 7-8A; p = 0.43**), as when as when normalized by dry weight (**Figure 7-8B**; p = 0.07;1.6 ± 0.7 % for edge and 2.5 ± 1.7 % for center) or by OHP content (**Figure 7-8C**; p = 0.43; 13.3 ± 5.3 % for edge and 11.0 ± 5.4 % for center).

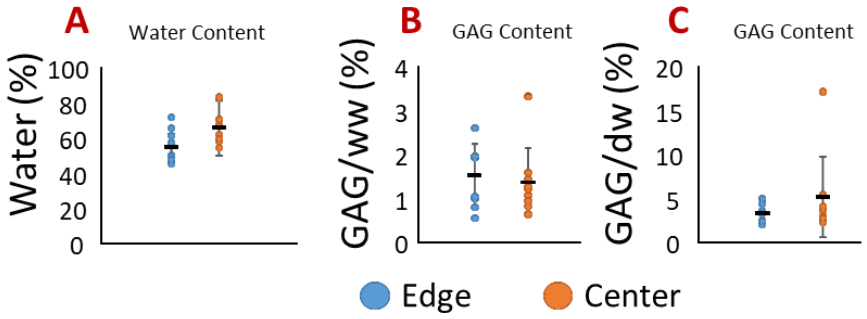

Figure 7-6: *Biochemical composition (A) water content (B) GAG over wet weight (C) GAG over dry weight for edge and center regions*

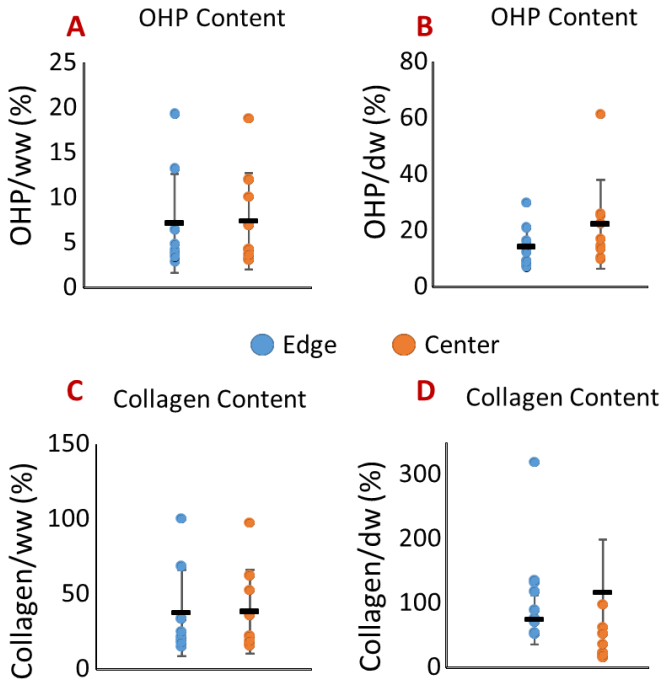

Figure 7-7: *Biochemical composition (A) OHP over wet weight (B) OHP over dry weight (C) Estimated collagen over wet weight and (D) estimated collagen over dry weight for edge and center regions*

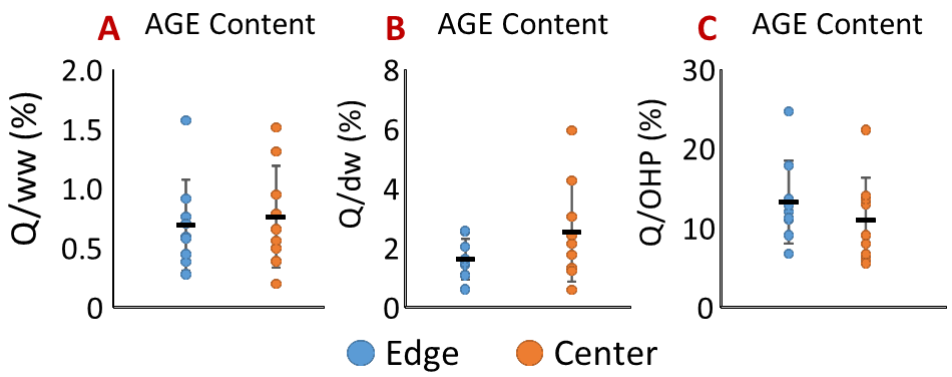

Figure 7-8: *Quinine content (as a proxy for AGE content) normalized by (A) wet weight (B) Dry weight and (C) OHP content*

7.3.3 Fiber Orientation

Orientation analysis from SHG images showed variation in alignment of collagen orientation. However, not all samples followed the same pattern of higher alignment with increasing distance from the surface edge. Representative images are shown in **Figure 7-8**.

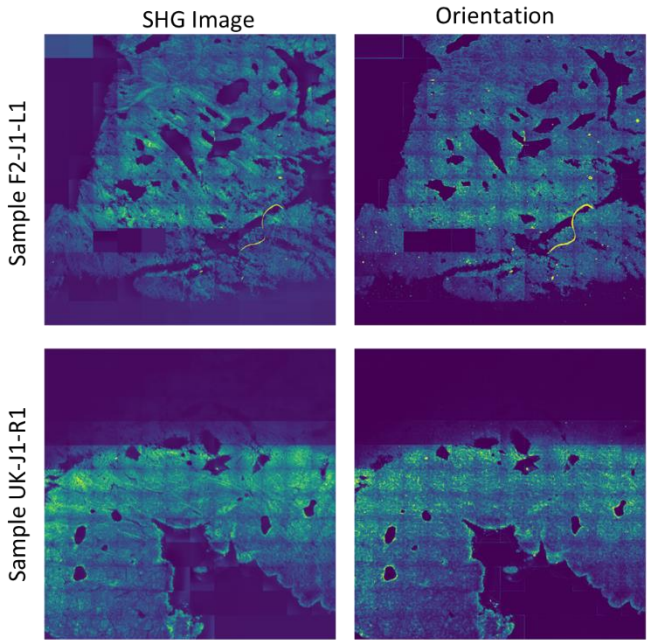

Figure 7-9: *Representative images of meniscus collagen orientation. The left column represents the obtained SHG image, in which higher image intensity is correlated with SHG signal. The right column shows higher intensity with increased fiber alignment within a 12x 12 μm window.*

7.4 Discussion

This study aimed to validate nanoindentation as a method to characterize local changes in mechanics due to composition and structure in soft materials. Local mechanics of healthy bovine meniscus were characterized through nanoindentation methods, while structure was evaluated through qualitative imaging and composition was evaluated through biochemical assays.

The overall modulus values measured for bovine meniscus were 4.8 ± 1.7 MPa. These values are higher than some reported previously for indentation and in unconfined and confined compression (0.1-1.5 MPa),[124,190,198,206] but within the same order of magnitude. They are also in the same order of magnitude as values seen for tensile modulus evaluated in a range of orientations (5-150 MPa).[37,197] However, previous studies using atomic force microscopy (AFM), which is a more localized form of nanoindentation given the smaller tip diameters, have reported indentation moduli to be several orders of magnitude lower (20-200 kPa).[189,191,201] It should be noted that AFM studies have typically used tip diameters as small as 5μm, which is within the observed range of collagen fiber diameter observed in other studies.[194] These studies also opt for analysis based on the Hertz contact model, which has been observed to significantly underestimate modulus values when compared to Oliver-Pharr methods due to viscoelastic effects in the effective area calculation.[207] .

Li *et al.* saw a higher effective indentation modulus when collagen fibers were oriented parallel to the indentation direction than on the surface, where orientation may be characterized as mostly perpendicular to the surface.[189] They attributed this difference to lateral constraints, with fibers being constrained laterally by other fiber bundles in the circumferential direction, while surface fibers had more space to deform. From the imaging analysis that shows a higher organization in the center regions, as well as the indentation direction presented here, a similar result was expected but a difference was only observed in horn samples (**Figure 7-5C**). A power analysis suggested that a sample size of 20 would have been able to detect a statistical difference with 80% power between center and edge moduli for the averaged horn and middle regions. Differences in fiber orientation between horn and middle regions are uncommon in juvenile meniscus, as radial tie-fibers become thicker and more tightly organized with maturation, increasing modulus.[201,203]

OHP content was evaluated as a proxy for collagen. Working with the premise that most of the collagen found in the meniscus is Type I collagen and that there is a 5.2:1 Collagen to OHP ratio for bovine specimens(Chapter 5), collagen was measured to be about 37.4% of the wet weight of the meniscus, which is similar values collected from the literature for junior bovine samples (~33% of wet weight) and higher than the expected values for human meniscus, which are more commonly reported (~22% of wet weight).[15,179] We also observed collagen content in the 30% range for other mammals like pigs, which may be more similar to bovine in overall composition than typically reported human values.[208] GAG content normalized over dry weight was slightly higher in overall meniscus samples (4.3 ± 2.7 %) than values seen in the human literature (~2% of dry weight), but GAG over wet weight was lower than those reported for juvenile bovine (~3 % GAG/ww).[15,179,209] However, we see from the data that the average overall water content (58.1 ± 6.3) was lower than the expected water content for soft tissue such as meniscus (~65-70%).[15,179] It is possible that the raw values reported here were affected by dehydration after a freeze-thaw cycle, as our water content results are consistent with a previous study that evaluated this effect.[210] It has also been reported that GAG and water fractions may increase with age for bovine menisci.[211] Pig

menisci have also reported similar collagen and GAG values over wet weight as those observed here (25-30 % Coll/ww, 1.5-3% GAG/ww).[208]

There were no detected differences in GAG content from edge to center regions. There are two possible explanations for this lack of GAG discrepancy. First, regional variability of GAG tends to be in the radial direction, with the inner avascular "white" zone showing a higher concentration of proteoglycans than the outer "red" zone of the meniscus.[193] Samples were not taken in this radial direction, and as such could not be observed. Second, the edge samples taken in this study encompass a distance of about 1mm from the surface. Moyer et al[212] previously showed that the surface is only GAG-deficient for about 600 μm in depth, meaning that about 40% of our sample would have similar GAG content to center regions.

Quinine was quantified as a proxy for AGE content within the menisci. There were no regional differences in AGE content when normalized by wet weight, dry weight, or OHP content (**Figure 7-6**). Crosslinking in collagen fibers due to AGE content has been shown to increase stiffness in soft tissues,[152] and as such would have been a possible source of variation in local mechanics. AGE content normalized by dry weight (2.1 ± 1.0 %) was an order of magnitude lower than reported AGE content for juvenile swine meniscus, but in addition to being a different species this particular study used pyridinoline, not quinine, as a proxy for AGE content.[208] Not all AGE's necessarily increase with age or degeneration in the meniscus and thus we cannot conclude that this data necessarily corresponds with what is expected of juvenile bovine menisci,[213] but it is reported here with the hope it becomes a reference point for other researchers interested in native menisci composition.

SHG imaging of menisci samples revealed regional variation, but was not always consistent with the expected features of high organization in the center of the sample when compared to the surface (edge) region. By highlighting areas of narrower distributions, we would expect to see orientation images feature lower intensity in the surface region (approximately 600 μm from the edge of the meniscus image) and much higher intensity near the center, where circumferential and radial fibers are highly organized in a single direction. Li et al showed similar observations, plotting angle distributions for surface and circumferential fibers imaged through scanning electron microscopy.[189] Our analysis showed "rows" of high intensity (**Figure 7-8**), seemingly more aligned with the borders of the imaging field of view than with native tissue features. It is possible that the artificial segments image were broken into (that is, the 12 x 12 μm windows in which orientation distribution was evaluated) affect the quantitative analysis, as organization between elements of neighboring segments is not taken into account. We also observe some regions of high organization near the very edge of some images. It should be noted that our analysis is limited by certain factors. First, this study only collected representative images from two menisci; thus, it is impossible to draw definitive conclusions beyond demonstrating a proof-of-concept. Second, we imaged into the circumferential direction, which means many fibers were presumably coming out of the plane, which may impact the SHG signal. Finally, there is a possibility meniscus sample preparation (scalpel cuts and microtoming) affected fiber orientation at the surface.

In conclusion, we were able to collect nanoindentation data of healthy bovine meniscus; however, the current method did not observe localized differences. This may be due to a lack of compositional differences observed with the biochemical assays. It is possible that age and diseases that result in greater variations in tissue composition will lead to greater differences in local mechanics. Regardless, this testing approach may be beneficial for characterizing regional

differences in engineered tissues that have shown greater matrix production on the construct periphery.

Chapter 8: Conclusions and Outlook

The overall goal of this dissertation was to explore how the mechanical properties of hydrogels can be evaluated and manipulated to support functional tissue engineered constructs. The research presented looked at relationships between rheological mechanical properties and manufacturability, relationships between composition and compressive mechanics, and relationship between composition and ECM production in gel scaffolds. While the work in this dissertation has focused on basic science as opposed to direct clinical application or evaluation, it is my hope that this information will be useful to tissue engineering researchers looking as they continue to improve and implement new strategies for the mechanical repair and replacement of injured tissue, in particular those of the knee joint.

Some specific take-away messages from this dissertation are:

1. *Extrusion printing was used to manufacture tissue-engineering scaffolds from agarose-alginate gels (Chapter 2).*
   Agarose-alginate co-gels were successfully extruded into basic macro-porous shapes, and demonstrated similar rheological properties to Pluronic, a control gel known for its manufacturability but limited by bulk mechanical properties and its water solubility. Extrusion printing is a useful tool for tissue-engineering researchers looking to improve nutrient diffusion in their hydrogel scaffolds, as macroporosity lowers the distance nutrients must travel during 3D cell culture, and allows for more complex geometries than casting, which would require the manufacture of a mold.

2. *Compressive mechanical properties of agarose-alginate gels were influenced by inducing ionic crosslinks (Chapter 3).*
   The compressive mechanical properties of a crosslinked agarose-alginate mix were evaluated. Crosslinking the alginate portion of the gel with a calcium chloride solution changed the short-term relaxation behavior of the bulk gel, making it relax more slowly at first, despite eventually reaching a similar overall relaxation as the non-crosslinked gel. Measured mechanical properties also demonstrated some-size dependence, but not enough aspect ratios were evaluated to establish a trend.
3. *Collagen type I to ortho-hydroxiproline ratios varied depending on collagen gel source (Chapter 4)*
   It is important for researchers to consider source when using the OHP assay to evaluate collagen content in scaffolds with commercial collagen Type I gels. Rat-tail and bovine collagen I gels demonstrated a species difference with respect to Collagen/OHP ratios, suggesting there is not a single perfect "multiplier" to obtain collagen from OHP data. Previous studies in the literature have been inconsistent with how collagen is estimated, using collagen/OHP relationships established for different types of collagen (collagen Type II) or rounding scalar factors to the nearest ten.

4. *Gel interfaces did not inherently lower the tensile failure properties of the bulk gel. (Chapter 5)*
   When allowing materials with different composition, specifically collagen content, the interface was not weaker than a bulk continuous material. This is important, because interfaces between dissimilar materials affect the clinical success of scaffolds that aim to imitate tissues with distinct regions such as the disc. Combined with the manufacturability

of hydrogels seen in Chapter 2, this finding encourages the creation of more complex tissue engineering scaffolds to better imitate the load transmission mechanisms seen in native tissues that include composition gradients.

5. *The effect of collagen type I to improve the tissue engineering properties of agarose gels was dose-dependent (Chapter 6).*
   Collagen was observed to increase chondrocyte bioactivity within agarose-collagen scaffolds, but this effect was slight and only did so at low concentrations. Larger concentrations of collagen were actually detrimental to matrix deposition and long-term compressive mechanics within agarose scaffolds, and as such it is not a recommended method of improving the functionality of tissue-engineered constructs.

6. *Micron-scale indentation could not differentiate regional mechanics in the circumferential plane due to collagen structure in juvenile bovine menisci (Chapter 7).*
   Indentation is a powerful tool for characterizing local mechanics, but was not effective at distinguishing differences in a soft tissue such as meniscus under the setup presented in Chapter 7. While the possibility exists that there were simply no differences to be detected due to the early developmental stage of the samples, the region-specific collagen structure of meniscus had been well-documented, which is why the tissue was chosen to validate the localized indentation technique, with hopes of using it to characterize gel interfaces such as the ones described in Chapter 5.

The primary contribution of this dissertation is to expand the existing literature on the mechanics of hydrogels, specifically agarose-based gels and co-gels. Agarose, agarose-alginate, and agarose-collagen gels were exposed to a series of mechanical characterizations including unconfined compression, tension, and shear oscillation. These series of experiments provided insight into how changing composition, either initially through adding an additional gel component or through biological ECM composition, affected the short and long-term responses to mechanical loading within agarose-based hydrogel scaffolds under different conditions. As future tissue-engineering researchers brainstorm ways to improve the mechanical functionality of their three-dimensional gel scaffolds, they will be able to come back to this work and establish composition-mechanics relationships.

The work presented here was limited by a number of factors. First, it must be noted that sample size is a limitation in many of the studies here, particularly in studies that include biological material such as chondrocytes or native tissues (Chapters 2, 6, & 7). Sample size itself is limited by availability or long mechanical test durations which make a high sample size capable of unequivocally proving a hypothesis unfeasible. However, the effort has been made to use different tools such as appropriate statistical tests and power analyses to gain insight into the relationships described in this work. Appropriate sample sizes are even more important with native tissues, as they present high variability depending on differences in age, loading, genetics, and other factors between donors.

Another limitation is that the mechanical characterization techniques described here are not necessarily representative of *in vivo* loading scenarios. Native tissues see dynamic loads, and experience complex loads beyond uniaxial or pure shear stresses. However, monotonic ramps and stress relaxation in unconfined compression performed in chapters 2, 3, 4, & 6 still give important mechanical properties such as linear and equilibrium moduli, and, perhaps more importantly, serve

to compare directly with known properties from native tissues in the literature tested under similar conditions.

In conclusion, this dissertation expands the literature on the mechanical properties of hydrogels used for tissue engineering, in particular agarose and agarose-blends. These materials have been widely used towards the development of 3D constructs to mechanically repair damaged tissue, and the series of studies presented here will continue to give researchers insight into the relationships between hydrogel composition, mechanical behavior, and matrix deposition when used as tissue engineered scaffolds.

References

1. Nijhuis, W. H. *et al.* Current concepts in osteogenesis imperfecta: Bone structure, biomechanics and medical management. *J. Child. Orthop.* **13**, 1–11 (2019).
2. Brody, L. T. Knee osteoarthritis: Clinical connections to articular cartilage structure and function. *Phys. Ther. Sport* **16**, 301–316 (2015).
3. Choi, J. Y. *et al.* Thickness of the meniscal lamellar layer: Correlation with indentation stiffness and comparison of normal and abnormally thick layers by using multiparametric ultrashort echo time MR imaging. *Radiology* **280**, 161–168 (2016).
4. Bonnevie, E. D. & Mauck, R. L. Physiology and Engineering of the Graded Interfaces of Musculoskeletal Junctions. *Annu. Rev. Biomed. Eng.* 403–431 (2018).
5. Asadian, M. *et al.* Fabrication and plasma modification of nanofibrous tissue engineering scaffolds. *Nanomaterials* **10**, (2020).
6. López-Marcial, G. R. *et al.* Agarose-Based Hydrogels as Suitable Bioprinting Materials for Tissue Engineering. *ACS Biomater. Sci. Eng.* **4**, 3610–3616 (2018).
7. Caliari, S. R. & Harley, B. A. C. Collagen-GAG Materials. in *Materials of Biological Origin* 280–300 (2011).
8. Bezci, S. E. *et al.* Radial variation in biochemical composition of the bovine caudal intervertebral disc. *JOR Spine* 1–13 (2019). doi:10.1002/jsp2.1065
9. Bezci, S. E., Nandy, A. & O'Connell, G. D. Effect of Hydration on Healthy Intervertebral Disk Mechanical Stiffness. *J. Biomech. Eng.* **137**, 101007 (2015).
10. Oungoulian, S. R. *et al.* Wear and Damage of Articular Cartilage with Friction Against Orthopaedic Implant Materials. *J. Biomech.* **48**, 1957–1964 (2015).
11. Krishnan, R., Kopacz, M. & Ateshian, G. A. Experimental verification of the role of interstitial fluid pressurization in cartilage lubrication. *J. Orthop. Res.* **22**, 565–570 (2004).
12. Johansson, P., Marklund, P., Björling, M. & Shi, Y. Effect of humidity and counterface material on the friction and wear of carbon fiber reinforced PTFE composites. *Tribol. Int.* **157**, (2021).
13. Bhosale, A. M. & Richardson, J. B. Articular cartilage: Structure, injuries and review of management. *Br. Med. Bull.* **87**, 77–95 (2008).
14. Sophia Fox, A. J., Bedi, A. & Rodeo, S. A. The basic science of articular cartilage: structure, composition, and function. *Sports Health* **1**, 461–468 (2009).
15. Fox, A. J. S., Bedi, A. & Rodeo, S. A. The Basic Science of Human Knee Menisci: Structure, Composition, and Function. *Sports Health* **4**, 340–351 (2012).
16. Seitz, A. M. *et al.* Knee Joint Menisci Are Shock Absorbers: A Biomechanical In-Vitro Study on Porcine Stifle Joints. *Front. Bioeng. Biotechnol.* **10**, 1–11 (2022).
17. Cassidy, J. J., Hiltner, A. & Baer, E. Hierarchical Structure of the Intervertebral Disc. **8207**, (2009).

18. Cortes, D. H., Jacobs, N. T., DeLucca, J. F. & Elliott, D. M. Elastic, Permeabilty and Swelling Properties of Human Intervertebral Disc Tissues : A Benchmark for Tissue engineering. *J. Biomech.* **47**, 2088–2094 (2015).

19. Malandrino, A. Chapter 6: Intervertebral DIsc. in *Biomechanics of the Spine* 89–103 (2018).

20. Yang, B. & Connell, G. D. O. GAG content , fiber stiffness , and fiber angle affect swelling - based residual stress in the intact annulus fibrosus. (2018).

21. Bunt, C. W., Jonas, C. E. & Chang, J. G. Knee pain in adults and adolescents: The initial evaluation. *Am. Fam. Physician* **98**, 576–585 (2018).

22. Ostendorf, RobertDe Koning, M. H., Van De Stadt, R. J. & Van Kempen, G. P. J. OSTEOARTHRITIS Cyclic loading is h a r m f u l to articular cartilage from which. *Osteoarthr. Cartil.* 275–284 (1995).

23. Hsu, H. & Siwiec, R. M. Knee osteoarthritis. *StatPearls* **67**, 240–241 (2021).

24. Buckwalter, JA ; Mankin,HJ; Grodzinsky, A. Articular Cartilage and Osteoarthritis. in *AAOS Instructional Course Lectures* **54**, 466–480 (2005).

25. Guglielmo, D. *et al.* State-Specific Severe Joint Pain and Physical Inactivity Among Adults with Arthritis — United States, 2017. *MMWR. Morb. Mortal. Wkly. Rep.* **68**, 381–387 (2019).

26. Bliddal, H., Leeds, A. R. & Christensen, R. Osteoarthritis, obesity and weight loss: Evidence, hypotheses and horizons - a scoping review. *Obes. Rev.* **15**, 578–586 (2014).

27. Fleming, B. C., Hulstyn, M. J., Oksendahl, H. L. & Fadate, P. D. Ligament Injury, Reconstruction, and Osteoarthritis. *Curr. Opin. Orthop.* **16**, 354–362 (2005).

28. Wheaton, M. & Jensen, N. The ligament injury connection to osteoarthritis. *J. Prolotherapy* **2**, 294–304 (2010).

29. Englund, M. *et al.* Meniscal Tear In Knees Without Surgery and the Development of Radiographic Osteoarthritis Among Middle-Aged and Elderly Persons. *Arthritis Rheum.* **60**, 831–839 (2009).

30. Kan, H. S. *et al.* Non-surgical treatment of knee osteoarthritis. *Hong Kong Med. J.* 127–133 (2019).

31. Rönn, K., Reischl, N., Gautier, E. & Jacobi, M. Current Surgical Treatment of Knee Osteoarthritis. *Arthritis* **2011**, 1–9 (2011).

32. Peng, H. *et al.* Osteotomy Around the Knee: The Surgical Treatment of Osteoarthritis. *Orthop. Surg.* **13**, 1465–1473 (2021).

33. Skou, S. T. *et al.* Total knee replacement and non-surgical treatment of knee osteoarthritis: 2-year outcome from two parallel randomized controlled trials. *Osteoarthritis and Cartilage* **26**, 1170–1180 (2018).

34. Barazanchi, A., Li, K., Al-Amleh, B., Lyons, K. & Waddell, J. Mechanical Properties of

Laser-Sintered 3D-Printed Cobalt Chromium and Soft-Milled Cobalt Chromium. *Prosthesis* **2**, 313–320 (2020).

35. Fang, L., Leng, Y. & Gao, P. Processing and mechanical properties of HA/UHMWPE nanocomposites. *Biomaterials* **27**, 3701–3707 (2006).

36. Boschetti, F., Pennati, G., Gervaso, F., Peretti, G. M. & Dubini, G. Biomechanical properties of human articular cartilage under compressive loads. *Biorheology* **41**, 159–166 (2004).

37. Ferroni, M., Belgio, B., Peretti, G. M., Di Giancamillo, A. & Boschetti, F. Evolution of meniscal biomechanical properties with growth: An experimental and numerical study. *Bioengineering* **8**, (2021).

38. Pal, S. *Design of artificial human joints & organs*. *Design of Artificial Human Joints & Organs* **9781461462**, (2014).

39. Martin, J. R., Watts, C. D., Levy, D. L. & Kim, R. H. Medial Tibial Stress Shielding: A Limitation of Cobalt Chromium Tibial Baseplates. *Journal of Arthroplasty* **32**, 558–562 (2017).

40. Bendich, I., Lawrie, C. M., Riegler, V., Barrack, R. L. & Nunley, R. M. The Impact of Component Design and Fixation on Stress Shielding After Modern Total Knee Arthroplasty. *Journal of Arthroplasty* **37**, S221–S225 (2022).

41. Aggarwal, V. K. *et al.* Revision total knee arthroplasty in the young patient: Is there trouble on the horizon? *J. Bone Jt. Surg. - Ser. A* **96**, 536–542 (2014).

42. Price, A. J. *et al.* Knee replacement. *Lancet* **392**, 1672–1682 (2018).

43. Bayliss, L. E. *et al.* The effect of patient age at intervention on risk of implant revision after total replacement of the hip or knee: a population-based cohort study. *The Lancet* **389**, 1424–1430 (2017).

44. Jones, I. A., Togashi, R., Wilson, M. L. & Heckmann, N. Intra-articular treatment options for knee osteoarthritis. *Nat. Rev.* **15**, 77–90 (2019).

45. Dubey, N. K. *et al.* Combating osteoarthritis through stem cell therapies by rejuvenating cartilage: A review. *Stem Cells Int.* **2018**, (2018).

46. Carey, J. L. *et al.* Autologous Chondrocyte Implantation as Treatment for Unsalvageable Osteochondritis Dissecans: 10- to 25-Year Follow-up. *Am. J. Sports Med.* **48**, 1134–1140 (2020).

47. Davies, R. L. & Kuiper, N. J. Regenerative Medicine: A Review of the Evolution of Autologous Chondrocyte Implantation (ACI) Therapy. *Bioengineering* **6**, 1–16 (2019).

48. Vonk, L. A., Roël, G., Hernigou, J., Kaps, C. & Hernigou, P. Role of matrix-associated autologous chondrocyte implantation with spheroids in the treatment of large chondral defects in the knee: A systematic review. *Int. J. Mol. Sci.* **22**, (2021).

49. Schuette, H. B., Kraeutler, M. J., Schrock, J. B. & McCarty, E. C. Primary Autologous Chondrocyte Implantation of the Knee Versus Autologous Chondrocyte Implantation

After Failed Marrow Stimulation: A Systematic Review. *Am. J. Sports Med.* **49**, 2536–2541 (2021).

50. Ebert, J. R., Fallon, M., Wood, D. J. & Janes, G. C. An accelerated 6-week return to full weight bearing after matrix-induced autologous chondrocyte implantation results in good clinical outcomes to 5 years post-surgery. *Knee Surgery, Sport. Traumatol. Arthrosc.* **29**, 3825–3833 (2021).

51. Binder, H. *et al.* Clinical evaluation after matrix-associated autologous chondrocyte transplantation: A comparison of four different graft types. *Bone Jt. Res.* **10**, 370–379 (2021).

52. Merkely, G., Ogura, T., Ackermann, J., Barbieri Mestriner, A. & Gomoll, A. H. Clinical Outcomes after Revision of Autologous Chondrocyte Implantation to Osteochondral Allograft Transplantation for Large Chondral Defects: A Comparative Matched-Group Analysis. *Cartilage* **12**, 155–161 (2021).

53. Migliorini, F., Eschweiler, J., Goetze, C., Tingart, M. & Maffulli, N. Membrane scaffolds for matrix-induced autologous chondrocyte implantation in the knee: a systematic review. *Br. Med. Bull.* **140**, 50–61 (2021).

54. Khoo, W. *et al.* Fracture behavior of multilayer fibrous scaffolds featuring microstructural gradients. *Mater. Des.* **184**, 1–9 (2019).

55. Ifkovits, J. L., Sundararaghavan, H. G. & Burdick, J. a. Electrospinning fibrous polymer scaffolds for tissue engineering and cell culture. *J. Vis. Exp.* 51525 (2009). doi:10.3791/1589

56. Martin, J. T. *et al.* In Vitro Maturation and In Vivo Integration and Function of an Engineered Cell-Seeded Disc-like Angle Ply Structure (DAPS) for Total Disc Arthroplasty. 1–13 (2017). doi:10.1038/s41598-017-15887-4

57. Jun, I., Han, H. S., Edwards, J. R. & Jeon, H. Electrospun fibrous scaffolds for tissue engineering: Viewpoints on architecture and fabrication. *Int. J. Mol. Sci.* **19**, (2018).

58. Rodriguez-Cabello, J. C., Gonzalez De Torre, I., González-Pérez, M., González-Pérez, F. & Montequi, I. Fibrous Scaffolds From Elastin-Based Materials. *Front. Bioeng. Biotechnol.* **9**, (2021).

59. Roberts, J. J. & Martens, P. J. Engineering biosynthetic cell encapsulation systems. in *Biosynthetic Polymers for Medical Applications* 205–240 (2016).

60. O'Connell, G. D., Nims, R. J., Green, J., Ateshian, G. A. & Hung, C. T. Time and Dose-dependent Effects of Chondroitinase ABC on Growth Of Engineered Cartilage. *Eur. Cells Mater.* **27**, 312–320 (2015).

61. Bian, L. *et al.* Influence of Decreasing Nutrient Path length on the Development of Engineered Cartilage. *Osteorthritis Cartil.* **17**, 677–685 (2009).

62. Mauck, R. L. *et al.* Functional tissue engineering of articular cartilage through dynamic loading of chondrocyte-seeded agarose gels. *J. Biomech. Eng.* **122**, 252–260 (2000).

63. López-Marcial, G. R. *et al.* Agarose-Based Hydrogels as Suitable Bioprinting Materials for Tissue Engineering. *ACS Biomater. Sci. Eng.* **4**, 3610–3616 (2018).

64. Pluen, A., Netti, P. A., Jain, R. K. & Berk, D. A. Diffusion of macromolecules in agarose gels: comparison of linear and globular configurations. *Biophys. J.* **77**, 542–52 (1999).

65. Mauck, R. L. *et al.* Functional Tissue Engineering of Articular Cartilage Through Dynamic Loading of Chondrocyte-Seeded Agarose Gels. *J. Biomech. Eng.* **122**, 252 (2000).

66. O'Connell, G. D. *et al.* Toward Engineering a Biological Joint Repleacement. *Computer (Long. Beach. Calif).* **144**, 724–732 (2012).

67. Ng, K. W. *et al.* A layered agarose approach to fabricate depth-dependent inhomogeneity in chondrocyte-seeded constructs. *J. Orthop. Res.* **23**, 134–141 (2005).

68. Kuo, C. K. & Ma, P. X. Ionically crosslinked alginate hydrogels as scaffolds for tissue engineering : Part I . Structure , gelation rate and mechanical properties engineering : Part 1 . Structure , gelation rate and mechanical properties. *Biomaterials* **22**, 511–521 (2001).

69. Lee, K. Y. & Mooney, D. J. Alginate : properties and biomedical applications. **37**, 106–126 (2012).

70. Cao, N., Chen, X. B. & Schreyer, D. J. Influence of Calcium Ions on Cell Survival and Proliferation in the Context of an Alginate Hydrogel. *ISRN Chem. Eng.* **2012**, 1–9 (2012).

71. Baniasadi, M. & Minary-jolandan, M. Alginate-Collagen Fibril Composite Hydrogel. *Materials (Basel).* **8**, 799–814 (2015).

72. Müller, M., Öztürk, E., Arlov, Ø., Gatenholm, P. & Zenobi-Wong, M. Alginate Sulfate–Nanocellulose Bioinks for Cartilage Bioprinting Applications. *Ann. Biomed. Eng.* **45**, 210–223 (2017).

73. Gruber, H. E., Hoelscher, G. L., Leslie, K., Ingram, J. A. & Hanley, E. N. Three-dimensional culture of human disc cells within agarose or a collagen sponge: Assessment of proteoglycan production. *Biomaterials* **27**, 371–376 (2006).

74. Ahearne, M. Introduction to cell – hydrogel mechanosensing. *Interface Focus* **4**, (2014).

75. Lake, S. P. & Barocas, V. H. Mechanical and Structural Contribution of Non-Fibrillar Matrix in Uniaxial Tension : A Collagen-Agarose Co-Gel Model. *Ann. Biomed. Eng.* **39**, 1891–1903 (2011).

76. Cambria, E. *et al.* Cell-Laden Agarose-Collagen Composite Hydrogels for Mechanotransduction Studies. *Front. Bioeng. Biotechnol.* **8**, 1–14 (2020).

77. Köpf, M., Campos, D. F. D., Blaeser, A., Sen, K. S. & Fischer, H. A tailored three-dimensionally printable agarose-collagen blend allows encapsulation, spreading, and attachment of human umbilical artery smooth muscle cells. *Biofabrication* **8**, (2016).

78. Hinton, T. J. *et al.* Three-dimensional printing of complex biological structures by freeform reversible embedding of suspended hydrogels. *Sci. Adv.* **1**, e1500758–e1500758 (2015).

79. Yuan, L. *et al.* Effects of Composition and Mechanical Property of Injectable Collagen I/II Composite Hydrogels on Chondrocyte Behaviors. *Tissue Eng. - Part A* **22**, 899–906 (2016).

80. Lai, V. K. *et al.* Swelling of Collagen-Hyaluronic Acid Co-Gels : An In Vitro Residual Stress Model. *Ann. Biomed. Eng.* **44**, 2984–2993 (2016).

81. Ren, X. *et al.* Engineering zonal cartilage through bioprinting collagen type II hydrogel constructs with biomimetic chondrocyte density gradient. *BMC Musculoskelet. Disord.* **17**, 1–10 (2016).

82. Kilmer, C. E. *et al.* Collagen Type I and II Blend Hydrogel with Autologous Mesenchymal Stem Cells as a Sca ff old for Articular Cartilage Defect Repair. *ACS Biomater. Sci. Eng.* 3464–3476 (2020).

83. Goodman, S. *et al.* Tissue ingrowth and differentiation in the bone-harvest chamber in the presence of cobalt-chromium-alloy and high-density-polyethylene particles. *J. Bone Joint Surg. Am.* **77**, 1025–1035 (1995).

84. O'Connell, G., Garcia, J. M. & Jamali, A. A. 3D Bioprinting: New directions in articular cartilage tissue engineering. *ACS Biomater. Sci. Eng.* acsbiomaterials.6b00587 (2017). doi:10.1021/acsbiomaterials.6b00587

85. O'Connell, G. D., Leach, J. K. & Klineberg, E. Tissue engineering a biological repair strategy for lumbar disc herniation. *Biores. Open Access* **11**, 3045–3053 (2014).

86. Duarte Campos, D. F., Blaeser, A., Buellesbach, K. & Sen, K. S. Bioprinting Organotypic Hydrogels with Improved Mesenchymal Stem Cell Remodeling and Mineralization Properties for Bone Tissue Engineering. *Adv. Healthc. Mater.* **5**, 1336–1345 (2016).

87. Ford, A. *et al.* Large Modular Engineered Cartilage Surfaces with Evenly Distributed Properties. *J. Tissue Eng. Regen. Med.* 5

88. Nicodemus, G. D. & Bryant, S. J. Cell Encapsulation in Biodegradable Hydrogels for Tissue Engineering Applications. *Tissue Eng. Part B. Rev.* **14**, 149–165 (2008).

89. Muller, M., Becher, J., Schnabelrauch, M. & Zenobi-Wong, M. Nanostructured Pluronic hydrogels as bioinks for 3D bioprinting. *Biofabrication* **7**, 35006 (2015).

90. Jeong, J. H., Moon, Y. M., Kim, S. O., Yun, S. S. & Shin, H. I. Human Cartilage Tissue Engineering with Pluronic and Cultured Chondrocyte Sheet. *Key Eng. Mater.* **342**–**343**, 89–92 (2007).

91. Tan, A. R. & Hung, C. T. Concise review: Immunological properties of ocular surface and importance of limbal stem cells for transplantation. *Stem Cells Transl. Med.* (2017).

92. Bian, W., Liau, B., Badie, N. & Bursac, N. Mesoscopic hydrogel molding to control the 3D geometry of bioartificial muscle tissues. *Nat. Protoc.* **4**, 1522–1534 (2009).

93. Stanton, M. M., Samitier, J. & Sánchez, S. Bioprinting of 3D hydrogels. *Lab Chip* **15**, 3111–3115 (2015).

94. Mouser, V. H. M. *et al.* Yield stress determines bioprintability of hydrogels based on

gelatin-methacryloyl and gellan gum for cartilage bioprinting. *Biofabrication* **8**, 035003 (2016).

95. Ribeiro, A. *et al.* Assessing bioink shape fidelity to aid material development in 3D bioprinting. *Biofabrication* **10**, (2018).

96. Smith, P. T., Basu, A., Saha, A. & Nelson, A. Chemical modification and printability of shear-thinning hydrogel inks for direct-write 3D printing. *Polymer* **152**, 42–50 (2018).

97. Adamkiewicz, M. & Rubinsky, B. Cryogenic 3D Printing for tissue engineering. *Int. J. Disaster Risk Reduct.* 36–44 (2015). doi:10.1016/j.actamat.2015.02.029

98. Wang, L. *et al.* Evaluation of sodium alginate for bone marrow cell tissue engineering. **24**, 3475–3481 (2003).

99. Wei, J. *et al.* 3D Printing of an extremely tough hydrogel. *RSC Adv.* **5**, 81324–81329 (2015).

100. Albro, M. B., Rajan, V., Li, R., Hung, C. T. & Ateshian, G. A. Characterization of the Concentration-Dependence of Solute Diffusivity and Partitioning in a Model Dextran-Agarose Transport System. *Cell Mol Bioeng* **2**, 295–305 (2009).

101. Lee, B. H., Li, B. & Guelcher, S. A. Gel microstructure regulates proliferation and differentiation of MC3T3-E1 cells encapsulated in alginate beads. *Acta Biomaterialia* **8**, 1693–1702 (2012).

102. Augst, A. D., Kong, H. J. & Mooney, D. J. Alginate hydrogels as biomaterials. *Macromol. Biosci.* **6**, 623–633 (2006).

103. DeKosky, B. J. *et al.* Hierarchically Designed Agarose and Poly(Ethylene Glycol) Interpenetrating Network Hydrogels for Cartilage Tissue Engineering. *Tissue Eng. Part C Methods* **16**, 1533–1542 (2010).

104. Duan, B., Hockaday, L. A., Kang, K. H. & Butcher, J. T. 3D Bioprinting of heterogeneous aortic valve conduits with alginate/gelatin hydrogels. *J. Biomed. Mater. Res. - Part A* **101 A**, 1255–1264 (2013).

105. Peng, J. & Wang, C.-H. An Investigation on the Influence of Pore Size and Porosity of Sponge on Maximum Cell Concentration. 1–9 (2004).

106. Lee, K. Y. & Mooney, D. J. Alginate: properties and biomedical applications. *Prog Polym Sci.* **37**, 106–126 (2012).

107. Diniz, I. M. A. *et al.* Pluronic F-127 hydrogel as a promising scaffold for encapsulation of dental-derived mesenchymal stem cells. *J. Mater. Sci. Mater. Med.* **26**, 1–10 (2015).

108. Gioffredi, E. *et al.* Pluronic F127 Hydrogel Characterization and Biofabrication in Cellularized Constructs for Tissue Engineering Applications. in *Procedia CIRP* **49**, 125–132 (The Author(s), 2016).

109. Ozbolat, I. T. & Hospodiuk, M. Current advances and future perspectives in extrusion-based bioprinting. *Biomaterials* **76**, 321–343 (2016).

110. Baird, D. G. & Collias, D. I. *Polymer Processing: Principles and Design*. (John Wiley & Sons, Ltd, 2014).

111. Blaeser, A. *et al.* Controlling Shear Stress in 3D Bioprinting is a Key Factor to Balance Printing Resolution and Stem Cell Integrity. *Adv. Healthc. Mater.* **5**, 326–333 (2016).

112. Zhao, Y., Li, Y., Mao, S., Sun, W. & Yao, R. The influence of printing parameters on cell survival rate and printability in microextrusion-based 3D cell printing technology. *Biofabrication* **7**, (2015).

113. He, Y. *et al.* Research on the printability of hydrogels in 3D bioprinting. *Sci. Rep.* **6**, 1–13 (2016).

114. Jang, T. S. *et al.* 3D printing of hydrogel composite systems: Recent advances in technology for tissue engineering. *Int. J. Bioprinting* **4**, 1–28 (2018).

115. Markstedt, K. *et al.* 3D bioprinting human chondrocytes with nanocellulose-alginate bioink for cartilage tissue engineering applications. *Biomacromolecules* **16**, 1489–1496 (2015).

116. Suntornnond, R., Tan, E. Y. S., An, J. & Chua, C. K. A highly printable and biocompatible hydrogel composite for direct printing of soft and perfusable vasculature-like structures. *Sci. Rep.* **7**, 1–11 (2017).

117. Sarker, M., Izadifar, M., Schreyer, D. & Chen, X. Influence of ionic crosslinkers (Ca 2+ /Ba 2+ /Zn 2+) on the mechanical and biological properties of 3D Bioplotted Hydrogel Scaffolds. *J. Biomater. Sci. Polym. Ed.* **29**, 1126–1154 (2018).

118. Paxton, N. *et al.* Proposal to assess printability of bioinks for extrusion-based bioprinting and evaluation of rheological properties governing bioprintability. *Biofabrication* **9**, (2017).

119. Talukdar, S., Nguyen, Q. T., Chen, A. C. & Sah, R. L. Effect of initial cell seeding density on 3D-engineered silk fibroin scaffolds for articular cartilage tissue engineering. *Biomaterials* **32**, 8927–8937 (2011).

120. Ouyang, L., Highley, C. B., Rodell, C. B., Sun, W. & Burdick, J. A. 3D Printing of Shear-Thinning Hyaluronic Acid Hydrogels with Secondary Cross-Linking. *ACS Biomater. Sci. Eng.* **2**, 1743–1751 (2016).

121. Wu, Z. *et al.* Bioprinting three-dimensional cell-laden tissue constructs with controllable degradation. *Sci. Rep.* **6**, 24474 (2016).

122. Kisiday, J. D., Liebig, B. E. & Goodrich, L. R. Adult ovine chondrocytes in expansion culture adopt progenitor cell properties that are favorable for cartilage tissue engineering. *J. Orthop. Res.* **38**, 1996–2005 (2020).

123. Xia, T., Liu, W. & Yang, L. A review of gradient stiffness hydrogels used in tissue engineering and regenerative medicine. *J. Biomed. Mater. Res. - Part A* **105**, 1799–1812 (2017).

124. Mahmood, M. F., Clarke, M. J. & Riches, D. P. Proteoglycans exert a significant effect on

human meniscal stiffness through ionic effects. *Clinical Biomechanics* **77**, (2020).

125. Gu, W. Y., Yao, H., Huang, C. Y. & Cheung, H. S. New insight into deformation-dependent hydraulic permeability of gels and cartilage, and dynamic behavior of agarose gels in confined compression. *J. Biomech.* **36**, 593–598 (2003).

126. Danso, E. K., Julkunen, P. & Korhonen, R. K. Poisson's ratio of bovine meniscus determined combining unconfined and confined compression. *J. Biomech.* **77**, 233–237 (2018).

127. Ng, K. W., Ateshian, G. A. & Hung, C. T. Zonal chondrocytes seeded in a layered agarose hydrogel create engineered cartilage with depth-dependent cellular and mechanical inhomogeneity. *Tissue Eng. Part A* **15**, 2315–2324 (2009).

128. Seidel, J. O. *et al.* Long-term culture of tissue engineered cartilage in a perfused chamber with mechanical stimulation. *Biorheology* **41**, 445–58 (2004).

129. Vunjak-Novakovic, G. *et al.* Bioreactor cultivation conditions modulate the composition and mechanical properties of tissue-engineered cartilage. *J. Orthop. Res.* **17**, 130–138 (1999).

130. Lake, S. P., Hald, E. S. & Barocas, V. H. Collagen-agarose co-gels as a model for collagen-matrix interaction in soft tissues subjected to indentation. *J. Biomed. Mater. Res. - Part A* **99 A**, 507–515 (2011).

131. Cao, W. *et al.* Dynamic mechanical loading facilitated chondrogenic differentiation of rabbit BMSCs in collagen scaffolds. *Regen. Biomater.* 99–106 (2019). doi:10.1093/rb/rbz005

132. Kuhn, K. C. J. L., Ciarelli, M. J. & Goldstein, S. A. THE ELASTIC MODULI OF HUMAN SUBCHONDRAL , TRABECULAR , AND CORTICAL BONE TISSUE AND THE SIZE-DEPENDENCY OF CORTICAL BONE MODULUS *. *J. Biomech.* **23**, (1990).

133. Lim, S., Huff, R. D., Veres, J. E., Satish, D. & O'Connell, G. D. Disc geometry measurement methods affect reported compressive mechanics by up to 65%. *JOR Spine* 2–9 (2022). doi:10.1002/jsp2.1214

134. Harikajimi, P. & Nejad, F. M. Chapter 3. Mechanical models of viscoelasticity. in *Applications of Viscoelasticity* 27–60 (2021).

135. Papanicolaou, G. C. & Zaoutsos, S. P. Viscoelastic constitutive modeling of creep and stress relaxation in polymers and polymer matrix composites. in *Viscoelastic constitutive modeling* 3–57 (2019).

136. Groth, K. M. & Granata, K. P. The viscoelastic standard nonlinear solid model: predicting the response of the lumbar intervertebral disk to low-frequency vibrations. *J Biomech Eng* **130**, 031005 (2008).

137. O'Connell, G. D., Jacobs, N. T., Sen, S., Vresilovic, E. J. & Elliott, D. M. Axial creep loading and unloaded recovery of the human intervertebral disc and the effect of degeneration. *J. Mech. Behav. Biomed. Mater.* **4**, 933–942 (2011).

138. Ed-Daoui, A. & Snabre, P. Poroviscoelasticity and compression-softening of agarose hydrogels. *Rheol. Acta* **60**, 327–351 (2021).

139. Patel, J. M., Wise, B. C., Bonnevie, E. D. & Mauck, R. L. A Systematic Review and Guide to Mechanical Testing for Articular Cartilage Tissue Engineering. *Tissue Eng. - Part C Methods* **25**, 593–608 (2019).

140. Zhao, C. *et al.* Gelation of Na-alginate aqueous solution: A study of sodium ion dynamics via NMR relaxometry. *Carbohydr. Polym.* **169**, 206–212 (2017).

141. Veen, A. J. Van Der, Bisschop, A., Mullender, M. G. & Dieën, J. H. Van. Modelling creep behaviour of the human intervertebral disc. *J. Biomech.* **46**, 2101–2103 (2013).

142. Engler, A. J., Sen, S., Sweeney, H. L. & Discher, D. E. Matrix Elasticity Directs Stem Cell Lineage Specification. *Cell* **126**, 677–689 (2006).

143. Kumar, A., Placone, J. K. & Engler, A. J. Understanding the extracellular forces that determine cell fate and maintenance. *Dev.* **144**, 4261–4270 (2017).

144. Zhou, M., Werbner, B. & O'Connell, G. D. Fiber engagement accounts for geometry-dependent annulus fibrosus mechanics: A multiscale, Structure-Based Finite Element Study. *J. Mech. Behav. Biomed. Mater.* **115**, (2021).

145. Khan, A. S., Balzer, J. E., Wilgeroth, J. M. & Proud, W. G. Aspect ratio compression effects on metals and polymers. *J. Phys. Conf. Ser.* **500**, (2014).

146. Middendorf, J. M. *et al.* Multiscale mechanics of tissue - engineered cartilage grown from human chondrocytes and human - induced pluripotent stem cells. *J. Orthop. Res.* 1–9 (2020). doi:10.1002/jor.24643

147. Harris, J. R., Graham, J. & Rickwood, D. *Cell Biology Protocols*. *Cell Biology Protocols* (2006). doi:10.1002/0470033487

148. Zeugolis, D. I., Paul, R. G. & Attenburrow, G. Factors influencing the properties of reconstituted collagen fibers prior to self-assembly: Animal species and collagen extraction method. *J. Biomed. Mater. Res. - Part A* **86**, 892–904 (2008).

149. Sorushanova, A., Skoufos, I., Tzora, A., Mullen, A. M. & Zeugolis, D. I. The influence of animal species, gender and tissue on the structural, biophysical, biochemical and biological properties of collagen sponges. *J. Mater. Sci. Mater. Med.* **32**, (2021).

150. Hollander, A. P. *et al.* Increased damage to type II collagen in osteoarthritic articular cartilage detected by a new immunoassay. *J. Clin. Invest.* **93**, 1722–1732 (1994).

151. O'Connell, G. D. *et al.* Toward Engineering a Biological Joint Replacement. *J Knee Surg* **25**, 187–196 (2012).

152. Werbner, B. *et al.* Non-enzymatic glycation of annulus fibrosus alters tissue-level failure mechanics in tension. *Journal of the Mechanical Behavior of Biomedical Materials* **126**, (2022).

153. Cheung, H. S. Distribution of Type I , II , III and V in the Pepsin Solubilized Collagens in Bovine Menisci. **8207**, (2009).

154. Rumian, A. P., Wallace, A. L. & Birch, H. L. Tendons and Ligaments Are Anatomically Distinct But Overlap in Molecular and Morphological Features — A Comparative Study in an Ovine Model. 458–464 (2007). doi:10.1002/jor

155. Stegemann, H. & Stalder, K. Determination of hydroxyproline. *Clin. Chim. Acta* **18**, 267–273 (1967).

156. Brydges, C. R. Effect Size Guidelines , Sample Size Calculations , and Statistical Power in Gerontology. *Innov. Aging* **3**, 1–8 (2019).

157. Monaco, J. Ecological Fallacy. in *Encyclopedia of Behavioral Medicine* (eds. Gellman, M. D. & Turner, J. R.) 644 (Springer New York, 2013). doi:10.1007/978-1-4419-1005-9_1017

158. Schwartz, S. The fallacy of the ecological fallacy: The potential misuse of a concept and the consequences. *Am. J. Public Health* **84**, 819–824 (1994).

159. Kurniawan, N. A., Wong, L. H. & Rajagopalan, R. Early stiffening and softening of collagen: Interplay of deformation mechanisms in biopolymer networks. *Biomacromolecules* **13**, 691–698 (2012).

160. Hoy, D. *et al.* A systematic review of the global prevalence of low back pain. *Arthritis Rheum.* **64**, 2028–2037 (2012).

161. Whatley, B. R. & Wen, X. Intervertebral disc (IVD): Structure, degeneration, repair and regeneration. *Mater. Sci. Eng. C* **32**, 61–77 (2012).

162. Ashinsky, B. G. *et al.* Degeneration alters structure-function relationships at multiple length-scales and across interfaces in human intervertebral discs. *J. Anat.* 1–13 (2020). doi:10.1111/joa.13349

163. Sahoo, M. M. *et al.* Significance of Vertebral Endplate Failure in Symptomatic Lumbar Disc Herniation. *Glob. Spine J.* **7**, 230–238 (2017).

164. Thomopoulos, S., Marquez, J. P., Weinberger, B., Birman, V. & Genin, G. M. Collagen fiber orientation at the tendon to bone insertion and its influence on stress concentrations. *J. Biomech.* **39**, 1842–1851 (2006).

165. Genin, G. M. *et al.* Functional Grading of Mineral and Collagen in the Attachment of Tendon to Bone. *Biophys. J.* **97**, 976–985 (2009).

166. Heidari, H. & Taylor, H. Multilayered microcasting of agarose-collagen composites for neurovascular modeling. *Bioprinting* **e00069**, (2020).

167. Kelly, B. E., Bhattacharya, I., Heidari, H. & Shusteff, M. Volumetric additive manufacturing via tomographic reconstruction. *Science (80-.).* **d**, 1075–1079 (2019).

168. Kokkinis, D., Bouville, F. & Studart, A. R. 3D Printing of Materials with Tunable Failure via Bioinspired Mechanical Gradients. *Adv. Mater.* **1705808**, 1–9 (2018).

169. Fujita, Y., Duncan, N. A. & Lotz, J. C. Radial Tensile Properties of the Lumbar Annulus Fibrosus are Site and Degeneration Dependent. *J. Orthop. Res.* **15**, 814–819 (1997).

170. Liu, Z., Meyers, M. A., Zhang, Z. & Ritchie, R. O. Functional gradients and heterogeneities in biological materials : Design principles , functions , and bioinspired applications. *Prog. Mater. Sci.* **88**, 467–498 (2017).

171. Gu, G. X., Chen, C., Richmond, D. J. & Buehler, M. J. Bioinspired hierarchical composite design machine learning : simulation , additive manufacturing , and experiment. *Mater. Horizons* **5**, 939–945 (2018).

172. Bartell, L. R., Fortier, L. A., Bonassar, L. J. & Cohen, I. Measuring microscale strain fields in articular cartilage during rapid impact reveals thresholds for chondrocyte death and a protective role for the superficial layer. *J. Biomech.* **48**, 3440–3446 (2015).

173. Dong, L. *et al.* The effect of collagen hydrogels on chondrocyte behaviors through restricting the contraction of cell/hydrogel constructs. *Regen. Biomater.* **8**, 1–10 (2021).

174. Vogel, Ch. & Marcotte, E. M. Insights into the regulation of protein abundance from proteomic and transcriptomatic analyses. *Nat Rev Genet* **13**, 227–232 (2013).

175. Greenbaum, D., Colangelo, C., Williams, K. & Gerstein, M. Comparing protein abundance and mRNA expression levels on a genomic scale. *Genome Biol.* **4**, (2003).

176. Little, C. J., Bawolin, N. K. & Chen, X. Mechanical properties of natural cartilage and tissue-engineered constructs. *Tissue Eng. - Part B Rev.* **17**, 213–227 (2011).

177. Lake, S. P., Hadi, M. F., Lai, V. K. & Barocas, V. H. Mechanics of a Fiber Network Within a Non-Fibrillar Matrix : Model and Comparison with Collagen-Agarose Co-gels. *Ann. Biomed. Eng.* **40**, 2111–2121 (2012).

178. Römgens, A. M., Van Donkelaar, C. C. & Ito, K. Contribution of collagen fibers to the compressive stiffness of cartilaginous tissues. *Biomech. Model. Mechanobiol.* **12**, 1221–1231 (2013).

179. Baylon, E. G. & Levenston, M. E. Osmotic Swelling Responses Are Conserved Across Cartilaginous Tissues With Varied Sulfated-Glycosaminoglycan Contents. *J. Orthop. Res.* **38**, 785–792 (2020).

180. Han, G., Boz, U., Eriten, M. & Henak, C. R. Glycosaminoglycan depletion increases energy dissipation in articular cartilage under high-frequency loading. *Journal of the Mechanical Behavior of Biomedical Materials* **110**, (2020).

181. Han, Y. L. *et al.* Cell contraction induces long-ranged stress stiffening in the extracellular matrix. *Proc. Natl. Acad. Sci. U. S. A.* **115**, 4075–4080 (2018).

182. Ulrich, T. A., Lee, T. G., Shon, H. K., Moon, D. W. & Kumar, S. Microscale mechanisms of agarose-induced disruption of collagen remodeling. *Biomaterials* **32**, 5633–5642 (2011).

183. Ebenstein, D. M. Nano-JKR force curve method overcomes challenges of surface detection and adhesion for nanoindentation of a compliant polymer in air and water. *J. Mater. Res.* **26**, 1026–1035 (2011).

184. Ebenstein, D. M. & Pruitt, L. A. Nanoindentation of soft hydrated materials for

application to vascular tissues. *Wiley Intersci.* 222–232 (2004). doi:10.1002/jbm.a.20096

185. Bansal, S. *et al.* Meniscal repair : The current state and recent advances in augmentation. *J. Orthop. Res.* 1–15 (2021). doi:10.1002/jor.25021

186. Andrews, S. H. J. *et al.* Tie-fibre structure and organization in the knee menisci. *Journal of Anatomy* **224**, 531–537 (2014).

187. Bansal, S. *et al.* Structure, Function, and Defect Tolerance with Maturation of the Radial Tie Fiber Network in the Knee Meniscus. *J Orthop Res* **38**, 2709–2720 (2020).

188. Aspden, R. M., Yarker, Y. E. & Hukins, D. W. L. Collagen orientations in the meniscus of the knee joint. *J. Anat.* **140**, 371–380 (1985).

189. Li, Q. *et al.* Micromechanical anisotropy and heterogeneity of the meniscus extracellular matrix. *Acta Biomaterialia* **54**, 356–366 (2017).

190. Coluccino, L. *et al.* Anisotropy in the Viscoelastic Response of Knee Meniscus Cartilage. *J. Appl. Biomater. Funct. Mater.* **15**, 77–83 (2017).

191. Sanchez-Adams, J., Wilusz, R. E. & Guilak, F. Atomic force microscopy reveals regional variations in the micromechanical properties of the pericellular and extracellular matrices of the meniscus. *J. Orthop. Res.* **31**, 1218–1225 (2013).

192. Sanchez-Adams, J., Willard, V. P. & Athanasiou, K. A. Regional variation in the mechanical role of knee meniscus glycosaminoglycans. *J. Appl. Physiol.* **111**, 1590–1596 (2011).

193. Danso, E. K. *et al.* Structure-function relationships of human meniscus. *J. Mech. Behav. Biomed. Mater.* **67**, 51–60 (2017).

194. Kambic, H. E. & McDevitt, C. A. Spatial organization of types I and II collagen in the canine meniscus. *J. Orthop. Res.* **23**, 142–149 (2005).

195. Hedayati, M. & Kipper, M. J. Atomic force microscopy of adsorbed proteoglycan mimetic nanoparticles: Toward new glycocalyx-mimetic model surfaces. *Carbohydr. Polym.* **190**, 346–355 (2018).

196. Qian, L. & Zhao, H. Nanoindentation of Soft Biological Materials. *Micromachines* **9**, (2018).

197. Abdelgaied, A. *et al.* Comparison of the biomechanical tensile and compressive properties of decellularised and natural porcine meniscus. *Journal of Biomechanics* **48**, 1389–1396 (2015).

198. Moyer, J. T., Abraham, A. C. & Haut Donahue, T. L. Nanoindentation of Human Meniscal Surfaces. *J. Biomech.* **45**, 2230–2235 (2012).

199. Moyer, J. T. Regional Comparisons of Nano-Mechanical Properties of the Human Meniscus; Structure and Function. *Proquest LLC* (2012).

200. Pordzik, J. *et al.* Analysis of proteoglycan content and biomechanical properties in arthritic and arthritis-free menisci. *Appl. Sci.* **10**, 1–12 (2020).

201. Li, Q. *et al.* Impacts of maturation on the micromechanics of the meniscus extracellular matrix. *Journal of Biomechanics* **72**, 252–257 (2018).

202. Campagnola, P. Second Harmonic Generation Imaging Microscopy: Applications to Diseases Diagnostics. *Anal. Chem.* **83**, 3224–3231 (2012).

203. Pinsard, M. *et al.* Maturation of the Meniscal Collagen Structure Revealed by Polarization-Resolved and Directional Second Harmonic Generation Microscopy. *Sci. Rep.* **9**, 1–11 (2019).

204. Werbner, B. *et al.* Saline-polyethylene glycol blends preserve in vitro annulus fibrosus hydration and mechanics: An experimental and finite-element analysis. *Journal of the Mechanical Behavior of Biomedical Materials* **125**, (2022).

205. Oliver, W. C. & Pharr, G. M. An improved technique for determining hardness and elastic modulus using load and displacement sensing indentation experiments. *J. Mater. Res,* **7**, 1564–1583 (1992).

206. Baro, V. J. *et al.* Functional characterization of normal and degraded bovine meniscus: Rate-dependent indentation and friction studies. *Bone* **51**, 232–240 (2012).

207. Kontomaris, S. V. & Malamou, A. Hertz model or Oliver & Pharr analysis? Tutorial regarding AFM nanoindentation experiments on biological samples. *Mater. Res. Express* **7**, (2020).

208. Gonzalez-Leon, E. A., Hu, J. C. & Athanasiou, K. A. Yucatan Minipig Knee Meniscus Regional Biomechanics and Biochemical Structure Support its Suitability as a Large Animal Model for Translational Research. *Front. Bioeng. Biotechnol.* **10**, 1–12 (2022).

209. Wu, J., Xu, J., Huang, Y., Tang, L. & Hong, Y. Regional-specific meniscal extracellular matrix hydrogels and their effects on cell-matrix interactions of fibrochondrocytes. *Biomed. Mater.* **17**, (2022).

210. Lewis, P. B. *et al.* Multiple Freeze-Thaw Cycled Meniscal Allograft Tissue: A Biomechanical, Biochemical, and Histologic Analysis. *J. Orthop. Res.* **25**, 49–55 (2007).

211. Ling, C. H., Lai, J. H., Wong, I. J. & Levenston, M. E. Bovine Meniscal Tissue Exhibits Age- and Interleukin-1 Dose-Dependent Degradation Patterns and Composition-Function Relationships. *J. Orthop. Res.* 801–811 (2016). doi:10.1002/jor.23096

212. Moyer, J. T., Priest, R., Bouman, T., Abraham, A. C. & Haut Donahue, T. L. Indentation properties and glycosaminoglycan content of human menisci in the deep zone. *Acta Biomaterialia* **9**, 6624–6629 (2013).

213. Takahashi, M., Suzuki, M., Kushida, K., Hoshino, H. & Inoue, T. The effect of aging and osteoarthritis on the mature and senescent cross-links of collagen in human meniscus. *Arthroscopy - Journal of Arthroscopic and Related Surgery* **14**, 366–372 (1998).